Dissertation zur Erlangung des Doktorgrades
der Fakultät für Chemie und Pharmazie
der Ludwig-Maximilians-Universität München

Development of a mCherry-DMDEx23 Positive Read-Out *In Vitro* Platform for Screening PMO-Xenopeptide Conjugates

Anna-Lina Lessl

aus

Hannover, Deutschland

2023

Erklärung

Diese Dissertation wurde im Sinne von § 7 der Promotionsordnung vom 28. November 2011 von Herrn Prof. Dr. Ernst Wagner betreut.

Eidesstattliche Versicherung

Diese Dissertation wurde eigenständig und ohne unerlaubte Hilfe erarbeitet.

München, 20.12.2023

.....

Anna-Lina Lessl

Dissertation eingereicht am	20.12.2023
1. Gutachter:	Prof. Dr. Ernst Wagner
2. Gutachter:	Ass.-Prof. Dr. Ulrich Lächelt
Mündliche Prüfung am	22.02.2024

Don't let the Muggles get you down.

Ron Weasley

Table of content

1. Introduction

This chapter provides a brief introduction into the research field of molecular therapeutics and associated delivery strategies. It is not considered to be a complete review of the whole scientific area.

1.1 Gene Expression Regulation

Gregor Mendel described the concept of genes as inheritable units causing disappearance and reappearance of a specific phenotype over several generations. The fact that the genotype results in a specific phenotype under specific conditions leads to the conclusion of specific mechanisms that regulate expression of different genes. The regulation of gene expression is according to necessity concerning endogenous conditions and environmental factors.[1-5] The International Human Genome Sequencing Consortium underlined the complexity of the human genome and its conversion into proteome. The majority of DNA in the human genome belongs to non-coding DNA which is transcribed into non-coding RNAs – including transfer (tRNA), ribosomal (rRNA), small nuclear RNAs (snRNA), and other regulatory factors.[2] Beside non-coding DNA, 30 000 to 40 000 protein-coding genes are present in the human genome, which consist of short exons and long introns. The gene expression pathway is influenced at many different levels. In addition to several genomic factors, such as genome architecture, histone modifications, DNA methylation, and chromosome topology[6], various post-transcriptional modifications take place to obtain a higher eukaryotic proteome diversity. Especially, RNA processing is one important process which extends the number of protein variants.[7]

1.1.1 Pre-mRNA Processing

Starting with genomic DNA as blueprint for every protein that is expressed in an eukaryotic organism, the information is transcribed into RNA taking the journey to be translated into a protein.[8] The transcription of DNA information into precursor messenger RNA (pre-mRNA) is regulated by transcription factors cis-elements, promotor, enhancer, and silencer sequences and performed by RNA-Polymerase II. Simultaneous to pre-mRNA generation, it undergoes three main processing steps resulting in mature messenger RNA (mature mRNA).[9]

First, 5' end capping with methylated guanosine (m^7G) occurs (**Figure 1a**). Via enzymatic catalysis through a triphosphatase, a guanyl transferase, and a methyl transferase as capping complex, addition of m^7G to the 5' triphosphate terminus (pppN) of pre-mRNA occurs resulting in a 7-methylguanosine-triphosphate (m^7GpppN).[10] The addition of m^7G protects the 5' end of RNA from degradation by exonucleases, facilitate the transport into the cytosol, and supports mRNA interaction with ribosomes during translation.[9, 11, 12]

5' end capping is followed by pre-mRNA splicing (**Figure 1b**), which plays a crucial role in diversification of the eukaryotic proteome. The observation of the polycistronic character of bacterial genes in 1977 led to further investigations of eukaryotic genes, which appeared to be a mosaic sequence consisting of exons divided by introns, which have to be removed precisely.[7, 13] Generally, mature mRNA consists of joined exons only.

The final step and therefore termination of RNA processing is the endonucleolytic cleavage 10-30 nucleotides downstream of a specific signal sequence. The cleavage is followed by polyadenylation of the 3' end of the RNA by polyadenylate polymerase which consumes ATP (**Figure 1c**).[11] The poly(A) tail at the 3' end enhances stability of the mRNA and plays an essential role in translational efficiency, and defines the half-life of mature mRNA.[14]

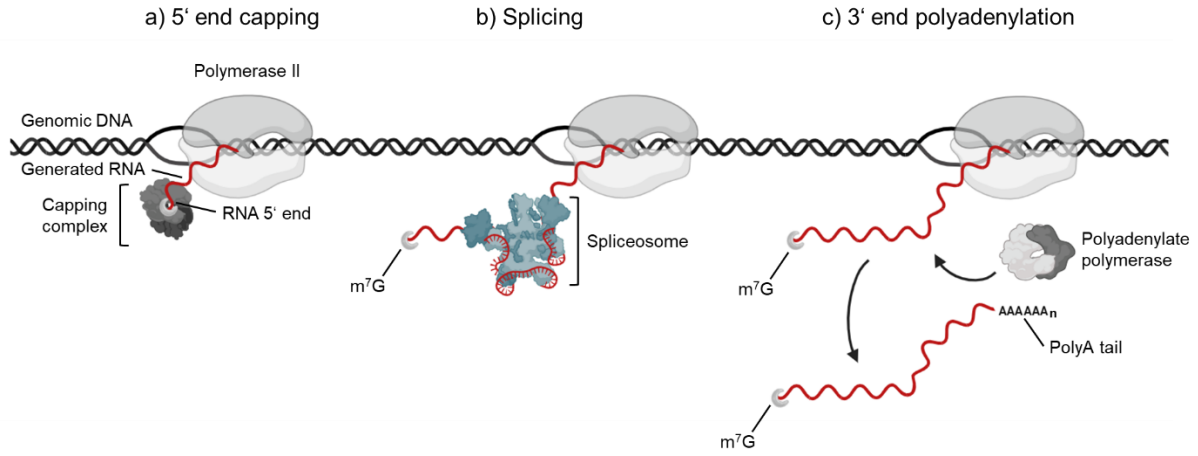

Figure 1 Schematic illustration of pre-mRNA processing. a) Pre-mRNA is generated by polymerase II. The capping complex forms a 7-methylguanosine (m^7G) at the 5' end of the RNA. **b)** During elongation, the spliceosome excises introns and ligates exons in the splicing process. **c)** As soon as polymerase II ends transcription of the gene, the RNA is cleaved, and a polyA-tail is added by the polyadenylate polymerase which terminates transcription. Figure was created using Biorender.com.

5’ end capping and 3’ end polyadenylation are conserved processes, whereas the process of splicing is a highly variable and complex regulated process in which regulating elements define the exon composition of mature mRNA.[15] The catalysis and recognition of these elements is done by the spliceosome. Spliceosomes are large ribonucleoprotein (RNP) complexes consisting of the uracil-rich small nuclear RNPs (snRNP) U1, U2, U4, U5 and U6 in association with at least 300 associated proteins. The different snRNPs recognize and bind specific sequences of introns.[16, 17] The essential binding sites are the conserved intronic cis-elements: 5’ splice site, located at the 5’ end of each intron, the 3’ splice site located at the 3’ end of each intron, and the branching point located 18-40 nucleotides upstream of the 3’ splice site.[16, 18] The ends of introns have conserved motifs. At the 5’ splice site (donor splice site) containing a nearly invariant dinucleotide GU indicating the transition from exon to intron, and the 3’ splice site (acceptor splice site) containing a nearly invariant dinucleotide AG indicating the transition from intron to exon.[2, 19] The mechanism relies on two subsequent transesterifications ligating exons and eliminating the intron (**Figure 2**). Through binding of U1 to the donor splice site and binding of U2 to the branching point the A complex is generated. The tri-snRNP U4/U6·U5 joins the A complex and therefore forms the B complex. Cleavage of U1 and U4 leads to activation of the spliceosome, which enables lariat intermediate formation. The nucleolytic attack of the 2’OH-group of the branching point on the nucleotide of the 5’ splice site results in a phosphodiester bond and therefore the lariat intermediate. After completion of the first nucleolytic attack, the C complex is formed and catalyzes the second nucleolytic attack. Here, the free 3’ OH group of the released 5’ exon attacks the G nucleotide of the 3’ splice site. The second transesterification releases the post-splicing complex in form of the lariat structure including U2, U5, U6, and ligated exons.[16]

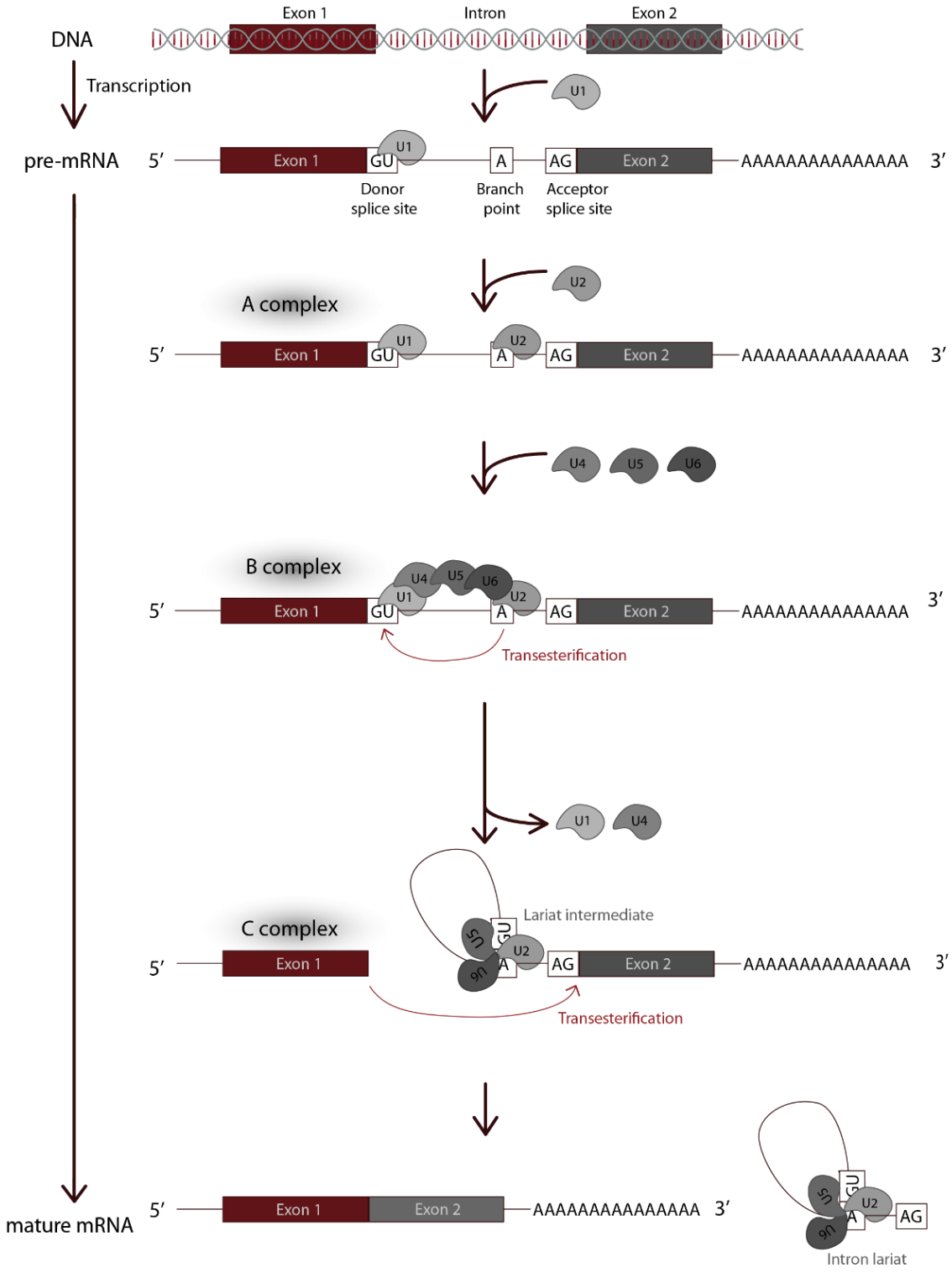

Figure 2 Schematic illustration of the progressive splicing mechanism. The recognition by spliceosome subunits is enabled by conserved sequences: donor splice site (5' splice site, GU), acceptor splice site (3' splice site, AG), and an adenine nucleotide (branch point, A). Binding of U1 to the donor splice site (5' splice site) and U2 to the branch point results in A complex. Association of tri-snRNP U4/U6·U5 to the A complex forms B complex. Cleavage of U1 and U4 activates the spliceosome which leads to the first transesterification and lariat intermediate formation resulting in the C complex. The second transesterification assembles exon sequences, and mature mRNA product and intron lariat are released.

1.1.2 Alternative Splicing

Constitutive splicing generally yields single transcripts from the pre-mRNA. The competition of at least two weak 5' or 3' splice sites mediated by additional splicing regulatory elements (SREs) results in alternative splicing.[20]

Consequently, a single primary transcript can lead to different mature mRNA sequences. The variability is caused by combinatorial effect of several different splice sites resulting in multiple protein isoforms (**Figure 3**) depending on cellular developmental stages and cell type.[21-24]

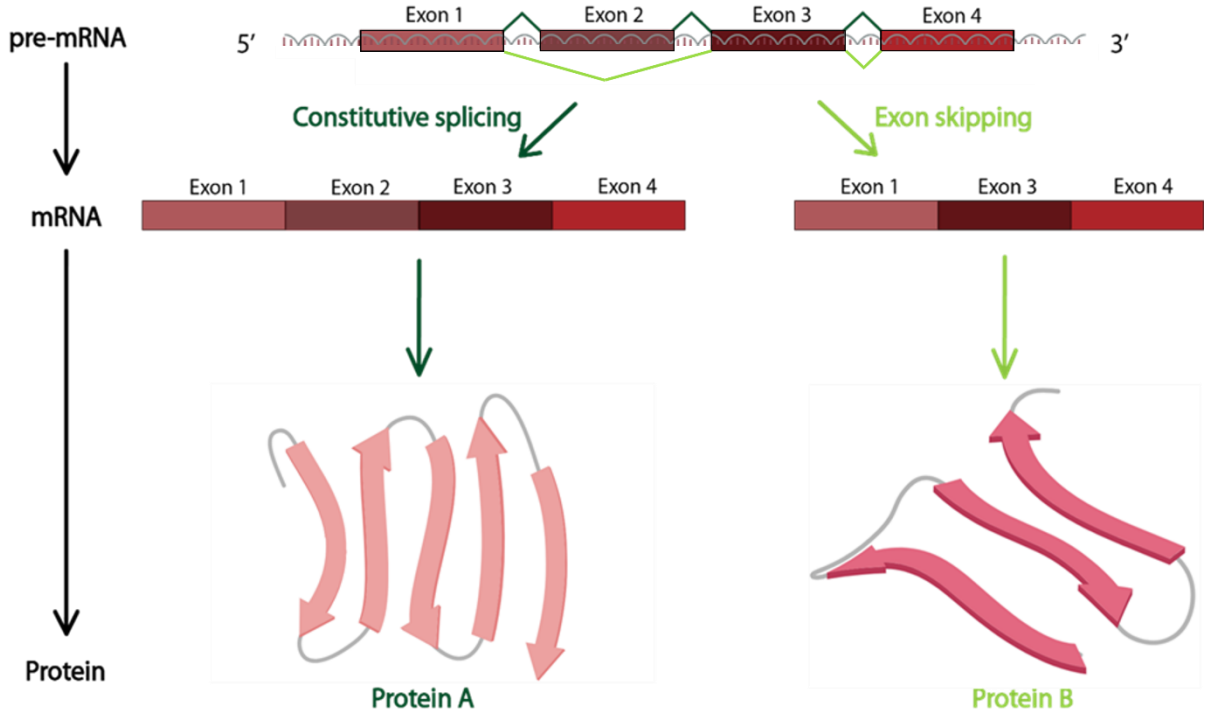

Figure 3 Schematic illustration of alternative splicing. Alternative splicing leads to diversification of the proteome due to various protein isoforms being expressed from one single pre-mRNA. After pre-mRNA formation, splicing occurs as one step of RNA processing. The constitutive way (left) shows the protein product after alignment of all pre-mRNA exons excluding all introns. Alternative splicing (right) commonly leads to exon skipping resulting in different isoforms. Figure was created using Biorender.com.

Trans-acting proteins and their cis-acting binding sites on the primary transcript regulate alternative splicing in an activating and inhibiting manner. Trans-acting proteins include activators and repressors, and cis-acting binding sites include silencers and enhancers.[25] These structures distinguish between pseudo and target exons and modulate the alternative splicing pattern. Exon skipping is a splicing variation which frequently occurs in humans in which one or more exons are completely spliced out resulting in a shorter

mature mRNA. Additional alternative splice modes are exon inclusion, alternative 3' splice sites, alternative 5' splice site, mutually exclusion exons, and intron retention (**Figure 4**).[15] In general alternative splicing leads to different protein isoforms. Since the recognition of cis-acting binding sites is highly important and sensitive, genomic mutations can make a significant effect disrupting canonical consensus sequences and defining exon-intron boundaries. Splice mutations can alter the mature mRNA sequence and lead to numerous human diseases.

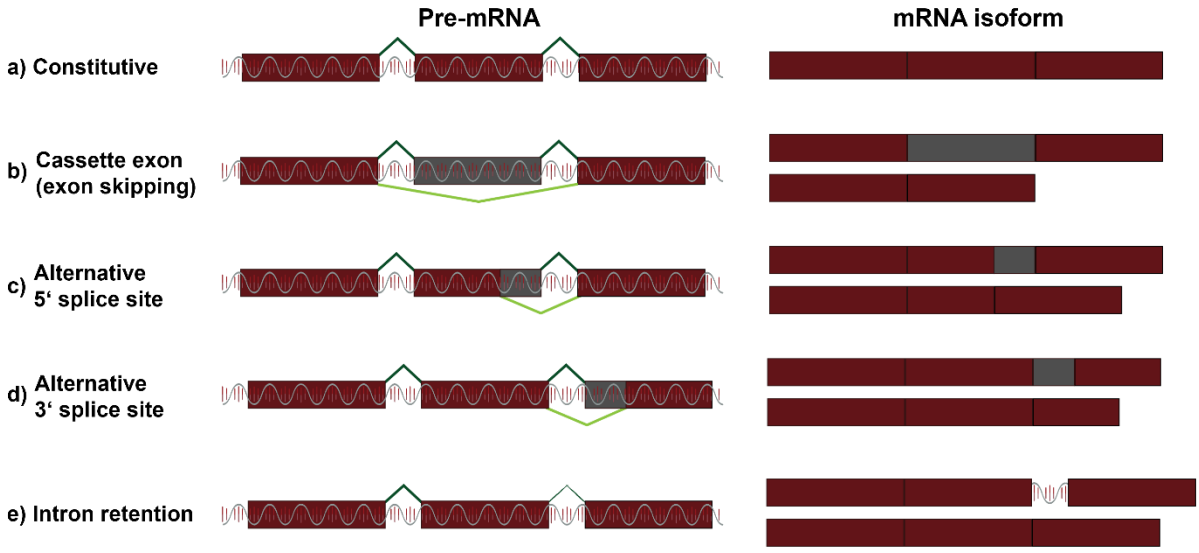

Figure 4 Classical forms of alternative splicing. The main alternative splicing patterns are divided into five common types: **a)** constitutive splicing where only introns are excluded; **b)** cassette exon where exons are included or skipped in order to generate different protein isoforms.[26] **c)** alternative 5' splice sites where the position of the 3' end of the exon shifts due to the change of the 5' splice site; **d)** alternative 3' splice sites where the position of the 5' end of the exon shifts due to the change of the 3' splice site; e) intron retention where introns are retained.

1.1.3 Aberrant Splicing

As explained above, splicing is a highly regulated and complex process with preserved sequence motifs. Small alterations of these regulation and recognition sites can modulate the splicing pattern significantly and lead to mutations in proteins and therefore loss of function. Genomic mutations affecting the splice pattern can either be frameshift, missense or non-sense mutations, which can lead to defective recognition of splice sites and therefore having an impact on the gene expression.[27] Mistakenly or partially present exons can be included or intron retention caused by activating cryptic splice sites can occur.[15] Cryptic splice sites can be activated after disruption of an original splice site or a *de novo* splice site can be created.[28] These defective mechanisms generate aberrant

mRNAs that encode for defective or incomplete protein isoforms or have a deficiency in stability. In addition to missense and silent mutations, coding single-nucleotide polymorphisms (cSNPs) are prone to affect pre-mRNA splicing.[29] Altering the reading frame or the composition of mature mRNA can be caused by complete or partial exclusion of necessary exons or complete or partial inclusion of redundant introns.[29] Mutations influencing mRNA splicing can induce several and severe diseases. The ratio of point mutations that are associated with human genetic disease causing RNA splicing alterations is striking and numbers 15%.[29]

1.1.4 Splice Mutations Originated Diseases

The high variability of genetic mutations leads to diversity of different diseases with varying severity.

β-Thalassemia is an autosomal recessive hematologic disease in which different mutations in the β-globin gene result in alteration of splicing.[30] Well known splicing mutations are located in exon 1, intron 1 and intron 2 of the β-globin gene.[31-33] A well-known point-mutation in intron 2 at position 705, called IVS2-705, activates aberrant splice sites and therefore leads to retention of intron parts in the β-globin mRNA.[30, 33]

Cystic fibrosis is a recessive severe pulmonary and pancreatic disease caused by mutations in the cystic fibrosis transmembrane conductance regulator (CFTR) gene. The CFTR is important for functionality of the cAMP-dependent transmembrane chloride channel that is expressed in secretory epithelium.[34] Approximately 12% of all reported CFTR mutations can be categorized as splicing mutations affecting cis-elements. More than 200 CFTR splice variants could be identified.[35]

Hutchinson-Gilford progeria syndrome (HGPS) is a rare genetic disease leading to noticeable accelerated ageing, postnatal growth retardation, atherosclerosis, and bone dysplasia.[36, 37] The mutated gene is LMNA, which serves as the blueprint for two distinct protein isoforms: prelamin A and lamin C. A point mutation (C→T) in exon 11 enhances recognition of a suboptimal donor splice site leading to a partial exon exclusion. This deletion creates a cryptic splice site that leads to expression of mutated prelamin A, called progerin. Progerin can not be processed and converted into mature lamin A due to the

absence of the proteolytic cleavage site.[38] This results in anchoring of progerin to the nuclear membrane which results in weakening cell growth.[34, 39-41]

Tautopathies, including Morbus Alzheimer, Parkinsonism, and frontotemporal dementia, are progressive neurodegenerative diseases caused by an abnormal ratio of microtubule associated protein tau (MAPT or tau) isoforms.[42] During brain maturation, six different tau isoforms are generated. Especially, mutations in exon 10 of the *MAPT* gene alter the relative ratio of isoform 3R and 4R with three or four tandem repeats of the microtubule-binding domain, respectively. This imbalance indirectly alters the hydrophilicity and unfolded structure of tau, leading to the misfolding and aggregation of tau polymers, which then form intracellular filaments.[43, 44]

Abnormalities in splicing have been shown to influence uncontrolled cell proliferation, cell migration which promote cancer development. In addition, the development of cancer is facilitated by resulting methylation changes and resistance to apoptosis, and chemotherapeutics. In this context, mutations effecting splice sites or spliceosomes contribute to tumorgenesis by inducing production of splice isoforms that enhance cancer progression.[45-49]

Beside these diseases, aberrant splicing can play a major role in pathogenesis of Duchenne muscular dystrophy (DMD)[50-55], retinitis pigmentosa[56], autism spectrum disorder[57-60], amyotrophic later sclerosis (ALS)[61], schizophrenia[62-64], and congenital myasthenic syndrome[65].[34, 41, 66] It is also related to infection, inflammation, and immune and metabolic disorders.[64, 67, 68]

As the mentioned exemplary diseases show: mutations affecting splicing processes can cause severe disorders. These disorders can be tackled at their source by targeting mRNA and influencing splicing.

1.2 Molecular Therapeutics – Tackle Diseases at its Source

In order to address a specific disease at its roots, knowledge of origin and mechanism of each disease, as well as genomic irregularities and resulting aberrations in gene expression must be acquired. The identification and biochemical characterization of the genome and genes began with the Human Genome Project, which provided the required

information.[2, 69] The knowledge about aberrant mechanisms of genetic diseases enabled development of biomedical research and led to molecular therapeutics. These molecular therapeutics offer the possibility of not only causal but also preventive treatment at the genomic level of severe and life-threatening diseases. Not only endogenous genetic defects but also viral infections and cancer could be medical indications.[70-77]

Before treating diseases at its roots, the classic way of treatment was modulation at the end of defective signaling pathways. Enzyme inhibition, metabolite supplementation, and interference in signal pathways were at common use. Another treatment approach was substitution of defective genes or introduction of new gene templates in plasmid (pDNA) and messenger RNA (mRNA) delivered by viral vectors.[70] An alternative way of therapy is to target the blueprint of all downstream activities by diverse modulations at the stage of mRNA biosynthesis and subsequent step of translation. RNA interference, single-stranded antisense-oligodeoxynucleotides (ODNs), genome editing via e.g. RNA-guided CRISPR/Cas9 system, and alternative splicing are ways to reach the target effect.[70, 78] The potential of molecular therapeutics can be also seen in increasing number of clinical trials of these approaches and approved products on the market.[72, 79-92] To translate potential therapeutics to clinical settings, important considerations must be taken into account. The product must exhibit sufficient stability, high transfection efficiency and good biocompatibility. In clinical gene therapy trials, predominantly viral vectors can be found.[72] The minority is carried out with non-viral formulations with a more simple and straight-forward system by using naked and chemically modified nucleic acids.[82, 84, 90, 93, 94] In addition to unsophisticated formulations, more complex carriers are used like lipid nanoparticles (LNPs) which showed their benefits especially as mRNA vaccine during the SARS-CoV-2 pandemic.[95] Moreover, LNPs encapsulating small-interfering RNAs reached the marked[83] and Cas9 mRNA LNPs could be used successfully in a clinical trial to achieve genetic correction *in vivo* in patients by CRISPR/Cas9/sgRNA[96]. Furthermore, the progress in this field is evident with the recent approval of Casgevy by the end of 2023. Casgevy is a genome-edited cellular therapy which was developed to treat sickle-cell disease and β-thalassemia. The therapy consists in transplanting hematopoietic stem cells which previously were edited by CRISPR/Cas9.[97, 98]

Additional, the group of antisense oligonucleotides (ASOs) can be used to specifically target splicing mechanism in mRNA processing. By using ASO, the splicing pattern is modified and consequently expression of a functional gene is restored. Since several acquired and inherited diseases are caused by genomic mutations leading to splicing aberrations, the approach of splicing modulation is a promising way to treat these kind of diseases.[99-101]

Antisense oligonucleotides as therapeutics

With the first reference of antisense oligonucleotides (ASOs) in 1978[102], the promising journey of an efficient tool for gene expression regulation started. The size of therapeutic ASOs is 15 – 30 nucleotides, which bind to complementary mRNA sequences. For the use of ASOs as a therapeutic tool, a more detailed understanding of their molecular mechanisms and the establishment of sufficient and safe delivery systems are required.

The focus of this chapter is on a specific group of ASOs that modulate pre-mRNA splicing termed splice switching oligonucleotides (SSOs). SSOs induce specific exclusion or inclusion of one or more exons.[37, 103, 104] If a carrier system is to be used to deliver SSOs, three main obstacles must be overcome: First, the intracellularly delivered amount of SSOs must be sufficient to induce a splice-switching effect. Secondly, a favorable pharmacokinetic profile has to be provided, featuring high stability of the carrier system and a low toxicity profile. And third, high specificity of the delivery has to be guaranteed to reduce off-target effects.[93, 105]

SSOs are artificial redesigns of natural nucleic acids that bind to pre-mRNA complementarily, generating a steric block that masks recognition sites for splicing factors. The altered recognition leads to alternative splicing patterns meaning inactivation or reactivation of splice sites.[101] Since SSOs are synthetic molecules, chemical modifications can be integrated during synthesis. These modifications can improve resistance against RNase H and general enzymatic degradation, therefore increases serum stability.[106, 107] To enable transfer to *in vivo* applications, an improved affinity of SSOs to pre-mRNA and a low immunogenicity have to be ensured.[49] In order to meet the requirements, chemical modifications of I) the phosphate backbone and II) carbohydrates can be implemented.

I) Alteration of phosphate backbone

The linker structure connecting nucleosides provides possibilities for modifications. The first reported improvement of SSOs was the transition from phosphodiester to the more stable phosphorothioate (PS) element. Another group of linker modified ASOs are phosphorodiamidate morpholino oligomers (PMOs) where bases are bound to morpholine rings. The modified morpholine containing nucleosides are linked through uncharged phosphorodiamidate groups. With these modifications, PMOs already showed promising efficacies in treatments of genetic diseases.[85-92, 106, 108] With their uncharged backbone and substituted carbohydrate, PMOs not only combine carbohydrate and backbone modification but also meet the requirements of resistance to enzymatic degradation, sequence specificity, lack of off-target effects and immunogenicity which are crucial for therapeutic antisense splice switching activity.[106, 108, 109] A critical hindrance of PMOs in therapeutic applications is one of their key benefits. The uncharged character of the PMO backbone limits delivery system approaches based on electrostatic interactions resulting in still insufficient intracellular PMO amounts *in vivo*. Additionally, PMOs exhibit minimal interactions with plasma proteins and therefore are rapidly excreted via the kidneys.[93]

II) Modifications of the carbohydrate

Several derivatives were developed showing a high stability and affinity to the target pre-mRNA. In particular, the 2'-hydrogen of ribose is a common position for modification with various residues: 2'-O-methyl (OMe) and 2'-methoxyethyl (MOE) or 2'-O-aminopropyl (AP), and 2'-fluoro (F) were used to generate general nuclease resistance and higher binding affinities to pre-mRNA.[110-112] These SSOs have the potential to be used in therapy against Alzheimer's disease[113], spinal muscular atrophy (SMA)[114], Duchenne muscular dystrophy (DMD)[115, 116], Huntington disease[117], hypercholesterolemia[118], and various types of cancer[49, 119]. Another possibility for modifying the carbohydrate element is to work with locked nucleic acid (LNA) oligomers, where the 1' oxygen is linked to the 4' carbon of ribose via a methylene bridge. This bridge locks the carbohydrate to 3'-endoconformation, thereby reducing the conformational flexibility of the ribose. The rigidity of LNAs increases binding affinity, as reflected by an increasing melting

temperature of approximately 5 °C per base. and additionally provides nuclease resistance.[120]

Beside that, peptide bonds can be used for the linkage of the nucleosides and substitute carbohydrates resulting in peptide nucleic acids (PNAs) with a polyamide backbone.[121, 122]

Different types of modification can be seen in **Figure 5**.

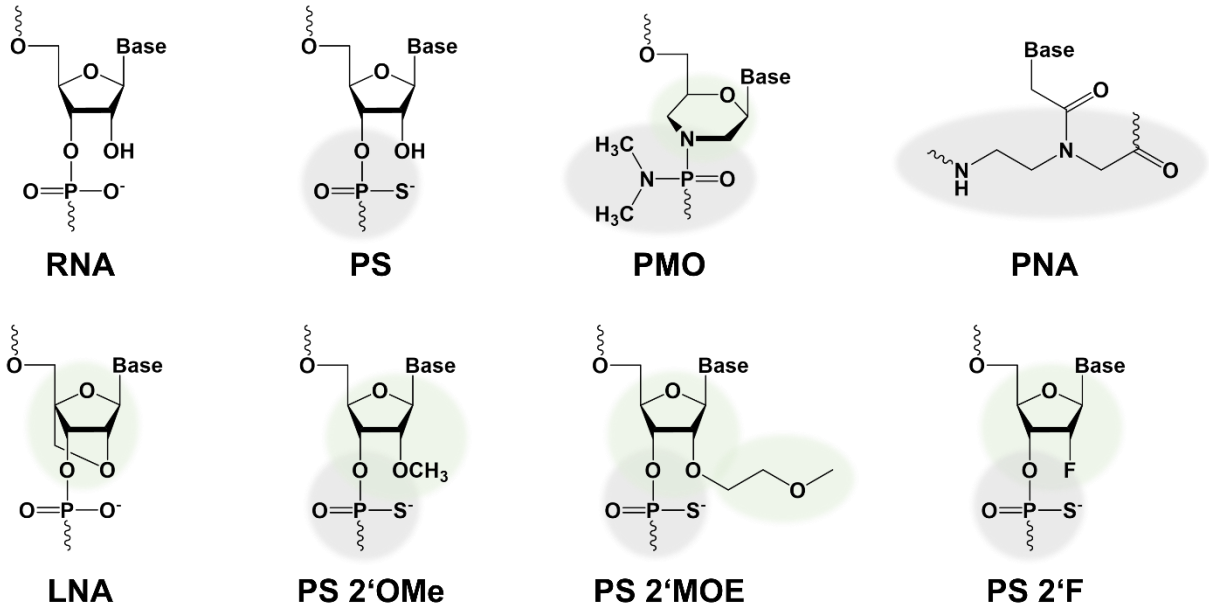

Figure 5 Schematic structures of different oligonucleotide analogues. RNA: Ribonucleic acid; PS: Phosphorothioate RNA; PMO: Phosphorodiamidate morpholino oligomer; PNA: Peptide nucleic acid, LNA: Locked-nucleic acid, PS 2'OMe: Phosphorothioate, 2'-O-methyl; PS 2'MOE: Phosphorothioate 2'-methoxyethyl; PS 2'F: Phosphorothioate 2'-fluoro. Grey: backbone alteration; green: carbohydrate modification.

Among others, two examples of SSOs approved by the FDA used for therapeutic treatments are nusinersen and eteplirsen.[84, 87, 114, 123]

Nusinersen (Spinraza™, Ionis Pharmaceuticals) is a PS 2'MOE (phosphorothioate with a methoxyethyl modification at the 2' position of the carbohydrate) used in order to treat the autosomal recessive disease spinal muscular atrophy (SMA). SMA is caused by mutations in the *survival motor neuro 1* (SMN1) gene.[124-127] This mutation leads to loss of function of SMN1 protein resulting in degradation of motor neurons, denervation, and muscle atrophy.[124, 125, 127]. Beside SMN1, the nearly identical SMN2 gene is present in the genome. *SMN1* and *SMN2* differ only in one single nucleotide, resulting in exon 7 exclusion in SMN2, leading to rapid degradation of the nonfunctional SMN2 RNA transcript.

Nusinersen targets the intronic splicing silencer N1 of SMN2, causing inclusion of exon 7 and resulting in functional SMN protein expression.[84, 114, 128]

Eteplirsen (Exondys 51™, Sarepta Therapeutics Inc.) is a therapeutic PMO against the severe x-linked recessive neuromuscular disorder Duchenne muscular dystrophy (DMD). DMD is caused by various mutations in the *dystrophin* (*DMD*) gene. DMD physiologically serves as membrane associated protein linking extracellular matrix with cytoskeletal actin and therefore stabilizes the muscle during muscle contractions. It is known that various mutations in the DMD gene either introduce stop codons or disrupt the reading frame. The mutation hotspot of the DMD gene reaches from exon 2-22 and 45 to 55.[55, 129] One frequently mutated exon is exon 51, leading to the inclusion of defective exon in approximately 13% of DMD patients. The frequency of defective exon 51 makes exon 51 a convenient target. Eteplirsen specifically targets a binding site near the junction between exon 51 and intron 51, causing exon 51 skipping and leading to restoration of the reading frame.[130] The resulting dystrophin-like protein is shorter, but still functional.[84, 87, 123, 128, 131, 132]

Another example for the potential of therapeutic ASOs is the development of milasen.[133] Milasen is a phosphorothioate oligomer with a 2'MOE modifications developed within one year for the 6-year-old patient Mila suffering from neuronal ceroid lipofuscinosis 7 (CLN7). CLN7 is a form of the rare and fatal neurodegenerative Batten's disease caused by a novel mutation.[133-135] Within only one year, the specific mutation in Mila's genome and the splice defect could be identified, the ASO sequence could be generated and validated, a toxicological study in rats, and the first application could be conducted. Even though the treatment with Milasen stabilized her condition, the disease was too far progressed by the time Mila was treated. Mila passed away in February 2021. However, Mila's personalized treatment showed the potential of further development in personalized medicine.[136] Among others, the customizable sequence of ASOs made it possible to design a highly adjusted ASO required for this "N-of-1" study.[133, 137, 138]

Additional ASO therapeutic on the market can be seen in the following table.

Table 1 Overview of approved antisense oligonucleotide-based therapeutics

Name, year of approval	Structural motifs	Medical indication
Vitravene® (fomivirsen)[139-142], 1998 Not longer on the market[143]	21-mer ASO, PS DNA	CMV retinitis
Kynamro® (mipomersen)[144-146], 2013	20-mer gapmer ASO, PS, 2'-O-MOE/2'-H	homozygous familial hypercholesterolemia
Exondys 51® (eteplirsen)[87, 109, 131], 2016	30-mer SSO, PMO, splicing modification (exon skipping)	Duchenne muscular dystrophy (DMD) skipping of exon 51
Vyondys 53® (golodirsen)[94, 109], 2019	25-mer SSO, PMO, splicing modification (exon skipping)	Duchenne muscular dystrophy (DMD) skipping of exon 53
Spinraza® (nusinersen)[147, 148], 2016	18-mer SSO, PS, 2'-O-MOE, splicing modification (exon inclusion)	spinal muscular atrophy
Tegsedi® (inotersen)[149, 150], 2018	20-mer gapmer ASO, PS, 2'O-MOE/2'-H	polyneuropathy of hereditary transthyretin-mediated amyloidosis (hATTR)
Waylivra® (volanesorsen)[151], 2019	20-mer gapmer ASO, PS, 2'-O-MOE/2'-H	familial chylomicronemia syndrome
Viltepso® (viltolarsen)[152], 2020	21-mer SSO, PMO, splicing modification (exon skipping)	Duchenne muscular dystrophy (DMD) skipping of exon 53
Amondys45® (casimersen)[153], 2021	22-mer SSO, PMO, splicing modification (exon skipping)	Duchenne muscular dystrophy (DMD) skipping of exon 45

1.3 Nucleic Acid Therapeutics and their Delivery

For efficient therapies using molecular therapeutics, intracellular delivery of sufficient amounts of therapeutic is necessary. The cellular uptake and intracellular fate, including endosomal escape, of unmodified macromolecules are determined by their limited biological stability, large size, and, in some cases, negative charge.[70] Irrespective of theoretical efficacy of the potential molecular therapeutics, the bottleneck for translation

into clinics and their therapeutic efficacy lies in the efficiency of their delivery. Hence, development of an efficient delivery system is important for molecular therapeutics in order to stabilize and protect the cargo and enable delivery to the target site. During development of carrier systems, considerations have to be taken into account regarding specific cargo properties, typical properties of the target tissue, intracellular target site and molecule, as well as the biochemical target mechanism.[154, 155]

Nucleic acid carriers can be roughly divided into viral and non-viral vectors. In 1972, the first viral vector expressing a foreign gene was generated.[156, 157] Since then, various viruses were adapted to serve as vectors. However, viral vectors have limitations such as a low capacity, challenges in large-scale virus production, potential immune response, and the risk of insertional mutagenesis.[158] Synthetic non-viral vectors are more flexible regarding their properties which can be adjusted and optimized considering cargo properties, toxicity, and immunogenicity.[159] These highly flexible synthetic systems are prone to be more promising regarding molecular therapeutic delivery, particularly for ASOs and SSOs.[160]

After application, therapeutic formulations have to face various obstacles, such as rapid clearance after systemic administration, enzymatic degradation and immune response in biological fluids, target cell penetration, and intracellular release including delivery to the intracellular target.[161] To address these hindrances, high flexibility of the artificial carrier synthesis is advantageous. Beside chemical modification of the nucleic acid itself, conjugation to carrier molecules[162] or supramolecular assembly into nanoparticles improve the stability and pharmacokinetic profile of the therapeutic formulation. The multidimensional nature of the delivery process can be divided into cellular uptake, and intracellular delivery and distribution. Each passage requires its own formulation demands, making it important to develop biodynamic flexibility in the carrier systems. Requirements for cellular uptake can differ in size, polydispersity, shape, surface charge, and surface hydrophobicity and hydrophilicity. These characteristics have an influence on interactions with serum proteins, impacting particle stability and identity due to emerging protein corona.[163, 164] The interaction with cell membranes is another important interaction of nanoparticles since majority of cellular uptake happens via endocytosis.

Carrier and cargo properties, as well as target cell type, influence the type of active endocytotic uptake mechanisms that take place.[165, 166]

Nonspecific interaction of positively charged delivery system with negatively charged cell surfaces leads, on one hand, to enhanced cellular uptake. On the other hand, increased surface tension of cell membranes caused by positively charged delivery systems and the resulting pore formation lead to higher cytotoxicity.[167-169] Hydrophobicity and interfacial forces between carrier systems and cell membranes enhance lipid membrane interactions.[170, 171] The requirements for the intracellular environment differ from cellular uptake since the cargo has to be released from the carrier system and continues its way to its intracellular destination. Entering the cell, encapsulated cargo usually is entrapped in vesicles or endosomes.[172] During several maturation steps, early endosomes get acidified and lysosomal enzymes are recruited which form a degrading environment. The escape from the endolysosomal compartment is a crucial step toward reaching the intracellular target site and is achieved via membrane disturbance.[173] One mechanism hypothesized to accomplish disintegration of the endosomal membrane is the so-called proton sponge effect of the endosomes using protonatable positively charged carriers, as first described by Jean-Paul Behr.[174, 175] The mechanism of the proton sponge effect was previously described as follows. Entrapped carrier formulations feature a specific buffering capacity through protonation of amino groups integrated into the carrier, leading to proton accumulation, followed by chloride influx into the endosomal lumen. Due to internal salt excess, the endosomes start to swell under osmotic pressure leading to membrane rupture.[174]

With proceeding investigation of the proton sponge effect and endosomal escape, another mechanism has come into focus, which is considered to be more likely to be involved in the endosomal escape by positively charged carrier systems. During maturation of endosomes, protonatable carrier systems get progressively protonated, leading to interactions with endosomal membranes that further lead to hydrophilic pore formation. These interactions are prone to destabilize lipid bilayers.[176-179]

After delivery of the carrier system into the cytoplasm, the intracellular transfer to the site of action continues with release of the cargo from the delivery system. Requirements for

extra- and intracellular delivery differ from each other regarding particle stability which means the design of carrier systems must be a compromise of stable extracellular assembly and intracellular disassembly. This balance of design ensures specific cargo release at the target intracellular region. In order to advance delivery to a specific target site, targeting approaches can be carried out by tagging the carrier system with specific localization tags like nuclear localization signal (NLS) peptides.[180]

As requirements for delivery of macromolecules are manifold, and carrier designs have to be flexible and adjustable, several approaches were investigated in the past in order to enhance intracellular delivery of macromolecules. Conjugations, complexations and inclusions with and in cationic polymers,[162, 181-184], peptides,[185, 186] proteins,[187] lipids,[188, 189] liposomes,[190-192] LNPs[193-197], and membrane translocating peptides[198] were studied. With increasing knowledge about the relationship between physicochemical properties and biological behavior, it is possible to achieve new and improved designs of carriers, in order to increase activity and decrease toxicity of the carrier systems.

Non-Viral Delivery Systems for Uncharged Nucleic Acids

Even though highly promising nucleic acid therapeutics indicate potential in antisense therapy within various clinical trials[199, 200], achieving sufficient amounts of ASO at the intracellular target site and ensure safe delivery strategies are the current bottlenecks. Especially, uncharged SSOs, such as PNAs and PMOs, with their beneficial properties, indicate high potential as antisense therapeutics that can be administered systemically without any modifications, conjugations, or formulations.[201] However, delivery of unformulated SSOs in sufficient amounts to the intracellular target site is insufficient since free SSOs are rapidly excreted after systemic administration and poorly taken up into cells.[202, 203] Promising efficacies of uncharged SSOs are limited by their delivery showing the importance of development of suitable carrier systems. A key requirement for the carrier system used for delivery of SSOs is an improvement in tissue-specific delivery, increased potency in lower doses and a reduction of off-target effects and toxicity. In contrast to natural or other negatively charged nucleic acids, uncharged nucleic acids can not be complexed by positively charged carrier systems. In order to formulate ASOs independent from ionic charges, strategies with covalent modifications, such as

conjugation to targeting ligands or carrier systems, and nanoparticle-based approaches, meaning incorporation into drug delivery systems were developed. So far, different strategies for delivery improvement based on cell penetrating peptides (CPPs) have been established.[204-208] Additionally, guanidine dendrimers[209], cationic backbones[210], and lipidic modifications[211] have been used to enhance delivery efficiency.

The focus of this work was on the highly promising PMOs which already showed encouraging *in vivo* transfection efficiencies with several delivery approaches. Especially, the strategy of covalently conjugated CPPs to PMOs showed striking results in pre-clinical DMD and SMA mouse models.[186, 212-214] The mechanism of delivery via CPPs is a subject of controversial discussion. Initially, the assumption of direct translocation across cell membranes was made, but also it was stated that the positively charged CPPs interact with the negatively charged cell surface, which leads to the initiation of endocytic pathways[215-222] Even though PMO–CPP conjugates yielded remarkable results *in vivo*, CPPs show fast enzymatic degradation in biological fluids, insufficient endosomal escape, endosomal entrapment, and high toxicity.

Since investigation of disease origins continues and gained knowledge about the pathophysiological mechanism improves, several potential target sites for SSOs were identified.[101, 103, 223] Combination of pathogenetic knowledge and insights regarding delivery system designs would lead the structural group of SSOs a big step forward toward being established SSO-based therapeutics.

1.4 Sequence-Defined Oligo(ethylenamino) Amide Xenopeptides

Sequence-defined oligomers bearing an oligo(ethylenamino) amide backbone demonstrated potential in delivery of various therapeutic cargos, such as nucleic acids[162, 183, 224-228], proteins[182, 189], and drugs[229, 230]. The artificial xenopeptides (XPs) are composed of a collection of building blocks with different characteristics. Natural α-amino acids, artificial oligoamino acids, and hydrophobic fatty acids are present in XPs in different combinations. The group of XPs can be divided into 2-arm[231], 3-arm[224], 4-arm[232, 233], comb architecture[234], T-shaped[162, 183, 224] based on their different topologies. Using the synthesis method of combinatorial solid-phase peptide synthesis makes it possible to generate peptides with defined sequences.[235] The combinatorial synthesis technique enables

customized optimization to meet requirements of each cargo and the delivery target tissue and site (**Figure 6**). Oligomers consist of several different components with different properties to fine-tune the total oligomer characteristics. Protonatable building blocks, such as the artificial oligoamino acid succinyl-tetraethylenpentamine (Stp), contain several protonatable amines, which are partially protonated at physiological pH. The positively charged oligoamino acid enables complexation of negatively charged cargos such as nucleic acids which leads to nanoparticle formation. The favorable buffer capacity of Stp facilitates endosomal escape through ionization to overcome endosomal entrapment.[181, 236] Additional to artificial amino acids, natural amino acids are used to include more features. Terminal cysteines improve stability of the nanoparticles through crosslinking disulfide bonds.[236] Histidine improves the required endosomal buffering capacity to enable endosomal escape.[237] Another stabilizing effect can be included by introducing tyrosine tripeptide motifs that increase cargo incorporation and complex stabilization via π-stacking effect.[238] An additional important component is the fatty acid domain which not only stabilizes the delivery system via hydrophobic interactions, but also promotes lytic membrane interactions, which can lead to enhanced intracellular delivery.[239] An alternative approach to fine-tune the delivery system's bioactivity is modification of the hydrocarbon moieties or use of ionizable lipo amino fatty acids (LAFs).[162, 184, 240]

The topology which was used in this study was the T-shape, consisting of a backbone composed of natural, and artificial amino acids, and fatty acid domains at a branching point. The established topology of T-shapes could already successfully enable delivery of different therapeutic molecules.[162, 171, 229, 238, 241, 242]

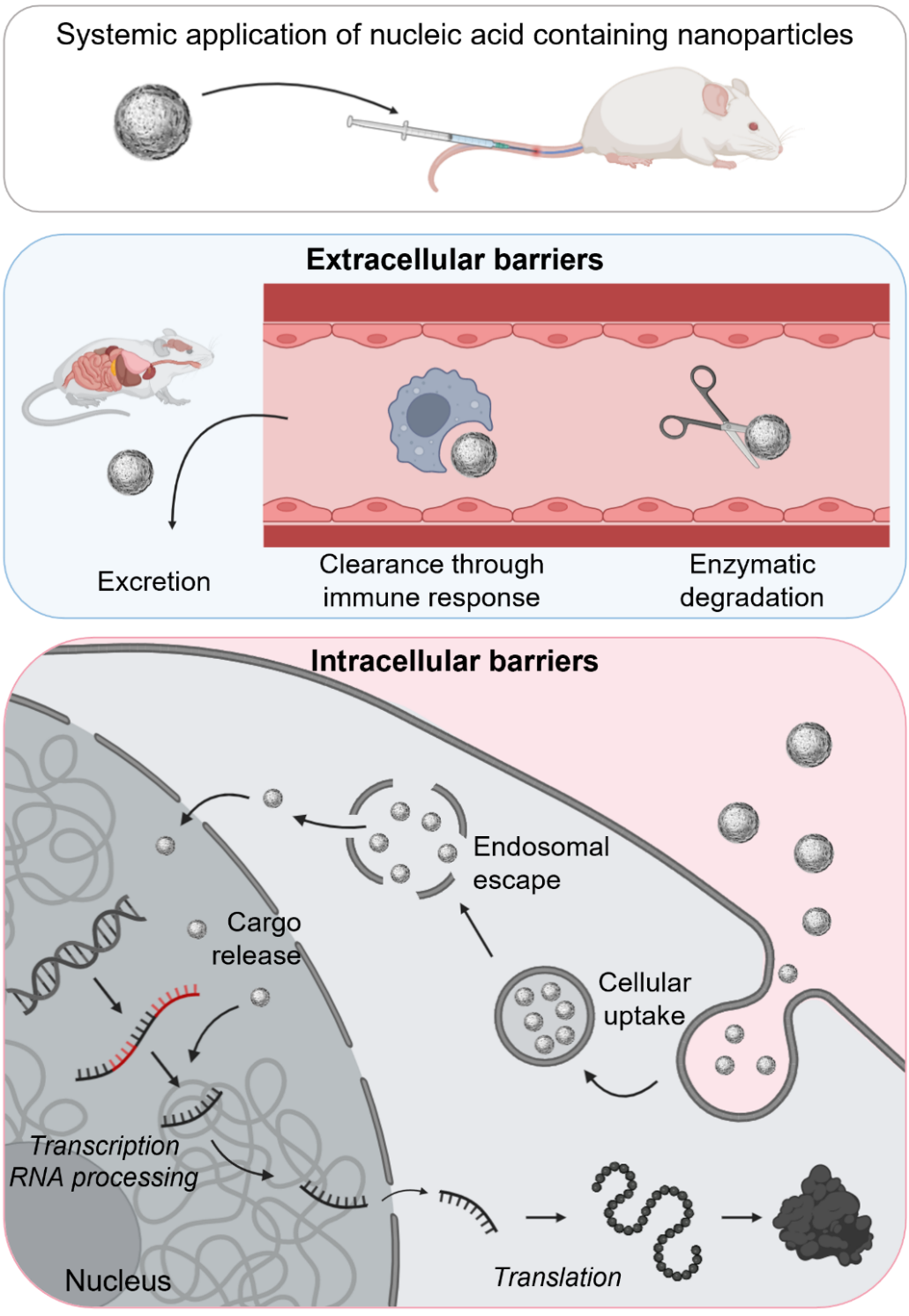

Figure 6 Extracellular and intracellular delivery barriers. After systemic application of nanoparticulate SSO formulations several different barriers have to be faced. Nonspecific biodistribution, fast excretion, clearance through immune cells, and enzymatic degradation are only a few of extracellular barriers. After reaching the cell, several cellular and intracellular barriers have to be managed. The first hurdle is the cellular uptake which is followed by endosomal escape to avoid degradation of the SSO cargo. Another critical requirement is the release of cargo from the formulation and reaching the target site in the nucleus. Figure was created using Biorender.com.

1.5 Aim of the Thesis

Therapy with artificial antisense oligonucleotides, focusing especially on splice switching oligonucleotides (SSOs), is a growing field with broad range of potential indications. Nonetheless, delivery of sufficient intracellular drug amounts is still limited. Due to the sequence specificity of SSOs, pre-evaluation *in vitro* requires a suitable test system to find a preselection for *in vivo* trials. Additionally, traditional *in vitro* reporter systems for PMOs rely on PMO sequences that can not be directly transferred into healthy *in vivo* systems.

The first aim of the thesis was the development and establishment of a new positive-read out system which can be used for splice switching oligomers (SSOs). The design of the system is based on PMO(Ex23) which induces DMD exon 23 skipping in wild-type or mdx mice. For this purpose, the mCherry-DMDEx23 reporter gene had to be designed and integrated stably into the genome of cells resulting in mCherry-DMDEx23 expressing cells which could be cultivated in cell culture. Molecular biological investigations of the stable HeLa mCherry-DMDEx23 had to be conducted in order to confirm that the mechanism of action is based on exon skipping. In addition, sequence specificity of the reporter had to be examined by using PMO(Ex23) and a PMO negative control. The establishment of a functional HeLa mCherry-DMDEx23 platform aimed at the generation of a screening platform enabling an in *vitro*-*in vivo* workflow which facilitates evaluation of PMO(Ex23) carriers without change of PMO sequences.

The second aim was identification of potent carriers for PMO delivery based on amphiphilic, ionizable XPs *in vitro* with subsequent confirmation *in vivo.*

2. Materials and Methods

This chapter has been adapted from:

Lessl AL, Pöhmerer J, Lin Y, Wilk U, Höhn M, Hörterer E, Wagner E, Lächelt U. mCherry on Top: A Positive Read-Out Cellular Platform for Screening DMD Exon Skipping Xenopeptide-PMO Conjugates. Bioconjugate Chemistry 2023 Nov 22.

DOI: 10.1021/acs.bioconjchem.3c00408

2.1 Materials

2.1.1 Solvents and Reagents

The following table summarizes the used solvents and reagents and the source of supply including their unique CAS number. For all experiments solvents and reagents were used in high quality.

Table 2 Chemicals and solvents in alphabetical order

Solvents and reagents	CAS number	Supplier
1-Hydroxybenzotriazole (HOBt)	123333-53-9	Sigma-Aldrich, Munich, Germany
2-Chlorotritylchloride resin	934816-82-7	Iris Biotech, Marktredwitz, Germany
Acetonitrile (ACN)	75-05-8	VWR Int., Darmstadt, Germany
Agar	9002-18-0	Th.Geyer, Renningen, Germany
Agarose	9012-36-6	Sigma-Aldrich, Munich, Germany
Ampicilin	69-53-4	Sigma-Aldrich, Munich, Germany
Bacto™ Tryptone	-	Th.Geyer, Renningen, Germany
Cell culture lysis buffer	-	Promega, Mannheim, Germany
Collagen A	9007-34-5	Biochrom, Germany
DAPI'(4',6-Diamidino-2-phenylindol)	28718-90-3	Sigma-Aldrich, Munich, Germany
DBCO-NHS ester (Dibenzocyclooctyne-N-hydroxysuccinimidyl ester)	-	Sigma-Aldrich, Munich, Germany
Dichloromethane	75-09-2	Bernd Kraft, Duisburg, Germany
Dimethyl sulfoxide (water free)	67-68-5	Sigma-Aldrich, Munich, Germany
Di-tert-butyl dicarbonate	24424-99-5	Sigma-Aldrich, Munich, Germany
D-luciferin sodium	103404-75-7	Promega, Mannheim, Germany
EDTA disodium salt dihydrate	6381-92-6	Sigma-Aldrich, Munich, Germany
Ethanol absolute	64-17-5	VWR Int., Darmstadt, Germany
Fetal bovine serum	-	Sigma-Aldrich, Munich, Germany

Fmoc-L-Gly-OH	29022-11-5	Iris Biotech, Marktredwitz, Germany
Fmoc-L-Lys(Dde)-OH	150629-67-7	Iris Biotech, Marktredwitz, Germany
Fmoc-L-Lys(Fmoc)-OH	78081-87-5	Iris Biotech, Marktredwitz, Germany
Fmoc-L-Lys(N_3)-OH	159610-89-6	Iris Biotech, Marktredwitz, Germany
Fmoc-L-Tyrosin(But)	71989-38-3	Iris Biotech, Marktredwitz, Germany
Fmoc-Stp(Boc3)-OH building block[235]	1268832-60-5	In-house synthesis
Gelred®	-	Sigma-Aldrich, Munich, Germany
HEPES	7365-45-9	Biomol, Hamburg, Germany
HBTU (Hexafluorophosphate)	94790-37-1	Multisyntech, Witten, Germany
Hydrazine monohydrate	7803-57-8	Sigma-Aldrich, Munich, Germany
Hydrochloric acid solution (1 M) (1 M HCl)	7647-01-0	Bernd Kraft, Duisburg, Germany
Isopropanol	67-63-0	Merck, Darmstadt, Germany
Linolenic acid (LenA)	463-40-1	Sigma-Aldrich, Munich, Germany
Lipofectamine™ 3000	-	ThermoFisher Scientific, Schwerte, Germany
Methanol	67-56-1	Iris Biotech, Marktredwitz, Germany
Methyl tert-butyl ether (MTBE)	1634-04-4	Brenntag GmbH, Essen, Germany
Millipore water	-	In-house purification
N,N-Diisopropylethylamine (DIPEA)	7087-68-5	Iris Biotech, Marktredwitz, Germany
N,N-Dimethylformamide (DMF)	68-12-2	Iris Biotech, Marktredwitz, Germany
N-hexane	110-54-3	Grüssing GmbH, Filsum, Germany
Ninhydrin	485-47-2	Sigma-Aldrich, Munich, Germany
N-Methyl-2-pyrrolidone (NMP)	872-50-4	Iris Biotech, Marktredwitz, Germany
n-octanol	111-87-5	Sigma-Aldrich, Munich, Germany
Nuclease-free water	-	Sigma-Aldrich, Munich, Germany
Paraformaldehyde (PFA)	50-00-0	Sigma-Aldrich, Munich, Germany
Penicillin/Streptomycin	-	Life Technologies, Carlsbad, USA
peqGold 1KB DNA ladder	-	VWR Int., Darmstadt, Germany
Phenol	108-95-2	Sigma-Aldrich, Munich, Germany
Piperidine	110-89-4	Iris Biotech, Marktredwitz, Germany
Potassium cyanide (KCN)	151-50-8	Sigma-Aldrich, Munich, Germany
Pybop® (Benzotriazol-1-yl-oxy tripyrrolidinophosphonium hexafluorophosphate)	128625-52-5	Multisyntech, Witten, Germany
Rhodamine phalloidin	219920-04-4	Life Technologies, Carlsbad, USA
Sephadex® G-10	9050-68-4	GE Healthcare, Freiburg, Germany
Sodium Acetate	S-5889	Sigma-Aldrich, Munich, Germany
Sodium chloride	7647-14-5	Sigma-Aldrich, Munich, Germany
Trifluoro acetic acid (TFA)	76-05-1	Iris Biotech, Marktredwitz, Germany

Triisopropylsilane (TIS)	6485-79-6	Sigma-Aldrich, Munich, Germany
Trypsin/EDTA	-	PAN Biotech GmbH, Aidenbach, Germany
Yeast Extract	-	PanReac AppliChem, Darmstadt Germany,

2.1.2 Buffers

Table 3 Buffers used for experimental procedures

Buffer	**Composition**
Agarose electrophoresis loading buffer	3 mL glycerine, 1.2 mL 0.5 M EDTA solution (pH 8.0), 2.8 mL H2O, 10 mg bromophenol blue
HBG	20 mM HEPES, 5% glucose, pH 7.4
LAR buffer	20 mM glycylglycine; 1 mM MgCl2; 0.1 mM EDTA; 3.3 mM DTT; 0.55 mM ATP; 0.27mM coenzyme A, pH 8–8.5
LB liquid media	1% bacto-trypton, 0.5% yeast extract, 0.5% sodium chloride
LB solid media	1% bacto-trypton, 0.5% yeast extract, 0.5% sodium chloride, 1.5% agar
PBS buffer	136.9 M NaCl, 2.68 M KCl, 8.1 M Na_2HPO_4, 1.47 M KH_2PO_4
10× TBE buffer	89 mM Trizma® base, 89 mM boric acid, 2 mM EDTA-Na2
10× NET gelatine	25g gelatina alba 1000 mL 10× NET (1.5 M NaCl, 0.05% EDTA (pH 8.0), 0.5 M Tris (pH 7.5), 0.5% Triton-X-100)

2.1.3 Kits

Table 4 Commercial kits used for experimental procedures

Kit	**Catalog number**	**Supplier**
qScript cDNA Synthesis Kit	95047	Quantabio, Beverly. Massachusetts, USA
QIAprep Spin Miniprep Kit	27106	Qiagen, Hilden, Germany
Qiagen Plasmid Maxi Prep	12163	Qiagen, Hilden, Germany
QIAquick PCR Purification Kit	28104	Qiagen, Hilden, Germany
QIAquick Gel Extraction Kit	28704	Qiagen, Hilden, Germany

2.1.3 Equipment for Solid-Phase Peptide Synthesis (SPPS)

Automated synthesis of the XP backbones was performed using a Biotage Syro Wave (Biotage AB, Uppsala, Sweden) peptide synthesizer. Disposable polypropylene (PP) syringe microreactors with the size of 10 mL purchased from Multisyntech (Witten, Germany) were used. Manual solid-phase synthesis was carried out using microreactors with polyethylene filters. The automated synthesis with the Biotage Syro Wave synthesizer was conducted with polytetrafluoroethylene (PTFE) filters. The size of the reactors was chosen according to resin amount. Manual reactions were carried out under steady shaking using an overhead shaker.

2.1.4 Proteins

Table 5 Proteins used for experimental procedures

Protein	Catalog number	Supplier
XmaI	R0180S	New England Biolabs, Ipswich, USA
NotI-HF	R3189S	New England Biolabs, Ipswich, USA
NdeI	R0111S	New England Biolabs, Ipswich, USA
Taq DNA polymerase	M0273X	New England Biolabs, Ipswich, USA
T4 DNA ligase	M0202S	New England Biolabs, Ipswich, USA
Anti-mCherry rabbit polyclonal antibody	#26765-1-AP	proteintech, Manchester, UK
IRDye 680RD Goat anti-rabbit	926-68071	Li-Cor, Lincoln, USA

2.1.5 Nucleic Acids

2.1.5.1 PMOs

Table 6 Phosphorodiamidate morpholine oligomers used for experimental procedures

PMO	Target	PMO Sequence	Modifications
PMO(705)	G point mutation at position 705 in intron 2 of the human β-globin gene (IVS2-705)	CCTCTTACCTCAGTTACAATTTATA	- Functionalization of 3'-end with DBCO - Functionalization of 3'-end with DBCO and 5'-end with AF647

PMO(Ex23)	Donor splice site of DMD intro 23	GGCCAAACCTCGGCTTACCTGAAAT	- Functionalization of 3' -end with DBCO

PMOs were purchased from Gene Tools, LLC (Philomath, USA) and contained a 3'-primary amine (PMO–NH_2) for DBCO functionalization.

2.1.5.2 Plasmid DNA (pDNA)

Table 7 pDNA used for experimental procedures

Name	Encoding	Supplier
pEGFP-N1/mCherry-DMDEx23	mCherry-DMDEx23 and eGFP	BioCat GmbH, Heidelberg, Germany
PB-CAG-GFPd2 pDNA[243]	GFPd2	AddGene #115665
Super piggyBac Transposase expression vector	PiggyBac Transposase	SBI, USA
PB-CAG-mCherry-DMDEx23-eGFP	mCherry-DMDEx23 and eGFP	In-house generation

2.1.5.3 PCR Primers

Primers were provided by Eurofins (Ebersberg, Germany).

Table 8 Primer sequences used for experimental procedures

Primer name	Sequence
mCherry-DMDEx23-eGFP_fwd	5'-ATCCCGGGGACTCAGATCTCGAGGCCACCAT'-3'
mCherry-DMDEx23-eGFP_rev	5'-TCGCGGCCGCTTTACTTGTACAGCT'-3'
mCherry-DMDEx23_SpliSwi_fwd	5'-GGAGGATAACATGGCCATC'-3'
mCherry-DMDEx23_SpliSwi_rev	5'-GTCCTTCAGCTTCAGCCTC'-3'
mCherry-DMDEx23_SpliSwi_nested_fwd	5'-GGAGTTCATGCGCTTCAAG'-3'
mCherry-DMDEx23_SpliSwi_nested_rev	5'-GCCGTCCTCGAAGTTCATC'-3'
DMD_Ex20-26 fwd	5'-CAGAATTCTGCCAATTGCTGA'-3' [244]
DMD_Ex20-26 rev	5'-TCACCAACTAAAAGTCTGCATT'-3' [245]
DMD_Ex20-24 fwd	5'-CCCAGTCTACCACCCTATCAGAG'-3' [244]
DMD_Ex20-24 rev	5'-CAGCCATCCATTTCTGTAAG'-3' [246]

2.1.6 Cell Culture

Table 9 Reagents for cell culture

Material	Supplier
Dulbecco's Modified Eagle's Medium (DMEM)	Life Technologies, Carlsbad, USA

Fetal bovine serum (FBS)	Life Technologies, Carlsbad, USA
Penicillin/Streptomycin	Life Technologies, Carlsbad, USA
Trypsin/EDTA	PANBiotech, Aidenbach, Germany

2.2 Methods

2.2.1 Solid-Phase Peptide Synthesis

Table 10 Summary of synthesized XP sequences

Xenopeptide ID	Backbone characteristic	Fatty acid	Sequence (N→C)
1195	Stp2	LenA	K(N_3)-Y_3-Stp_2-K[K(OleA)$_2$]-Stp_2-Y_3
1391	Stp	OleA	K(N_3)-Y_3-Stp-K(K(OleA)$_2$)-Stp-Y_3
1392	Stp	LinA	K(N_3)-Y_3-Stp-K(K(LinA)$_2$)-Stp-Y_3
1393	Stp	LenA	K(N_3)-Y_3-Stp-K(K(LenA)$_2$)-Stp-Y_3
1395	H-Stp-H	OleA	K(N_3)-Y_3-H-Stp-H-K(K(OleA)$_2$)-H-Stp-H-Y_3
1396	H-Stp-H	LinA	K(N_3)-Y_3-H-Stp-H-K(K(LinA)$_2$)-H-Stp-H-Y_3
1397	H-Stp-H	LenA	K(N_3)-Y_3-H-Stp-H-K(K(LenA)$_2$)-H-Stp-H-Y_3

The syntheses of XPs *#1391, #1392, #1393, #1396,* and *#1397* were performed by Dr. Yi Lin (Pharmaceutical Biotechnology, LMU München).

The azide-containing XPs used for conjugation and formulation of PMOs were synthesized and characterized as described previously.[162, 183] Table 10 provides an overview over the individual sequences, internal ID numbers and further descriptions. Sequence-defined lipo-oligoaminoamide XP were synthesized by standard Fmoc solid-phase peptide synthesis.

Schematic illustration of the manual SPPS algorithm is shown in **Figure 7**. A 2-chlorotrityl chloride resin was used, which was preloaded with the first amino acid Tyr(tBu)-OH. The artificial Fmoc- and Boc-protected amino acid Fmoc-Stp(Boc)3-OH was synthesized as previously reported [1, 5]. The sequences of the α-peptide backbones, excluding the N-terminal K(N_3) and side-chain lipid modification, were synthesized from C-terminus to N-terminus using a SyroWave synthesizer (Biotage, Uppsala, Sweden). Every coupling step was carried out twice with 4 eq. Fmoc-amino acid, 4 eq. HOBt, 4 eq. HBTU, and 8 eq. DIPEA in NMP/DMF (5 mL/g resin) for 12 min at 50 °C. Fmoc deprotection was carried out by 4

times incubation with 20% piperidine in DMF (7 mL/g resin) for 10 min. After each coupling and deprotection step, the resin was washed 5 times with DMF (10 mL/g resin) for 1 minute each. By including Fmoc-L-Lys(Dde)-OH in the backbone, an asymmetric branching point was introduced.

The N-terminal Fmoc-L-Lys(N_3)-OH coupling as well side-chain modifications of K(Dde) were performed manually as follows. Manual couplings were conducted at RT with 4 eq. Fmoc-protected amino acid, 4 eq. HOBt, 4 eq. PyBOP, and 8 eq. DIPEA in DCM/DMF (50/50) (10 mL/g resin) for 90 min using syringe microreactors and an overhead shaker followed by washing the resin three times with DMF and three times with DCM (10 mL/g resin each). The Fmoc protecting group was removed by incubating the resin with 20% piperidine in DMF (10 mL/g resin) four times for ten min. After the coupling and deprotection steps, a Kaiser test [2] was performed to confirm the accomplishment of the previous step. The N-terminus was protected with a Boc group by using 10 eq. Boc anhydride and 10 eq. DIPEA in DCM/DMF (10 mL/g resin). To enable chain elongation at the ε-amine of the Dde-protected lysine, the resin was incubated with 2% hydrazine hydroxide (v/v) in DMF (10 mL/g resin) for three times. The first and third incubation was performed for 5 min, the second incubation step took 7 min. The resin was washed for 10 times with DMF (10 mL/g resin), five times with 10% DIPEA (V/V) in DMF and five times with DCM. Fmoc-Lys(Fmoc)-OH was coupled and deprotected manually as described above. The final coupling step was performed by incubating the resin with 8 eq. of the desired fatty acid, 8 eq. HOBt, 8 eq. PyBOP, and 16 eq. DIPEA in DCM/DMF (50/50) (10 mL/g resin) for 90 min. After drying of the resin, the peptides were cleaved by using a cocktail consisting of trifluoroacetic acid (TFA)/triisopropylsilane (TIS)/H2O (95/2.5/2.5 v/v/v) (10 mL/g resin). The cleavage cocktail was cooled to 4 °C to avoid TFA-adduct formation,[6] added to the resin and incubated at RT for 20 min. Afterwards, the cleavage solution was transferred rapidly into 40 mL of precooled methyl-tert-butylether (MTBE)/n-hexane (50/50 v/v). The mixture was centrifuged, the supernatant was discarded and precipitated peptide dried. Purification of the peptide was conducted by size exclusion chromatography using an Äkta purifier system (GE Healthcare Bio-Sciences AB, Sweden) equipped with a P-900 solvent pump module, a UV-900 spectrophotometric detector, a pH/C-900 conductivity module, a Frac-950 automated fractionator, a Sephadex

G-10 column and 10 mM HCl in ACN (70/30 v/v) as solvent. Product fractions were combined and lyophilized to obtain the final product.

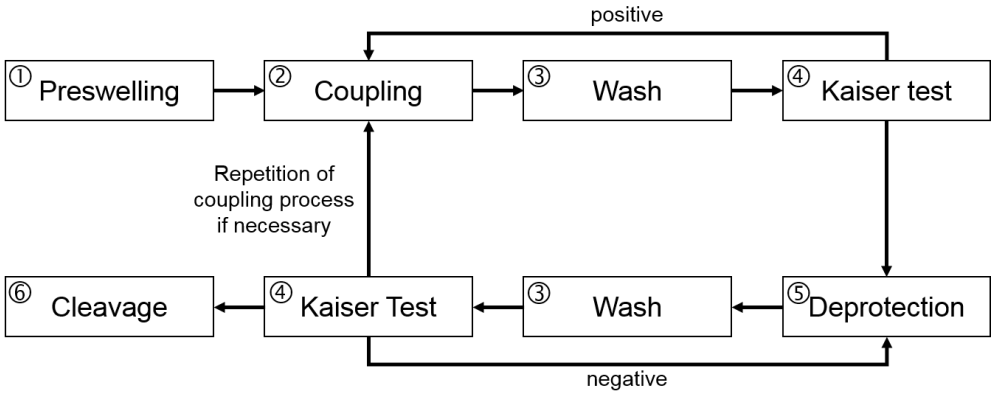

Figure 7 Schematic illustration the solid-phase synthesis algorithm during manual oligomer synthesis. 1) 2-Chlorotrityl chloride resin was swollen in DMF for 20 min. 2) The building block was solved in DCM, DIPEA was added. PyBOP and HOBt were solved together in DMF and added to the resin. The resin was incubated for 90 min. 3) The resin was washed three times with DMF; and three times with DCM. 4) One droplet of each aqueous 20 µM KCN in pyridine, ninhydrin in ethanol (5% w/v) and phenol in ethanol (80%, w/v) were added to a small amount of the resin. The resin was incubated for 5 min at 99 °C. (positive (blue): free amines, negative (colorless): protected amines). 5) Deprotection conditions were set depending on the protecting group. 6) The whole resin was incubated for 90 min with TFA/TIS/H2O (95/2.5/2.5 v/v/v). The cleaved product was precipitated in 30 mL of cooled mixture of MTBE/n-hexane (50/50 v/v).

2.2.2 PMO Functionalization

2.2.2.1 Synthesis of PMO–DBCO

1 µmol of 3' primary amine modified PMO (Gene Tools, USA) was dissolved in 300 µL water-free DMSO. 2.5 mg of DBCO-NHS ester (Sigma-Aldrich, Munich, Germany) was dissolved in 100 µL water-free DMSO and 0.3 µL DIPEA was added. The solutions were combined and incubated overnight at RT under shaking at 300 rpm.

The DBCO functionalized PMO was purified by size exclusion chromatography (SEC) using the Äkta purifier system (GE Healthcare Bio-Sciences AB, Uppsala, Sweden) comprising a P-900 solvent pump module, a UV-900 spectrophotometric detector, a pH/C-900 conductivity module, a Frac-950 automated fractionator, and a Sephadex G-10 column. The solvent composition was 30% ACN in Millipore water. The pooled product containing fractions were lyophilized, dissolved in water and analyzed by MALDI-MS.

To determine the concentration of dissolved PMO–DBCO, a 1:1000 dilution of the PMO–DBCO solution in 0.1 M HCl was prepared and the UV absorbance at 265 nm using UV/Vis

spectrophotometry was measured. The concentration was determined using following formula.

$$c[\mu M] = \frac{\text{dilution factor} \cdot \text{absorbance}}{extinction\ coeffincient} \cdot 10^6$$

Extinction coefficients of each PMO sequence can be found in Table 11.

Table 11 Extinction coefficient of used PMO sequences.

PMO	Extinction coefficient [$M^{-1}cm^{-1}$]	PMO Sequence
PMO(705)	259160	CCTCTTACCTCAGTTACAATTTATA
PMO(Ex23)	259210	GGCCAAACCTCGGCTTACCTGAAAT

2.2.2.2 PMO–Xenopeptide Conjugation

For the conjugation of PMO–DBCO and XP at a molar ratio of 1:3 PMO to XP, a dilution of PMO–DBCO (PMO(Ex23)–DBCO: stock solution in 20% acetonitrile ACN) in water; PMO(705)–DBCO in water; ~1000 µM) with the concentration of 100 µM and a dilution of the XP (stock solution of XP as HCl salt in water 1 mg/mL) with the concentration of 300 µM in water were prepared. Equal volumes of the solutions were combined and incubated overnight at room temperature (RT) with shaking at 300 rpm. The conjugate formulation solution was freeze-dried and reconstituted with the required volume of HBG to obtain the desired concentration. For fluorescently labeled PMO–XP conjugate formulations, 5% of PMO(Ex23)–DBCO was replaced by Alexa Fluor 647 (AF647) labeled PMO(705)–DBCO[162].

2.2.3 MALDI Mass Spectroscopy

MALDI mass spectroscopy was performed by Melina Grau and Tobias Burghardt (Pharmaceutical Biotechnology, LMU München).

As characterization method, the MALDI-ToF system was used. An approximately 1 mg/mL solution of each oligomer in Millipore water was prepared. 1.0 µL of a 10 mg/mL sDHB matrix solution (2,5-dihydroxybenzoic acid and 2-hydroxy-5-methoxybenzoic acid) in acetonitrile/water (3:7) with 0.1% (v/v) TFA, was spotted on a MTP AnchorChip (Bruker Daltonics, Bremen, Germany). 1.0 µL of the sample solution was added on the crystallized

matrix spot. Each mass spectrum was recorded using an Autoflex II mass spectrometer (Bruker Daltonik GmbH, Bremen, Germany).

2.2.4 Transmission Electron Microscopy (TEM)

TEM was performed by Susanne Kempter (Physics, soft condensed matter group, LMU München).

PMO–XP conjugate formulations were prepared in HEPES similar to as described in 2.2.2.2 PMO–Xenopeptide Conjugation. Samples contained either PMO(Ex23)–DBCO alone or PMO(Ex23)–XP conjugate formulations at a molar ratio of 1:3 PMO to XP. Carbon coated copper grids (Ted Pella, Inc. USA, 300 mesh, 3.0 mm O. D.) were hydrophilized with a plasma cleaner under argon atmosphere (420 V, 1 min). The grids were placed with the activated face down on top of 10 µL sample droplets for 20 s. Afterwards, the sample was removed with a filter paper and stained using a two-step process: first, the grid was washed with 5 µL staining solution (1.0% uranyl formate in water), which was removed immediately. Second, 5 µL of the same solution was left on the grid for 5 s. Afterwards, it was removed with a filter paper and grids were allowed to dry for 20 min. Grids were stored at room temperature. The samples were measured on a JEOL JEM-1100 electron microscope using 80 kV acceleration voltage. The surface diameter of PMO–XP conjugate nanomicelles were determined by measuring the diameter of the nanomicelles using the imageJ software (*#1195* containing formulations: n = 13; *#1395* containing formulations: n = 9).

2.2.5 LogD$_{7.4}$ Determination of PMO–Xenopeptide Conjugate Formulations

In order to determine the hydrophobicity of the PMO(Ex23)–XP conjugate formulations at a molar ratio of 1:3 PMO to XP, an octanol-water partition coefficient at pH 7.4 (logD$_{7.4}$) was determined as previously reported with adaptions. [183, 247] 10 µL of a 50 µM PMO–XP conjugate formulation containing 5% AF647–PMO(705)–DBCO and 95% PMO(Ex23)–DBCO was diluted with 90 µL of HBG buffer in a 1.5 mL reaction tube. 100 µL of n-octanol was added. After vortexing, the tube was shaken at 1400 rpm for 24 h. Afterwards, the tube was centrifuged and stored for 1 h at 4 °C. 70 µL of each phase was transferred into a 96-well plate and fluorescence was measured using Tecan Reader. AF647-labeled PMO

was excited at 640 nm and emission detected at 670 nm. Each solution was blanked with the used solvent. The distribution was calculated as $\log(F_{octanol}/F_{water})$ using the fluorescence intensities of each phase aliquot.

2.2.6 Cell Culture

HeLa cells are immortalized cells derived from cervical cancer cells.[248] HeLa wt, HeLa pLuc/705 and HeLa mCherry-DMDEx23 cells were cultured in DMEM low glucose (Sigma-Aldrich, St. Louis, USA) supplemented with 10% fetal bovine serum (FBS; Life Technologies, Carlsbad, USA), and 1% penicillin/streptomycin (P/S) (Life Technologies, Carlsbad, USA) at 37 °C and 5% CO_2 in a humidified atmosphere. The medium was changed every two days and cells were passaged at a confluency of approximately 80%.

HeLa pLuc/705 cells express *luciferase* gene containing the intron 2 of a human β-globin with a IVS2-705 mutation. HeLa mCherry-DMDEx23 cells contain the new *mCherry-DMDEx23* gene, which was designed in this work, with the *mdx* exon 23 including the nonsense point mutation.

2.2.7 Design of mCherry-Reporter for DMD Exon 23 Skipping

The mCherry sequence was split into two parts: 5'-mCherry and 3'-mCherry. The two regions were separated by the murine exon 23 sequence, containing the nonsense mutation of the *mdx* mouse model, flanked by intronic sequences of 154 bp at each side. The sequence of the reporter construct is provided in **Figure 38**. The construct was synthesized and cloned into a pEGFP-N1 vector by BioCat (Heidelberg, Germany). The pEGFP-N1/mCherry-DMDEx23 plasmid was used for initial transient reporter expression experiments. Additionally, the gene construct was subcloned into a modified PiggyBac plasmid (PB-CAG-GFPd2 was a gift from Jordan Green; Addgene plasmid #115665; http://n2t.net/addgene:115665; RRID:Addgene_115665)[243], which was used for generation of HeLa cells with stable reporter expression.

2.2.8 Flow Cytometry

Flow cytometry was used for the determination of mCherry expression as well as the cellular uptake of fluorescently labeled PMO formulations in HeLa mCherry-DMDEx23 cells. After individual treatments, cells were trypsinized and resuspended in 100 µL of FACS buffer,

consisting of 10% FBS in PBS supplemented with DAPI (1 µg/mL) to discriminate viable and dead cells. All samples were analyzed by flow cytometry using a CytoFLEX S flow cytometer (Beckman Coulter, Carlsbad, USA) equipped with a well-plate autosampler. DAPI was excited at 405 nm, and emission was detected at 450 nm. In splice switching experiments, mCherry was excited at 561 nm and, emission was detected at 610 nm. In the case of uptake experiments, AF647-labeled PMO was excited at 640 nm, and emission was detected at 670 nm. Only isolated and viable cells were evaluated. Flow cytometry data was analyzed using FlowJo X 10.0.7r2 flow cytometric analysis software by FlowJo, LLC (Ashland, USA). All experiments were performed in triplicate.

2.2.9 *In Vitro* Treatment of Transient HeLa mCherry-DMDEx23 Cells

Hela wt cells were seeded into a 96-well plate 24 h prior to transfection at a density of 5,000 cells per well. 200 ng pEGFP-N1/mCherry-DMDEx23 plasmid was transfected into each well using Lipofectamine 3000 (Thermo Fisher Scientific, Waltham, USA) according to the manufacturer's protocol. 24 h after the plasmid DNA transfection, cells were treated with the specified PMO conjugate formulations. The medium of the cells was replaced by 90 µL of fresh medium, and 10 µL of the PMO conjugate formulations was added. After 24 h of incubation, the medium was removed, each well was washed with 100 µL of PBS and the cells were analyzed by flow cytometry using a CytoFLEX S flow cytometer (Beckman Coulter, Carlsbad, USA) as described above.

2.2.10 Generation of PB-CAG-mCherry-DMDEx23-eGFP Plasmid

For the generation of stable mCherry-DMDEx23 reporter cells, the reporter gene construct was subcloned from pEGFP-N1/mCherry-DMDEx23 obtained from BioCat GmbH (Heidelberg, Germany) into a PiggyBac plasmid. PB-CAG-GFPd2 was a gift from Jordan Green (AddGene plasmid #115665; http://n2t.net/addgene:115665; RRID:Addgene_115665). First, the GFPd2 gene was cleaved out of PB-CAG-GFPd2 using the restriction enzymes XmaI (New England Biolabs, Ipswich, USA) and NotI (New England Biolabs, Ipswich, USA) in sequence. Intermediate and final purification was performed by gel electrophoresis (1% agarose; 100 V; 3 h) followed by gel extraction. The mCherry-DMDEx23-eGFP insert was generated by PCR amplification from pEGFP-N1/mCherry-DMDEx23 using Taq DNA polymerase (NEB) and PCR primers which include

NotI and XmaI restriction sites at the 5' ends. The primers mCherry-DMDex23-eGFP_fwd (5'-ATCCCGGGGACTCAGATCTCGAGGCCACCATG-3'), mCherry-DMDex23-eGFP_rev (5'-TCGCGGCCGCTTTACTTGTACAGCTC-3') and following PCR conditions were used: initial denaturation (94 °C, 30 sec), 30 cycles (94 °C, 30 sec / 60 °C, 1 min / 68 °C, 1 min), final extension (68 °C, 5 min). The mCherry-DMDEx23-eGFP PCR product was purified by electrophoresis on a 1% agarose gel. Sticky ends were generated by digestion of the PCR amplicon with XmaI and NotI. Intermediate and final purification was performed by gel electrophoresis (1% agarose; 100 V; 3 h) followed by gel extraction. The obtained mCherry-DMDEx23-eGFP insert (~1291 bp) was integrated into the PB-CAG vector (5592 bp) by using standard cloning techniques. DH5alpha cells were transformed with the ligation reaction mixture and PB-CAG-mCherry-DMDEx23-eGFP plasmid was isolated using Qiagen Plasmid Maxi kit.

The plasmids pEGFP-N1/mCherry-DMDEx23 (#211367) and PB-mCherry-DMDEx23-eGFP (#211366) are deposited at Addgene.

2.2.11 Generation of Stable HeLa mCherry-DMDEx23 Cells

Hela wt cells were seeded in a 48-well plate at a density of 12,500 cells/well 24 h before transfection. The next day, 500 ng of Super piggyBac Transposase expression vector (SBI, CA, USA) and 200 ng of PB-CAG-mCherry-DMDEx23-eGFP plasmid were cotransfected using Lipofectamine 3000 (ThermoFisher Scientific, USA) according to the manufacturer's protocol. 48 h after pDNA treatment, the transfection mixture containing medium in each well was replaced by fresh medium. 3, 17, and 22 days after treatment, the cells were evaluated by flow cytometry as described above. The fluorescence of cells was determined by excitation of DAPI at 405 nm, detection of emission at 450 nm, excitation of eGFP at 488 nm and detection of emission at 530 nm. Only isolated and viable cells were evaluated. Flow cytometry data was analyzed using FlowJo X 10.0.7r2 flow cytometric analysis software by FlowJo, LLC (Becton, Dickinson and Company, USA). After expansion, cells were sorted to isolate viable and eGFP expressing cell populations using a BD FACSAriaFusion. The cell sorting was performed at the Core Facility Flow Cytometry of the Biomedical Center, LMU Munich by Dr. Lisa Richter (Biomedical Center Munich, Core Facility Flow Cytometry, LMU München). Flow cytometry data was analyzed using FlowJo (Tree

Star Inc.). Single cell clones were generated from the sorted polyclonal population of HeLa mCherry-DMDEx23 cells using limiting dilution method in 96-well plates. A suitable monoclonal HeLa mCherry-DMDEx23 cell line was selected by determining eGFP and mCherry expression after PMO(Ex23) treatments.

In order to confirm the presence of mCherry-DMDEx23 in the genomic DNA, genomic DNA was isolated from 1 Mio. HeLa mCherry-DMDEx23 cells using the QIAamp® DNA Mini kit according to manufacturer's protocol. The DNA concentration was evaluated and 300 ng of the genomic DNA was used to perform a PCR to amplify the mCherry-DMDEx23 gene using Taq polymerase (New England Biolabs, Ipswich, Massachusetts, USA), mCherry-DMDEx23-eGFP_fwd primer (5'-ATCCCGGGGACTCAGATCTCGAGGCCACCATG-3'), and mCherry-DMDEx23-eGFP_rev (5'-TCGCGGCCGCTTTACTTGTACAGCTC-3') primer. Following PCR conditions were used: initial denaturation (94 °C, 30 sec), 30 cycles (94 °C, 30 sec/60 °C, 1 min/68 °C, 1 min), and final extension (68 °C, 5 min).

The PCR product was analyzed on a 1% agarose gel in TBE buffer and visualized using GelRed® (Biotium, Hayward, CA, USA). Electrophoresis was run for 1.5 h at 100 V.

The target band (~2042 bp) indicating the whole mCherry-DMDEx23-eGFP gene was cut out and the DNA was isolated using QIAquick® Gel Extraction Kit (Qiagen, Hilden, Germany). The purified DNA fragment at concentrations of 10 ng/µL was sequenced by Eurofins GATC Biotech (Konstanz, Germany) with mCherry-DMDEx23-eGFP_fwd primer (5'-ATCCCGGGGACTCAGATCTCGAGGCCACCATG-3'), and mCherry-DMDEx23-eGFP_rev (5'-TCGCGGCCGCTTTACTTGTACAGCTC-3') primer.

2.2.12 Luciferase Activity Assay

24 h prior to transfection, 96-well plates (Corning ® Costar, Sigma-Aldrich, Germany) were coated with collagen and HeLa pLuc/705 cells were seeded at a density of 5,000 cells/well. 50 µM PMO–XP formulation was prepared as explained above. Prior to transfection, the medium in the 96-well plates was replaced by 90 µL of fresh medium, and 10 µL of the PMO(705)–XP formulation was added into each well. Cells were incubated at 37 °C and 5% CO_2 in a humidified atmosphere for 24 h. After incubation, the medium was removed and 100 µL of 0.5× cell lysis buffer (25 mM Tris, pH 7.8; 2 mM EDTA;

1 mM DTT; 10% glycerol, 1% Triton X-100) was added to each well to lyse the cells. The well plates were incubated for 30 min at RT. After the incubation, the 96-well plates were stored at –80 °C. The luminescence measurements were performed by using a Centro LB 960 plate reader luminometer from Berthold Technologies (Bad Wildbad, Germany). 500 µL of a 10 mM luciferin solution was diluted with 9.5 mL LAR buffer (20 mM glycylglycine; 1 mM MgCl2; 0.1 mM EDTA; 3.3 mM DTT; 0.55 mM adenosine 5′-triphosphate; 0.27 mM coenzyme A, pH 8-8.5). 35 µL of each cell lysate was transferred to a luminometer microplate and 100 µL of luciferin-LAR buffer was added to each well before the measurement. With a delay of 2 seconds, the relative light units were measured for 10 sec. To relate the luminescence of the treated cells to the background of untreated cells, the mean value of each group was divided by the mean of the HBG treated negative control cells and a 'fold increase' value was calculated for each group.

2.2.13 mCherry Expression Determined by Flow Cytometry

Stable HeLa mCherry-DMDEx23 cells were seeded into 96-well plates (Corning® Costar, Sigma-Aldrich, Munich, Germany) 24 h prior to treatments at a density of 5,000 cells/well. The medium in each well was replaced by 90 µL of fresh medium, 10 µL of the PMO–XP conjugate formulation was added into each well and the cells were exposed to the formulation for the specified incubation times at 37 °C and 5% CO_2 in a humidified atmosphere. For short-term incubations, the medium containing the PMO–XP conjugate formulation was replaced by fresh medium after the desired incubation time, and incubation was continued for a total time of 24 h. After the required total incubation time, the medium was removed, each well was washed with 100 µL of PBS, and cells were analyzed by flow cytometry using a CytoFLEX S flow cytometer (Beckman Coulter, Carlsbad, USA) as described above.

2.2.14 Cellular Uptake Determined by Flow Cytometry

Stable HeLa mCherry-DMDEx23 cells were seeded into 96-well plates (Corning® Costar, Sigma-Aldrich, Munich, Germany) 24 h prior to treatments at a density of 5,000 cells/well. The medium in each well was replaced by 90 µL of fresh medium, 10 µL of the PMO–XP conjugate formulation containing 5% AF647-labeled PMO was added into each well and the cells were incubated for 0.5 or 24 h, respectively. After the specified time, the medium was removed, each well was washed with 100 µL of PBS, and the cells were analyzed by flow

cytometry using a CytoFLEX S flow cytometer (Beckman Coulter, Carlsbad, USA) as described above.

2.2.15 Metabolic Activity Assay (MTT assay)

Cell viability was determined indirectly via the quantification of cellular metabolic activity with MTT assays. HeLa mCherry-DMDEx23 cells were seeded in 96-well plates at a density of 5,000 cells/well. 24 h after seeding, the medium was replaced by 90 µL of fresh medium and 10 µL of the PMO–XP conjugate formulation at the desired concentration was added to each well. After incubation for 24 h, 10 µL of 3-(4,5-dimethylthiazol-2-yl)-2,5-diphenyl-tetrazolium bromide (MTT, 5 mg/mL) was added to each well. After 2 h of incubation, the medium was removed, and the 96-well plates were stored at −80 °C overnight. 100 µL of DMSO was added per well to dissolve the purple formazan product. The 96-well plates were incubated for 30 min at 37 °C with constant shaking. The absorbance at λ = 590 nm of each well was measured with background correction at λ = 630 nm by using a microplate reader (Tecan Spark 10M, Tecan, Nänikon, Switzerland). The relative cell viability (%) was calculated by normalizing the values to control wells treated with HBG, according to the following equation:

$$cell\ viability\ [\%] = \frac{A(test)}{A(control)} \cdot 100\ \%$$

A difference of absorbance at λ = 590 nm and background correction at λ = 630 nm

2.2.16 Confocal Laser Scanning Microscopy (CLSM)

All CLSM experiments were performed by Miriam Höhn (Pharmaceutical Biotechnology, LMU München).

2.2.16.1 mCherry Expression Imaged by CLSM

15,000 HeLa mCherry-DMDEx23 cells/well were seeded in 8 well-Ibidi µ-slides (Ibidi, Planegg/Martinsried, Germany) in a total volume of 300 µL medium per well. The next day, medium was replaced by 270 µL of fresh medium. PMO–XP conjugate formulations in HBG were prepared at 25 µM as explained above and 30 µL was added to each well. 24 h after the treatment, the wells were washed three times with 300 µL of prewarmed PBS and cells were fixed with 4% paraformaldehyde in PBS for 40 min at RT. The wells were washed again three times with PBS. The cell nuclei were stained with DAPI (2 µg/mL) for 20 min under light protection at RT. The wells were washed once with PBS and 300 µL of fresh PBS was added. A

Leica-TCS-SP8 confocal laser scanning microscope (CLSM) equipped with an HC PL APO 63× 1.4 objective (Wetzlar, Germany) was used to record the images. DAPI emission was recorded at 460 nm and mCherry emission was recorded at 610 nm. All images were processed by using the LAS X software from Leica.

2.2.16.2 Uptake of PMO–XP Conjugate Formulations Imaged by CLSM

15,000 HeLa mCherry-DMDEx23 cells/well were seeded in 8 well-Ibidi µ-slides (Ibidi, Planegg/Martinsried, Germany) in a total volume of 300 µL medium per well. Cells were incubated at 37 °C and 5% CO_2 for 24 h before treatment with PMO–XP conjugate formulations containing 5% AF647-labeled PMO. The next day, the medium was replaced by 270 µL of fresh medium and 30 µL of a 25 µM PMO–XP conjugate formulation solution in HBG was added per well. 0.5 or 4 h after the treatment, the wells were washed thrice with 300 µL of prewarmed PBS and cells were fixed with 4% paraformaldehyde in PBS for 40 min at RT. The wells were washed again three times with PBS. F-actin was stained with rhodamine-phalloidin (1 µg/mL) overnight at 4 °C. Cell nuclei were stained with DAPI (2 µg/mL) for 20 min under light protection at RT. The wells were washed once with PBS and 300 µL of fresh PBS was added. A Leica-TCS-SP8 confocal laser scanning microscope (CLSM) equipped with an HC PL APO 63× 1.4 objective (Wetzlar, Germany) was used to record the images. DAPI emission was recorded at 460 nm, rhodamine at 580 nm and AF647 at 665 nm. All images were processed by using the LAS X software from Leica.

2.2.17 Western Blot

150,000 HeLa mCherry-DMDEx23 cells/well were seeded into a 6-well plate 24 h prior to PMO treatments. PMO formulations containing PMO(Ex23)–DBCO or PMO(705)–DBCO at a concentration of 25 µM were prepared with XP *#1195* as described above. Prior to the treatment, the medium was replaced by 900 µL of fresh medium and 100 µL of PMO formulations was added into the wells. After an incubation time of 24 h, cells were washed with PBS and lysed using 100 µL of 0.5× cell culture lysis buffer (Promega, Mannheim, Germany) supplemented with EDTA-free Protease Inhibitor Cocktail (Roche, Basel, Switzerland) per well. The cell lysates were stored at −80 °C for 18 h. After centrifugation for 10 min at 4 °C and 17,000g, 40 µL of a 1:4 dilution of each supernatant was added to the SDS sample buffer containing β-mercaptoethanol and incubated for 5 min at 95 °C and 2 min on ice. SDS-PAGE was performed using a 3.5% stacking and a 10% separating SDS-gel. The

proteins were transferred to a poly (vinylidene difluoride) (PVDF) blotting membrane. The membrane was incubated in 1× NET-gelatin (8.33 g of gelatina alba in 1 L of 1× NET containing 0.15 M NaCl, 0.005 M EDTA, and 0.05 M Tris, 0.05% Triton-X-100) for 2 h at room temperature and immunolabeled with a primary anti-mCherry antibody (anti-mCherry Rabbit polyclonal antibody, #26765-1-AP, proteintech, Manchester, UK) diluted 1:1,000 in 1× NET-gelatin overnight at 4 °C. The membrane was washed four times with 1× NET-gelatin and incubated with the secondary antibody (IRDye 680RD Goat anti-rabbit, Li-Cor, Lincoln, USA) diluted 1:10,000 in 1× NET-gelatin for 1 h at RT followed by four times washing with 1× NET gelatin. Membranes were imaged using an Odyssey Fa imaging system (Li-Cor, Lincoln, USA) and analyzed and quantified by Image Studio Software (Li-Cor, Lincoln, USA).

2.2.18 Bafilomycin A1 (BafA1) Assay

5,000 HeLa mCherry-DMDEx23 cells/well were seeded in 96-well plates one day prior to treatments. Two hours before PMO treatment, the medium in the wells was replaced by either fresh medium or medium supplemented with bafilomycin A1 (BafA1, Sigma-Aldrich, Munich, Germany) to obtain a final concentration of 200 nM BafA1 after PMO formulation addition. After two hours of preincubation with BafA1, the PMO formulations at concentrations 6.25, 3.125, and 1.5625 µM were added as explained above. Cells were incubated for 30 min and 4 h respectively and the medium was replaced by 100 µL of fresh medium. The cells were incubated for further 23.5 or 20 h, respectively, before determination of mCherry expression by flow cytometry as described above. Treatments were performed in triplicate.

2.2.19 RT-PCR of Reporter Exon Skipping *In Vitro*

Total RNA was isolated from PMO-treated and untreated HeLa mCherry-DMDEx23 cells using RNASolv (VWR International, Darmstadt, Germany) according to the manufacturer's protocol. 400 ng of RNA was used to generate cDNA using the qScript cDNA synthesis kit (Quantabio, Beverly, USA) according to the manufacturer's protocol. The region of interest was amplified by PCR with 150 ng of the cDNA, Taq polymerase (New England Biolabs, Ipswich, USA), the primers mCherry-DMDex23_SpliSwi_fwd (5'-GGAGGATAACATGGCCATCA-3'), mCherry-DMDex23_SpliSwi_rev (5'-GTCCTTCAGCTTCAGCCTCT-3'), and the following PCR conditions: initial denaturation (94 °C, 30 sec), 30 cycles (94 °C, 30 sec/60 °C, 1 min/68 °C, 1 min), and final extension (68 °C, 5 min).

After amplification, the PCR product was purified using a PCR purification kit (Qiagen, Hilden, Germany) according to the manufacturer's protocol. 1 µg of the purified PCR amplicon was digested overnight with 2 units of Nde I (New England Biolabs, Ipswich, USA). To ensure detachment of the restriction enzyme, SDS was added to a concentration of 0.2% and was incubated for 10 min at 65 °C. The digested DNA was purified using the PCR purification kit (Qiagen, Hilden, Germany). Second PCR was conducted with 100 ng of the purified DNA as template, the primers mCherry-DMDex23_SpliSwi_nested_fwd (5'-GGAGTTCATGCGCTTCAAGG-3'), and mCherry-DMDex23_SpliSwi_nested_rev (5'-GCCGTCCTCGAAGTTCATCA-3'), and the following PCR conditions: initial denaturation (94 °C, 30 sec), 30 cycles (94 °C, 30 sec/55 °C, 1 min/68 °C, 1 min), final extension (68 °C, 5 min).

The PCR product was analyzed on a 1% agarose gel in 1× TBE buffer containing GelRed® (Biotium, Hayward, USA). Electrophoresis was conducted for 1.5 h at 100 V and analyzed with Dark Hood DH-40 (biostep, Burkhardtsdorf, Germany) and the biostep argusX1 software. The band with the expected size of the DNA sequence with skipped DMD exon 23 (~280 bp) was cut out, and the DNA was isolated using a QIAquick® Gel Extraction Kit (Qiagen, Hilden, Germany). The purified DNA fragment was sequenced (Sanger) by Eurofins GATC Biotech (Konstanz, Germany) with the sequencing primers mCherry-DMDex23_SpliSwi_nested_fwd (5'-GGAGTTCATGCGCTTCAAGG-3') and mCherry-DMDex23_SpliSwi_nested_rev (5'-GCCGTCCTCGAAGTTCATCA-3').

2.2.20 Splicing Modulation *In Vivo*

Animal experiments were performed by veterinarians Jana Pöhmerer and Dr. Ulrich Wilk (Pharmaceutical Biotechnology, LMU München).

All animals were handled in accordance with the guidelines of the German Animal Welfare Act and were approved by the animal experiments ethical committee of the "Regierung von Oberbayern", District Government of Upper Bavaria, Germany.

6-week-old female BALB/c mice (BALB/cByJRj, Janvier, Le Genest-Saint-Isle, France) were housed in isolated ventilated cages under pathogen-free condition with a 12 h light/dark interval. The mice were acclimated for seven days prior to treatments. Water and food were provided ad libitum. For splice switching in the physiological DMD gene, PMO formulations were prepared 48 h before intravenous injection as described above. The

freeze-dried PMO formulations were reconstituted with HBG to obtain a concentration of 375 µg PMO per 150 µL. The mice were randomly divided into three groups (n = 6 for PMO(Ex23)–1395, and n = 5 for free 3' primary amine modified PMO(Ex23) and PMO(705)–1395). 150 µL of PMO solution was injected intravenously into a lateral tail vein. 48 h after injection, the mice were euthanized and the brain, spleen, quadriceps femoris muscle, kidneys, liver, lung, and heart were harvested. For stabilization of the mRNA, the organs were incubated in RNAlater solution (Thermo Fisher Scientific, Waltham, USA) overnight at 4 °C and afterward stored at –20 °C. Each organ was manually homogenized using a mortar and pestle, and liquid nitrogen. The mRNA was isolated using the peqGOLD Total RNA Kit (VWR International, Darmstadt, Germany). 400 ng of the RNA was used to generate cDNA using the qScript cDNA synthesis kit (Quanta Biosciences, Gaithersburg, USA). To amplify the region of interest, 300 ng of the cDNA was used to perform a PCR with Taq polymerase (New England Biolabs, Ipswich, USA), the primers DMD_Ex20-26 fwd (5'- CAGAATTCTGCCAATTGCTGAG -3')[54], and DMD_Ex20-26 rev (5'- TCACCAACTAAAAGTCTGCATTG -3')[249] and the following conditions: initial denaturation (94 °C, 30 sec), 30 cycles (94 °C, 30 sec/55 °C, 1 min/68 °C, 1 min), and final extension (68 °C, 5 min).

The PCR products were purified using the PCR purification kit (Qiagen, Hilden, Germany). 100 ng of the purified PCR product was used to perform a second PCR with the primers DMD_Ex20-24 fwd (5'- CCCAGTCTACCACCCTATCAGAGC -3')[54], and DMD_Ex20-24 rev (5'- CAGCCATCCATTTCTGTAAGG -3')[56] and the following conditions: initial denaturation (94 °C, 30 sec), 30 cycles (94 °C, 30 sec/57 °C, 1 min/68 °C, 1 min), and final extension (68 °C, 5 min).

The final PCR products were analyzed by agarose gel electrophoresis (2% agarose gel; 100 V; 2 h). Individual band intensities were quantified and put into relation to the band of full-length DMD-Ex20-24 with a size of 633 bp by using ImageJ software.

To confirm the determined exon 23 skipping in PMO(Ex23)–1395 treated mice, the bands of the lung of animal C1 were purified by gel extraction using a QIAquick® Gel Extraction Kit (Qiagen, Hilden, Germany). The purified sequences were sequenced (Sanger) by

Eurofins GATC Biotech (Konstanz, Germany) with the primers DMD-Ex20-24 fwd and DMD-Ex20-24 rev at a concentration of 10 ng/µL.

2.2.21 Statistical Analysis

Unless otherwise stated, results are presented as arithmetic mean ± standard deviation (SD) and the number of replicates. The statistical significance of experiments was estimated using the two-tailed student's t-test. Significance levels are indicated with asterisks. **** $p \leq 0.0001$, *** $p \leq 0.001$, ** $p \leq 0.01$, * $p \leq 0.05$, and ns $p > 0.05$.

3. Results and Discussion

This chapter has been adapted from:

Lessl AL, Pöhmerer J, Lin Y, Wilk U, Höhn M, Hörterer E, Wagner E, Lächelt U. mCherry on Top: A Positive Read-Out Cellular Platform for Screening DMD Exon Skipping Xenopeptide-PMO Conjugates. Bioconjugate Chemistry 2023 Nov 22.

DOI: 10.1021/acs.bioconjchem.3c00408

3.1. Analysis of the Synthesized Xenopeptides

MALDI-MS analysis of resynthesized XPs *#1195* and *#1395*, confirmed successful synthesis. Only one mass peak with low difference to calculated molecular weight of the products was detected in each case. PMO–derivatives and conjugates were analyzed by MALDI-MS and one peak each could be observed corresponding to the calculated molecular weight.

3.2 PMO Delivery System using Click Chemistry

PMOs are artificial nucleic acid analogues with uncharged character which on the one hand improves their tolerability and half-life due to resistance against enzymatic degradation. On the other hand, the uncharged character dismisses the possibility of complexation with charged transfection agents. Kuhn et al. developed covalent PMO conjugation using lipid-modified XPs for enhanced PMO delivery.[162] To covalently bind PMOs to XPs, click reaction[250] in form of strain-promoted azide–alkyne cycloaddition (SPAAC)[251] was used (**Figure 8a**). For this purpose, 3' primary amine modified PMOs were previously functionalized with dibenzocyclooctyne-NHS ester (DBCO-NHS). As consequence, PMOs contain a functional group for further conjugation with azido-lysine containing XPs (**Figure 8b**).

In a previous work, it could be shown, that an excess of XPs in the formulation (molar ratio of 1:3 PMO/XP) strongly enhances transfection efficiency due to self-assembly into nanomicelles (**Figure 8c**).[162] The amphiphilic character of XPs which are conjugated to PMOs lead to the observed self-assembly in aqueous environment.

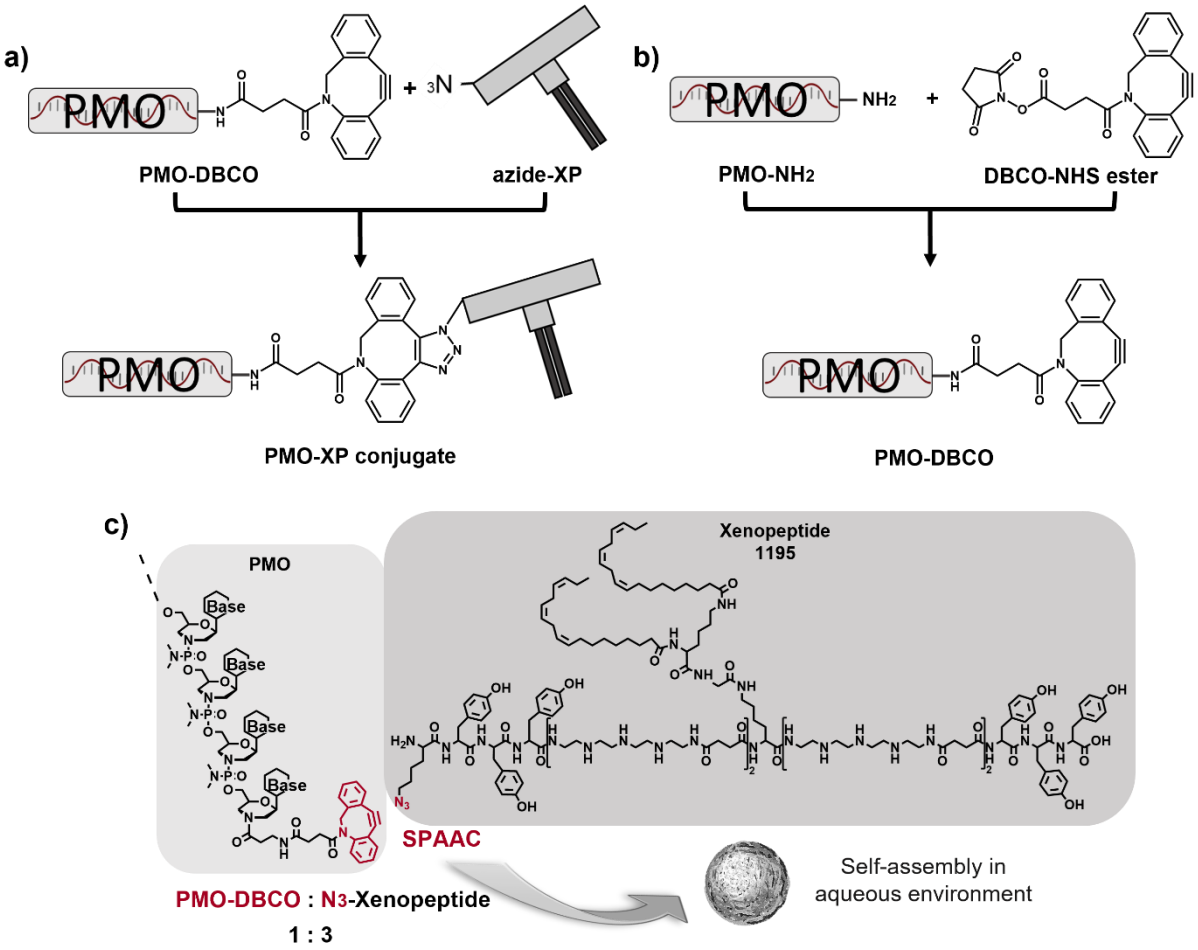

Figure 8 Illustration of functionalization and conjugation of PMO–DBCO and azide-containing xenopeptide (XP). a) Illustration of strain-promoted azide–alkyne cycloaddition (SPAAC) between PMO–DBCO and azide-XP. **b)** Functionalization of 3' primary amine of PMO with DBCO–NHS ester resulting in PMO–DBCO. **c)** Conjugation of PMO–DBCO and azide-containing XP (*#1195*) followed by nanomicelle formation in aqueous environment.

3.3 Design of new Reporter Gene mCherry-DMDex23

During development of nanotherapeutics, translation from in *vitro* to *in vivo* stages is generally challenging. For PMO conjugate formulations, this gap can be particularly critical, since different PMO sequences used in different screening models can exhibit very different properties. For this reason, in this work a workflow has been designed, which enables *in vitro* and *in vivo* screenings of PMO conjugate formulations without change of sequence (**Figure 9**). The basis for the screening platform is the PMO(Ex23) sequence, which mediates skipping of DMD exon 23 and is frequently used in the well-established *mdx* mouse model of DMD. The particular PMO has the advantage, that it can not only be used in transgenic *mdx* mice but does also induce exon skipping in healthy mice. For the

initial *in vitro* assessment, an *in vitro* reporter system was designed, which enables convenient screening of PMO conjugate formulations.

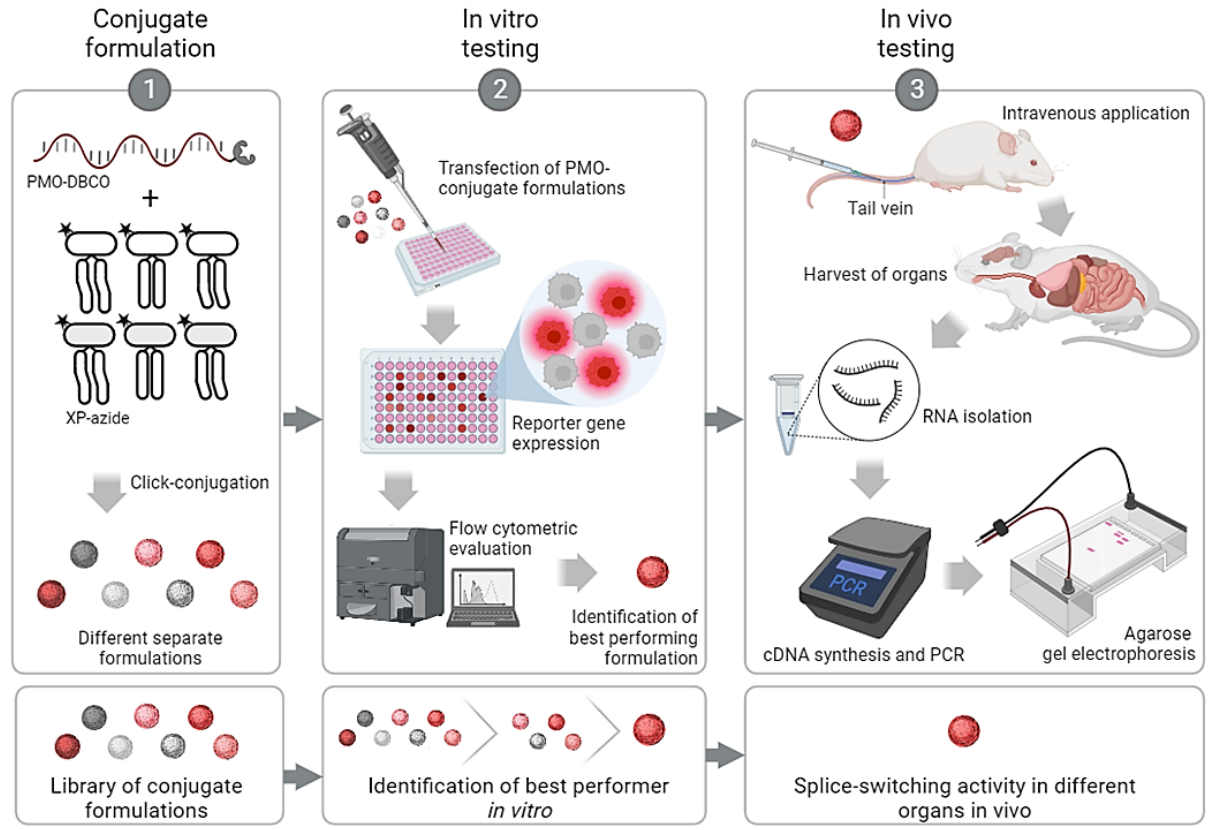

Figure 9 Schematic overview of the formulation generation *in vitro* and *in vivo* evaluation. 1) Generation of PMO–conjugate formulations using PMO(Ex23)–DBCO and azide-containing XPs via strain-promoted azide-alkyne cycloaddition (click conjugation). 2) *In vitro* screening of PMO conjugate formulations and identification of most potent candidates. 3) Evaluation of most potent PMO conjugate formulation *in vivo* using same PMO sequence and formulation composition. Figure was created using Biorender.com.

An intron–exon–intron sequence was implemented as the design of a fluorescent protein reporter in order to generate a positive read-out system activatable via exon skipping (**Figure 10a**). Based on the DMD *mdx* mouse model, the *dystrophin* exon 23 containing a nonsense mutation at nucleotides 28–30 was inserted as an interrupting exon into the *mCherry* gene between nucleotides 105 and 106. The exon was flanked by two artificial intronic sequences containing splice sites. The donor and acceptor splice sites contained conserved splice sequences which are required for functional splicing (**Figure 10b**).[29] The 5' splice sites between the 5' mCherry I and intron I, and mdx DMDEx23 and intron II are presented by the conserved sequence motif CAG | CTAAG. The 3' splice sites between intron I and mdx DMDEx23, and intron II and 3' mCherry II are presented by the conserved sequence motif TCTACAG | G. The 5' splice site (donor splice site) of the intron

downstream of *mdx* exon 23 was based on the physiological donor splice site sequence of DMD intron 23, which enables utilization of the same PMO(Ex23) sequence in the *in vitro* reporter system and *in vivo* experiments. Transcription and splicing of the *mCherry-DMDEx23* construct results in mRNA with the nonsense mutation of *mdx* exon 23 and no functional mCherry product after translation. Skipping of *mdx* exon 23 via a specific SSO such as PMO(Ex23) induces exon 23 skipping and by this restores the correct reading frame and induces the functional mCherry expression (**Figure 10c**).

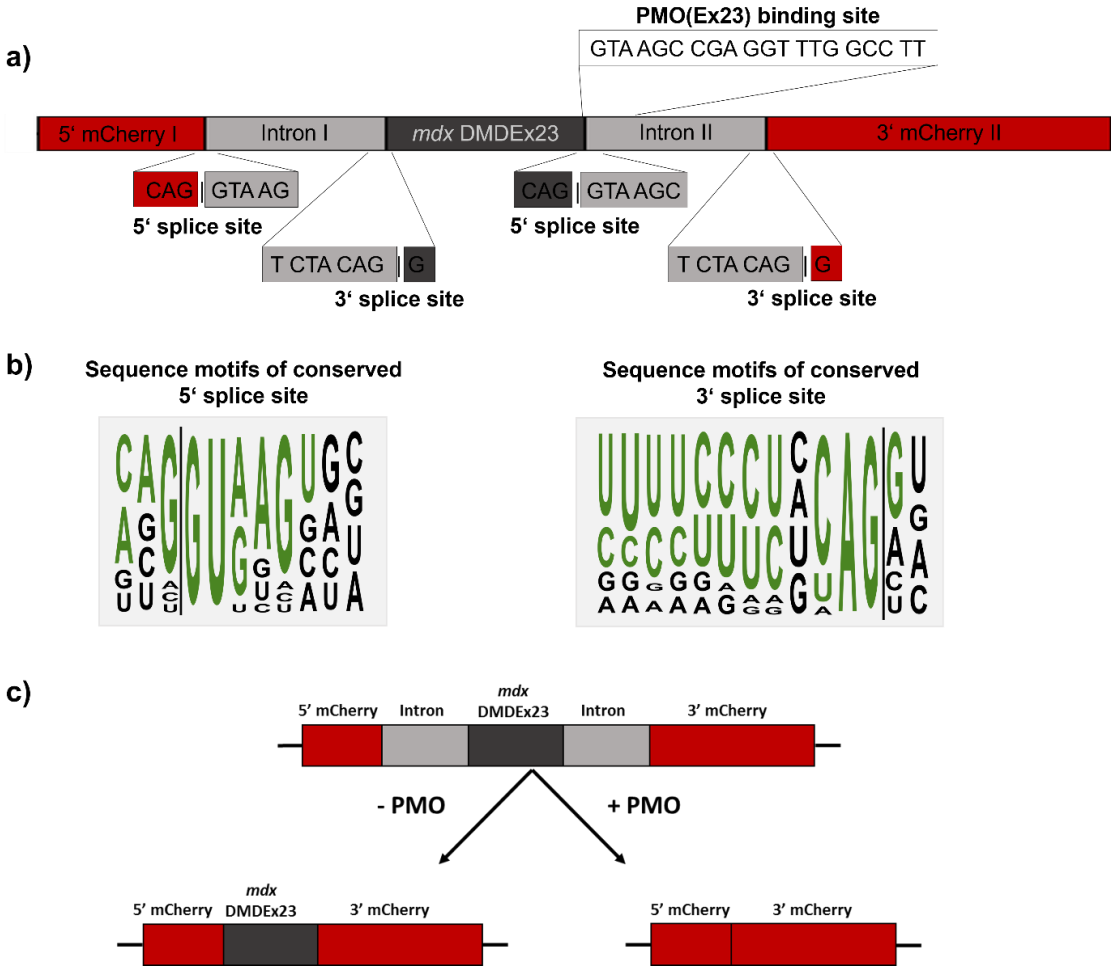

Figure 10 Design of new mCherry-DMDEx23 reporter. a) mCherry-DMDEx23 structure with splice site sequences. **b)** Required conserved sequences of 5’ splice site and 3’ splice site. **c)** Structure of mCherry-DMDEx23 construct and its mechanism in presence or absence of PMO(Ex23).

PMO(Ex23) forms a steric block at the donor splice site (5’ splice site) connecting exon 23 and intron 23. Following description refer to **Figure 11**.

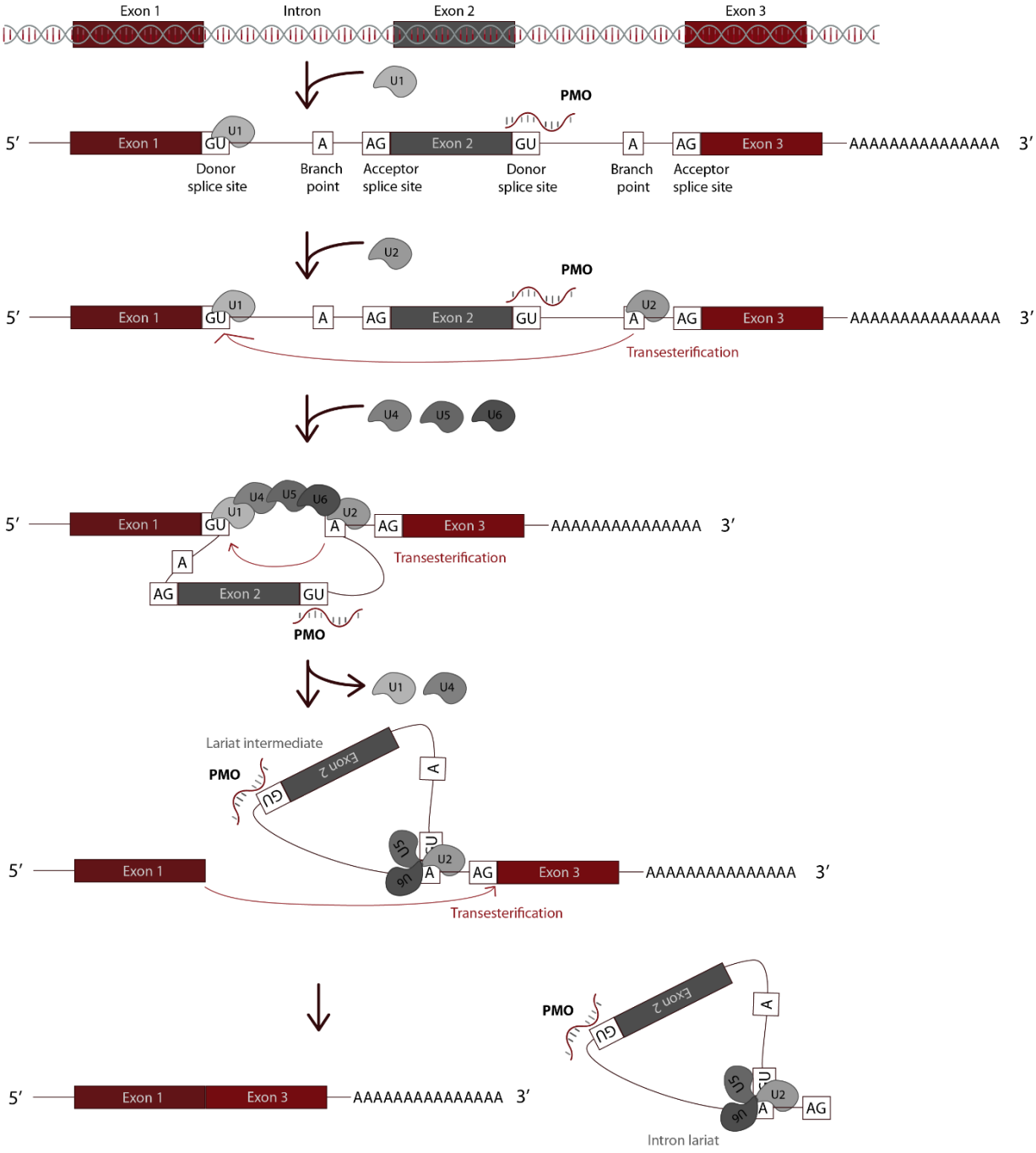

Figure 11 Schematic illustration of theoretical progressive splicing mechanism in presence of PMO. Recognition by spliceosome subunits is enabled by conserved sequences: the donor splice site (5' splice site, GU), acceptor splice site (3' splice site, AG), and an adenine nucleotide (branch point, A). Binding of U1 to the donor splice site (5' splice site) downstream of exon 1 and U2 to the branch point upstream of exon 3 resulting in A complex. Due to masking of donor splice site of exon 2 by PMO, exon 2 is not considered an exon. Association of tri-snRNP U4/U6·U5 to the A complex forming B complex. Cleavage of U1 and U4 activates the spliceosome which leads to the first transesterification and lariat intermediate formation resulting in the C complex. The second transesterification assembles the exon sequences and the mature mRNA product and intron lariat including exon 2 are released.

Due to blockage and therefore failed recognition of the donor splice site by the subunits of the spliceosome, the first transesterification takes place between exon 1 and exon 3 skipping exon 2. As a result, subsequently cleaved lariat structure includes exon 2 and the final splicing product is shorter consisting of ligated exon 1 and exon 3.

3.4 Transient Expression using pEGFP-N1/mCherry-DMDEx23

The *mCherry-DMDEx23* reporter gene was designed to evaluate transfection efficiency of sequence specific PMO conjugate formulations inducing exon skipping in the physiological DMD gene *in vivo*. For establishment of the reporter system, functionality and suitability of the reporter gene for detecting DMD exon 23 skipping were first validated in HeLa cells transiently transfected with the pEGFP-N1/mCherry-DMDEx23 plasmid (plasmid map shown in **Figure 36**). Successful pDNA delivery led to eGFP expression. After pEGFP-N1/mCherry-DMDEx23 treatment, the cells were treated with PMO using two different PMO sequences to show sequence specificity of the reporter. PMO(Ex23) was used to induce DMD exon 23 skipping, leading to functional mCherry expression. PMO(705) served as "negative control" since the sequence is not complementary to the target site. The ratio of eGFP and mCherry expressing cells was evaluated using flow cytometry (**Figure 12**).

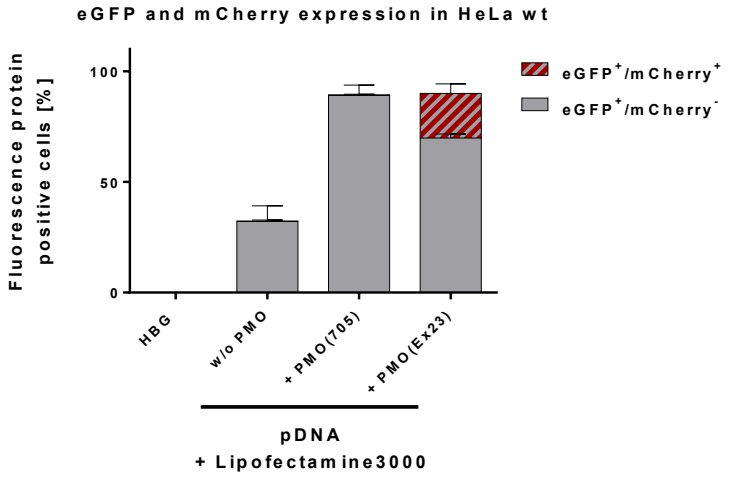

Figure 12 eGFP and mCherry expression of HeLa wt cells after transient transfection with pEGFP-N1/mCherry-DMDEx23 transfection and treatment with PMO–1195 conjugate formulations. 200 ng pEGFP-N1/mCherry-DMDEx23 per well were transfected with Lipofectamine 3000. PMO(705)–DBCO and PMO(Ex23)–DBCO were formulated with XP *#1195* at a molar ratio of 1:3 (PMO:XP) and used at a concentration of 2.5 µM.

Cells treated with pDNA and PMO conjugate formulations, regardless of the PMO sequence, showed a higher ratio of eGFP expressing cells, compared to the cells which were treated with pDNA only. The increase of eGFP expression can be explained by the construction of the pDNA and the position of *eGFP* and *mCherry-DMDEx23* in the *mCherry-DMDEx23-eGFP* gene. The eGFP gene sequence is located downstream of mCherry-DMDEx23 with no separate promoter of *mCherry-DMDEx23*. Stop codon read-through and noncanonical translation initiation could lead to a promotor independent eGFP expression. Noncanonical pathways can be induced and enhanced by cellular stress [252, 253] which could be caused by transfection agents. Another explanation is the additional Kozak consensus sequence and start codon between mCherry and eGFP. This phenomenon is described for fusion genes cloned into pEGFP-N1 vector. [254] Additionally, the usage of two subsequent transfections with different transfection agents could influence the eGFP expression. The addition of formulations containing *#1195* could also improve endosomal escape of pDNA which remained in endosomes.

Direct comparison between the two PMO variants confirmed sequence–specific response of the reporter system: treatment with PMO(Ex23)–1195 1:3 conjugate formulation led to 20% mCherry positive cells within the eGFP positive cell population, whereas treatment with PMO(705)–1195 1:3 did not induce mCherry expression.

In summary, a PMO sequence specific effect could be observed in HeLa cells transiently expressing mCherry-DMDEx23-eGFP leading to the assumption of functionality of the reporter gene. As a result, *mCherry-DMDEx23-eGFP* was used in order to establish a new stable reporter system based on the PMO(Ex23) sequence.

For the generation of a stable HeLa mCherry-DMDEx23 reporter cell line, *mCherry-DMDEx23* was integrated into a PiggyBac vector plasmid. Genomic integration was conducted by using the PiggyBac system and PB-mCherry-DMDEx23 pDNA delivery using Lipofectamine 3000.

3.5 Generation and Establishment of New Reporter Cell Line HeLa mCherry-DMDEx23

For evaluation of new carrier systems, a reporter system is required which reliably expresses an appropriate reporter which retains expression over several cell cycles. Since transient mCherry-DMDEx23-eGFP expressing HeLa cells showed PMO(Ex23) dependent mCherry expression, integration of mCherry-DMDEx23-eGFP into the genome of HeLa wt cells was the aim.

In order to do so, cells had to be treated simultaneously with the PiggyBac (PB) vector plasmid encoding the target *mCherry-DMDEx23* gene and additionally a PB-vector plasmid encoding the required transposase protein.

PiggyBac is a class II transposon (DNA-transposon) which is a mobile genetic element which can be transferred with the transposase protein via a "cut-and-paste" mechanism. Transposase induces single-strand breaks at the 3'ends of transposons resulting in a cascade of bond formations leading to ligation of transposons with the genomic DNA and therefore integration into the genome.[255-258]

3.5.1 Generation of PB Plasmid Containing *mCherry-DMDEx23*

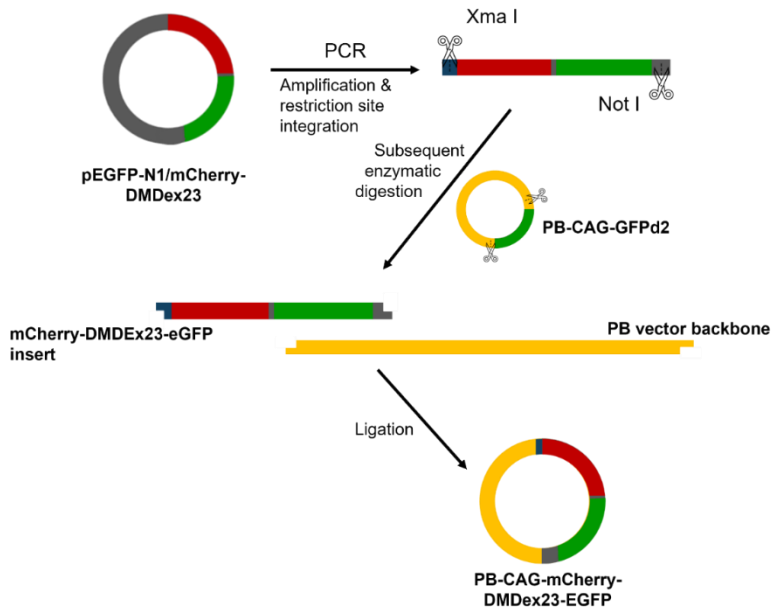

Figure 13 Schematic illustration of PB-mCherry-DMDEx23-eGFP generation.

The first step of the cell line generation was integration of the *mCherry-DMDex23* into the PB vector plasmid (**Figure 13**) via molecular cloning. For this purpose, *mCherry-DMDEx23-eGFP* was PCR amplified using pEGFP-N1/mCherry-DMDEx23 as template in order to include suitable terminal restriction sites via PCR primer design. A restriction site for Xma I was introduced at the 5' cloning site. A restriction site for Not I was introduced at the 3' cloning site. The mCherry-DMDEx23-eGFP PCR product served as insert which had to be integrated into the PB vector. The PB-CAG-GFPd2 plasmid served as template PB vector plasmid of which GFPd2 was cleaved to obtain the PB vector backbone. The mCherry-DMDEx23-eGFP insert and the PB vector backbone were ligated and amplified in DH6α E.coli. The plasmid map of the resulting PB-mCherry-DMDEx23-eGFP shown in **Figure 37**.

3.5.2 Generation of Stably Expressing HeLa mCherry-DMDEx23 Cells

HeLa wt cells were co-treated with 500 ng PB-mCherry-DMDEx23-eGFP vector plasmid and 200 ng of the Super PiggyBac Transposase expression vector (SBI, CA, USA) using Lipofectamine 3000 as transfection agent. The designed PB-mCherry-DMDEx23-eGFP contained the sequence of eGFP to serve as transfection control of the pDNA to facilitate evaluation. Three, 17, and 22 days after treatment, cells were evaluated using flow cytometry to determine the expression of eGFP (**Figure 14**).

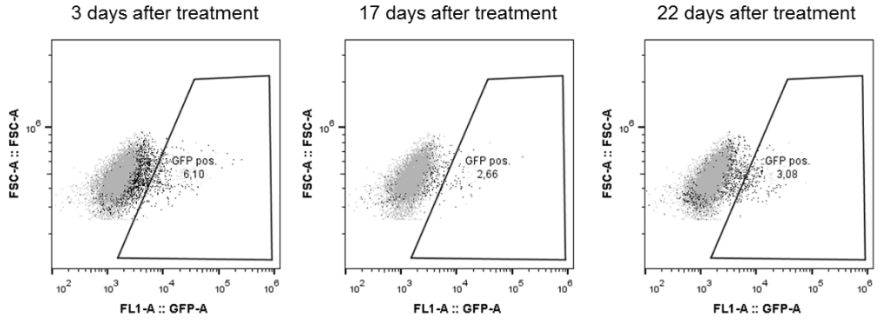

Figure 14 eGFP expression of HeLa cells treated with PiggyBac system. eGFP expression 3 days, 17 days, and 22 days after treatment with PB-CAG-mCherry-DMDEx23-eGFP and Super PiggyBac Transposase expression vector using Lipofectamine 3000. Grey: HBG treated HeLa wt cells; black: PB treated HeLa cells.

Three days after treatment, around 6.1% of the cells expressed eGFP which can also be caused by remaining plasmid in the cells. The decreasing eGFP signal over time was caused by elimination of the plasmid from the cells with remaining signal caused by stable integration of the reporter gene. In order to ensure complete plasmid removal and eGFP

expression caused by stably integrated reporter gene only, cells were cultivated for several more days. 22 days after treatment, the ratio of eGFP expressing cells decreased to approximately 3% which most likely are originated from stable integration of the whole *mCherry-DMDEx23-eGFP* into the genome. The cell population was expanded in order to sort eGFP positive cells indicating genomic presence of the whole reporter gene *mCherry-DMDEx23-eGFP* using fluorescence-activated cell sorting (FACS).

Figure 15 shows the gating strategy of the sorting process of eGFP positive HeLa-mCherry-DMDex23-eGFP mixed population in bulk. HeLa wt served as negative control sample to distinguish eGFP positive and negative cells in the treated cell sample. After gating the main population, single cell population and living cells, a total ratio of approximately 4.3% eGFP positive cells could be collected ("mixed population") numbering 10,832 cells.

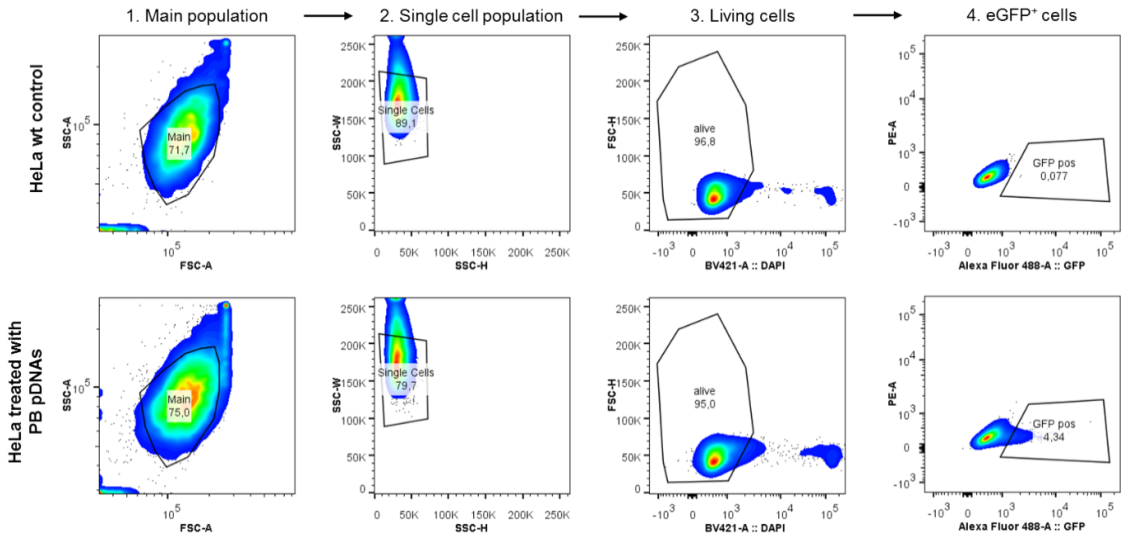

Figure 15 Gating strategy to sort eGFP positive cells. HeLa wt cells and HeLa cells treated with Super PiggyBac Transposase expression vector and PB-CAG-mCherry-DMDEx23-eGFP were sorted via fluorescence-activated cell sorting (FACS) 22 days after treatment. Sorting was performed by Dr. Lisa Richter (Biomedical Center Munich, Core Facility Flow Cytometry, LMU München).

The sorted mixed population was expanded, and monoclonal populations were generated by using limiting dilution method in 96-well plates. Only cell populations proposedly originating from one cell were taken into account. In total 20 monoclonal cell populations were obtained. In order to narrow down the test group, each clone was evaluated by the median fluorescence intensity (MFI, **Figure 16a**) and distributional width of the population regarding the eGFP signal (**Figure 16b**).

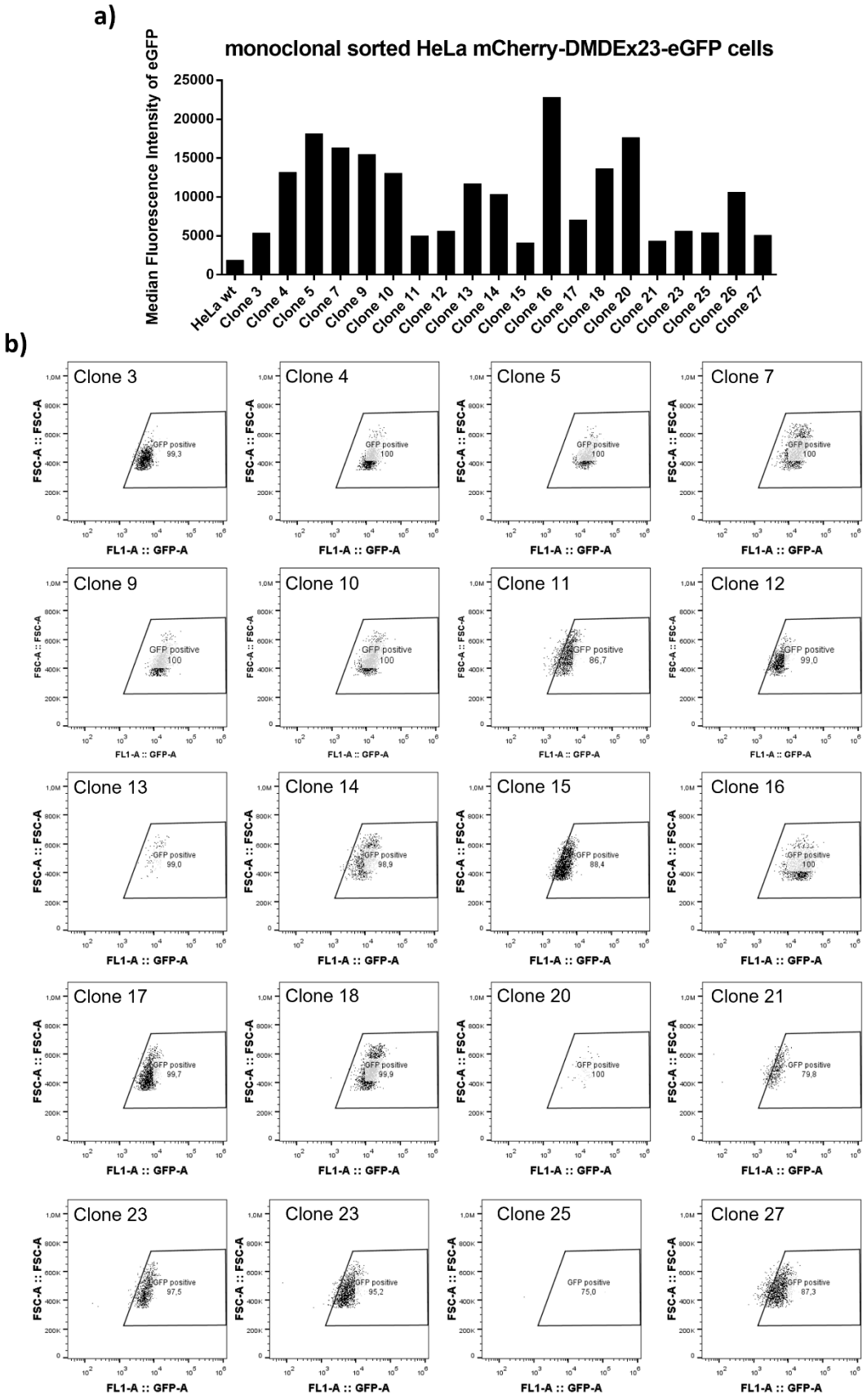

Figure 16 Monoclonal populations of sorted HeLa mCherry-DMDEx23 cells. a) Median fluorescence intensity (MFI) of eGFP of each monoclonal population. **b)** Forward scatter - eGFP dot plot of each monoclonal population.

The highest median fluorescence intensity of eGFP could be obtained in clone 16 but the distribution of the population was broad which excludes clone 16 for further testings. Additional high median fluorescence intensity values could be detected in clone 4, 5, 7, 9, 10, 18, and 20. The combination of median fluorescence and a narrow population distribution in the dot plot led to exclusion of several monoclonal populations and reducing the set to only five populations – clone 4, clone 5, clone 7, clone 9, and clone 10. The different eGFP MFI values and distribution can be caused by the locus of transposon integration and copy number. [259] The piggyBac transposon is inserted randomly into a tetranucleotide site TTAA by the transposase.[255-258] Suboptimal insertion loci can influence expression adversely. To ensure the usage of a cell population with a definite mCherry-DMDEx23-eGFP integration, a high eGFP MFI value and a narrow eGFP MFI value distribution were desirable.

For identification of a suitable monoclonal HeLa mCherry-DMDEx23 cell line, PMO(Ex23) was used together with the previously reported XP *#1195* conjugate formulation at a 1:3 ratio.[162] PMO(Ex23) induces exon 23 skipping in the mCherry-DMDEx23 reporter leading to functional mCherry expression.

The narrowed monoclonal HeLa mCherry-DMDEx23 population set consisting of clone 4, 5, 7, 9, and 10, were treated with PMO(Ex23)–1195 1:3 conjugate formulation at 2.5 µM and mCherry expression was determined. **Figure 17a** shows the comparison of each dot plot of PMO(Ex23) (green) and HBG (orange) treated monoclonal HeLa mCherry-DMDEx23 population in comparison to PMO(Ex23) (blue) and HBG (red) treated HeLa wt cells. Especially, the difference of mCherry expression of PMO(Ex23) and HBG treated monoclonal populations was considered (**Figure 17c**). Diagonal shift of HeLa wt cells treated with PMO(Ex23) conjugate formulations (**Figure 17a**) and slight increase of median fluorescence intensity (MFI) of eGFP (**Figure 17b**) could be caused by cellular stress resulting from conjugate formulation treatment.

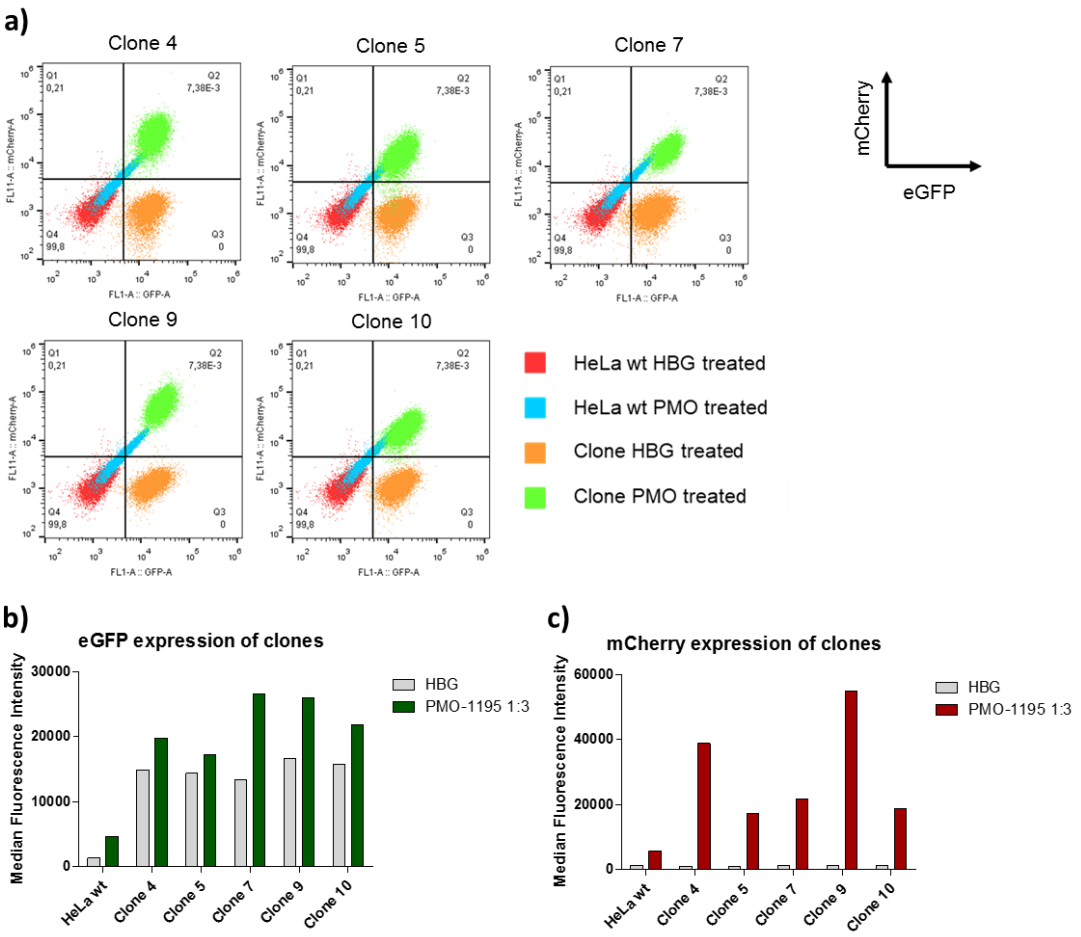

Figure 17 Identification of adequate monoclonal population. Monoclonal HeLa mCherry-DMDEx23 populations and HeLa wt cells were treated with PMO(Ex23)–1195 1:3 conjugate formulation at 2.5 µM for 24 h. eGFP and mCherry expression was evaluated using flow cytometry (FC). **a)** mCherry – eGFP dot plots of each monoclonal population in comparison to HeLa wt cells. **b)** Median fluorescence intensity of eGFP of each monoclonal population in comparison to HeLa wt treated with HBG and PMO(Ex23)–1195. **c)** Median fluorescence intensity of mCherry of each monoclonal population in comparison to HeLa wt treated with HBG and PMO(Ex23)–1195.

All monoclonal populations were treated with the same PMO(Ex23)–1195 1:3 sample but showed different increases in mCherry median fluorescence intensities. The monoclonal population originating from clone 9 showed highest sensitivity to PMO(Ex23) regarding mCherry expression. A reason for this could be the location of the integrated *mCherry-DMDEx23-eGFP* which could be more favorable in clone 9. Another possibility of the difference in median fluorescence intensities could be the number of copies which were integrated into the genome. The clear difference of mCherry MFI of PMO(Ex23) conjugate formulation and HBG treated, and the narrow distribution of the monoclonal population originating from clone 9 showed the potential of this monoclonal cell population.

To confirm the presence of the whole *mCherry-DMDEx23-eGFP* in the genome of HeLa mCherry-DMDEx23 cells, genomic DNA was isolated, and the gene sequence was PCR amplified. The PCR product was evaluated performing gel electrophoresis on a 1% agarose gel (**Figure 18**). The PCR product could be separated into three bands derived from amplification of the whole *mCherry-DMDEx23-eGFP* (~2042 bp), *mCherry-DMDEx23* without *eGFP* (~1290 bp), and *eGFP* only (~720 bp).

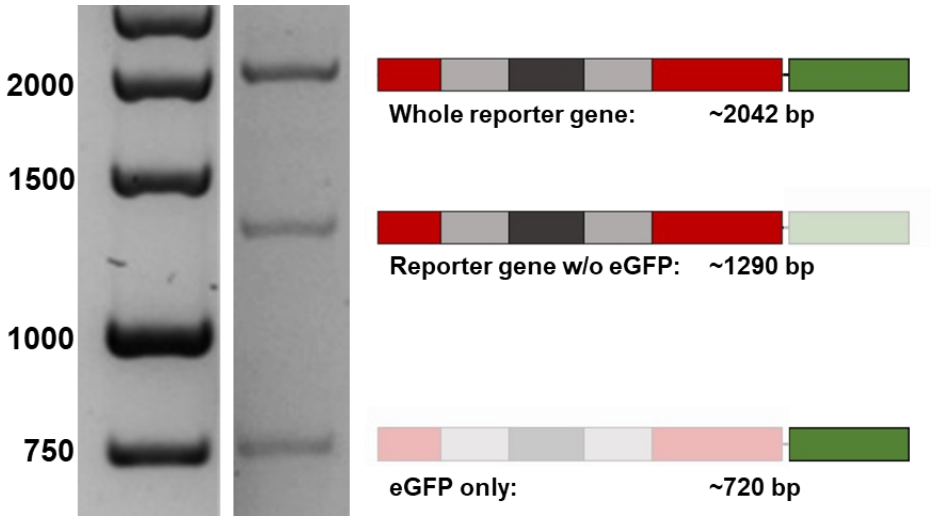

Figure 18 Verification of mCherry-DMDEx23 presence in HeLa mCherry-DMDEx23 genome. Genomic DNA of HeLa mCherry-DMDEx23 was isolated. mCherry-DMDEx23 was amplified using PCR and analyzed using agarose gel electrophoresis. Due to sequence similarity, sequences of mCherry-DMDEx23-eGFP, mCherry-DMDEx23 only, and eGFP only were obtained. Completeness of mCherry-DMDEx23-eGFP could be confirmed by Sanger sequencing after gel extraction of the corresponding band (~2042 bp).

The 5' and 3' terminal sequences of *mCherry* and *eGFP* sequences show a certain similarity which leads to additional amplification of incomplete reporter sequences. The band of the whole *mCherry-DMDEx23-eGFP* was extracted from the gel and the sample was Sanger sequenced confirming the target sequence. With this procedure, the presence of mCherry-DMDEx23-eGFP could be confirmed in the genomic DNA of HeLa mCherry-DMDEx23.

MFI of mCherry and eGFP of cells treated with PMO(Ex23) conjugate formulations and Sanger sequencing confirmation of the *mCherry-DMDEx23-eGFP* presence in the genome made the monoclonal HeLa mCherry-DMDEx23 cell line originating from clone 9 the reasonable candidate as new reporter cell line. As consequence this HeLa mCherry-DMDEx23 cells were used in all further *in vitro* experiments as reporter cell line.

3.5.3 mCherry-DMDEx23 Reporter System Validation

For further understanding and validation of the mCherry-DMDEx23 reporter system, the generated HeLa mCherry-DMDEx23 cells were treated with PMO–1195 1:3 conjugate formulations. PMO(705) conjugate formulations served as negative control without complementary binding site. The monoclonal reporter cell line was treated with PMO–1195 1:3 conjugate formulations at concentrations 2.5, 1.25, and 0.625 µM for 3 h (followed by 21 h incubation in fresh medium), 6 h (followed by 18 h incubation in fresh medium), 24, 48, and 72 h. The relative number of mCherry expressing cells (**Figure 19a**) and the median fluorescence intensities (MFI) of mCherry (**Figure 19b**) were determined by using flow cytometry. Evaluation of mCherry expression showed a concentration and time-dependent effect, where the increase of concentration and incubation time led to a higher ratio of mCherry positive cells, when treated with PMO(Ex23) conjugate formulation. In direct comparison, treatment with control conjugate formulation PMO(705)–1195 1:3 did not lead to substantial mCherry expression. The slight increase of the mCherry MFI of HeLa mCherry-DMDEx23 cells treated with negative control PMO(705) at increasing incubation time and concentration can be caused by cellular swelling and increasing internal complexity induced by cellular stress.[260]

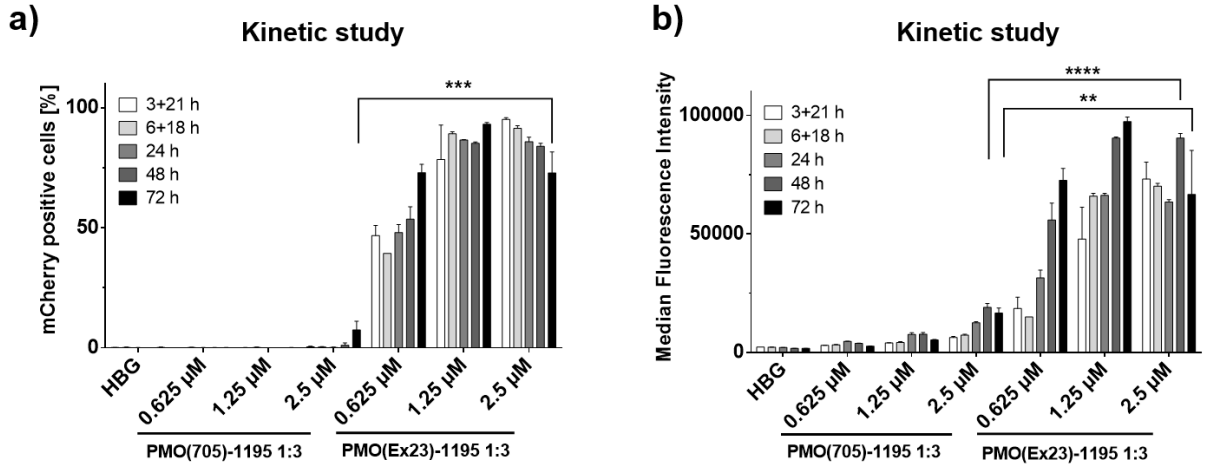

Figure 19 Establishment of the reporter system. a) mCherry positive HeLa mCherry-DMDEx23 cells (%) after incubation with PMO(Ex23) of PMO(705) conjugate formulations between 3 (+21 h) and 72 h. Extended incubation times without PMO before evaluation are indicated in brackets. **b)** Median mCherry fluorescence intensity (MFI) of HeLa mCherry-DMDEx23 cells after incubation with PMO(Ex23) of PMO(705) conjugate formulations between 3 (+21 h) and 72 h. Extended incubation times without PMO before evaluation are indicated in brackets.

To confirm the generation of the supposed mRNA splicing product and therefore the mechanism of action, a specific amplification approach was chosen: RNA was isolated from treated cells and reverse transcribed into cDNA. A nested PCR was carried out with an Nde I restriction digestion step between the two amplifications. DMD exon 23 contains the recognition site of Nde I, which leads to preferential amplification of DNA with skipped exon 23. Gel electrophoresis was used to analyze DNA samples obtained from HeLa mCherry-DMDEx23 cells treated with 2.5 µM PMO(Ex23)–1195 and PMO(705)–1195 1:3 or HBG buffer, respectively. Only in the case of PMO(Ex23)–1195 treated cells was a DNA band with a correct size of 280 bp detected (**Figure 20a**) and Sanger sequencing confirmed the correct sequence of mCherry reporter fragment after exon 23 skipping (**Figure 20b**).

In order to confirm the presence of the mCherry protein after successful PMO(Ex23) delivery, HeLa mCherry-DMDEx23 cells were treated for 24 h with PMO–DBCO conjugate formulations at 2.5 µM containing *#1195* and either PMO(Ex23)–DBCO or PMO(705)–DBCO as control. Cellular proteins were extracted, and a Western blot was performed using a primary rabbit anti-mCherry antibody and a secondary goat anti-rabbit antibody (**Figure 20c**). Only in case of cells treated with PMO(Ex23)–1195 1:3, mCherry protein could be detected further confirming the PMO sequence specificity and functionality of the reporter gene *mCherry-DMDEx23*.

To verify the functionality of the mCherry protein in a functional and imaging assay, a confocal laser scanning microscopy (CLSM) experiment was performed. HeLa mCherry-DMDEx23 cells were treated with PMO–1195 1:3 conjugate formulations for 24 h (**Figure 20d**). Only PMO(Ex23)–DBCO containing conjugate formulation could induce mCherry expression leading to cellular fluorescence.

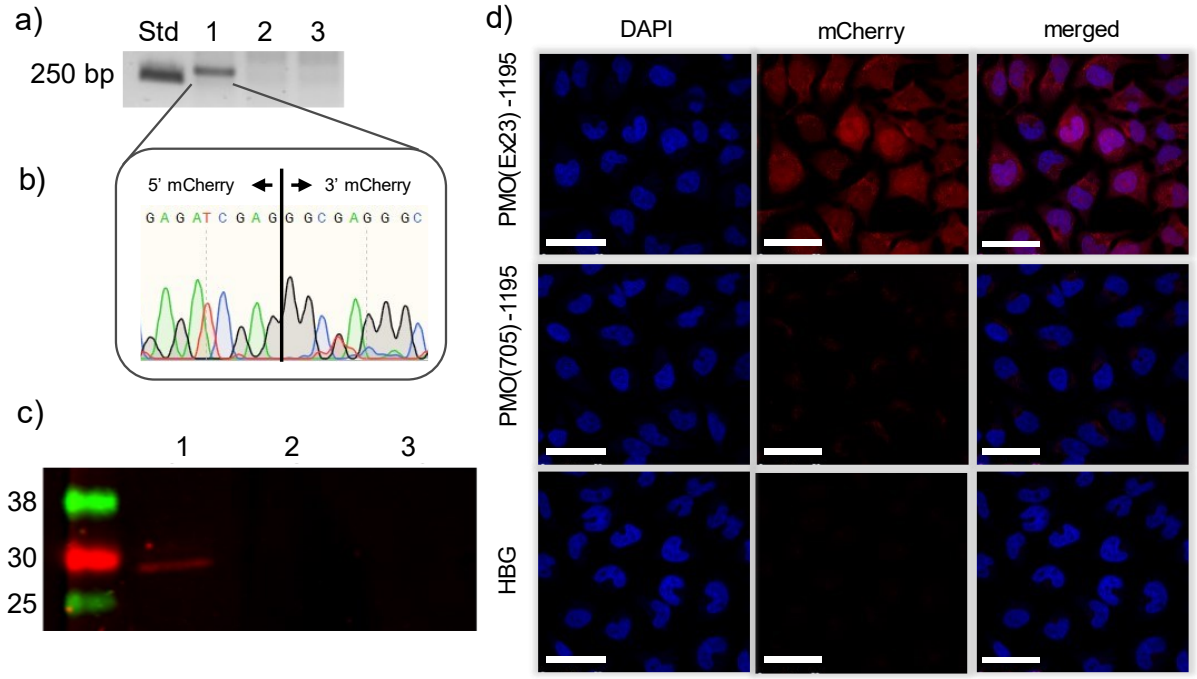

Figure 20 Establishment of new reporter system. a) Detection of mdx exon 23 skipping of mCherry-DMDEx23 mRNA by RT-PCR. Total RNA was extracted from cells 24 h after PMO(Ex23)–1195 and PMO(705)–1195 treatment (2.5 µM PMO). A sequence surrounding mdx exon23 in mCherry-DMDEx23 was amplified by RT-PCR. The band resulting from mdx exon 23skipping is shown (~280 bp). Std: DNA ladder; 1: PMO(Ex23)–1195; 2: PMO(705)–1195; 3: HBG. **b)** Exemplary Sanger sequencing results from the gel extracted band resulting from mdx exon 23 skipping (~280 bp). **c)** Detection of the mCherry protein by Western blotting. HeLa mCherry-DMDEx23 cells were treated with PMO(Ex23)–1195 and PMO(705)–1195 conjugate formulations (2.5 µM PMO) for 24 h. **d)** CLSM images of HeLa mCherry-DMDEx23 cells 24 h after transfection with PMO–1195 conjugate formulations containing PMO(Ex23)–DBCO or PMO(705)–DBCO respectively (2.5 µM PMO). Nuclei were stained with DAPI (blue), and mCherry is shown in red. Scale bar is 50 µm. CLSM experiment was performed by Miriam Höhn (Pharmaceutical Biotechnology, LMU Munich).

3.6 Screening of New Xenopeptides for PMO Delivery

Reporter cell lines are commonly used to assess the potential delivery system of choice to find favorable structural motifs and new best performers. To evaluate the ability of the reporter gene mCherry-DMDEx23 to serve as adequate reporter gene and to find highly potent carriers for PMO delivery, a small library of XPs with structural variations was screened. Variations in 1) presence of histidine (H), and 2) type of fatty acid was taken into account (**Figure 21**) which already showed efficient intracellular delivery of Cas9/sgRNA RNPs [183].

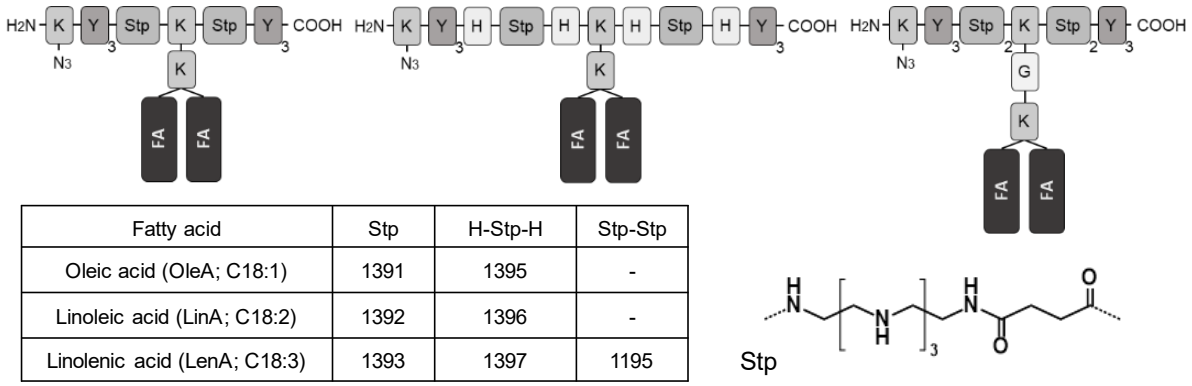

Fatty acid	Stp	H-Stp-H	Stp-Stp
Oleic acid (OleA; C18:1)	1391	1395	-
Linoleic acid (LinA; C18:2)	1392	1396	-
Linolenic acid (LenA; C18:3)	1393	1397	1195

Figure 21 Series of XP analogues screened for PMO delivery. Schematic illustrations of XP architectures classified according to the ionizable backbone into "Stp" (*#1391-#1393*), "H-Stp-H" (*#1395-#1397*) and "Stp-Stp" (*#1195*). The table summarizes individual fatty acids contained. K: lysine, Y: tyrosine; H: histidine; Stp: succinoyl tetraethylene pentamine; FA: fatty acid. Syntheses of *#1391,#1392, #1393, #1396, #1397* was performed by Dr. Yi Lin (Pharmaceutical Biotechnology, LMU München).

PMO–DBCO conjugate formulations of each oligomer were prepared in a molar ratio of 1:3 (PMO/XP). HeLa mCherry-DMDEx23 cells were used to screen the new XP library, using PMO(Ex23)–DBCO in order to skip *mdx* exon 23 and induce expression of functional mCherry. HeLa mCherry-DMDEx23 cells were treated with PMO(Ex23)–XP 1:3 conjugate formulations from 0.078 to 5 µM for 24 h and the ratio of mCherry expressing cells was evaluated (**Figure 22a**). The dose titration experiment ranging from 0.078 to 5 µM using the Stp1-library in comparison to *#1195* revealed new highly potent PMO carriers. In direct comparison to *#1195*. Histidine-containing XPs generally mediated higher transfection efficiencies even at low concentrations. Oleic acid, and linoleic acid (*#1395* and *#1396*) were found to be favorable structural elements in the new XP architectures. Over 90% of cells were mCherry positive after treatment with the most potent *#1395* and *#1396* conjugate formulations containing 156.25 nM PMO. In all cases, the ratio of mCherry expressing cells increased with an increasing PMO concentration. At the same time a dose dependent cytotoxicity at higher concentration was observed (**Figure 22b**), which illustrates the need for potent conjugate formulations with high activity at low doses.

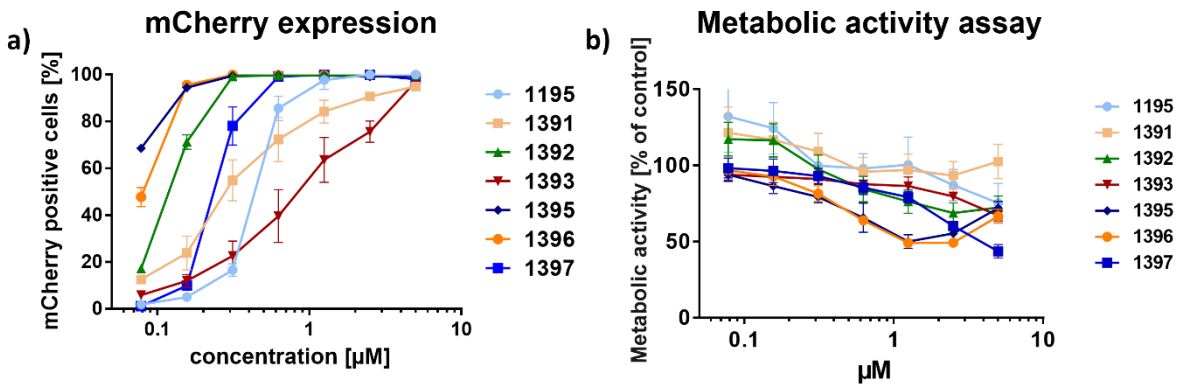

Figure 22 Structure-activity relationship of PMO(Ex23)–XP 1:3 conjugate formulations with an exposure time of 24 h. a) Splice switching activity in HeLa mCherry-DMDEx23 cells after 24 h treatment with PMO(Ex23)–XP 1:3 conjugate formulations (0.078-5 µM PMO). **b)** Dose-dependent effects of PMO(Ex23)–XP 1:3 conjugate formulations on metabolic acitivity of HeLa mCherry-DMDEx23 after 24 h treatment. PMO treatments ranged from 0.078125-5 µM. Syntheses of *#1391,#1392, #1393, #1396, #1397* was performed by Dr. Yi Lin (Pharmaceutical Biotechnology, LMU München).

In order to get a better assessment of the functionality of HeLa mCherry-DMDEx23 cells as reporter cell line, the well-established HeLa pLuc/705 cell line was used to screen the new XP library additionally. HeLa pLuc/705 cells contain *luciferase* which is interrupted by the thalassemic β-globin intron IVS2-705 between nucleotide 1268 and 1269. The thalassemic mutation in the β-globin intron generates an additional 5' splice site and therefore activates a cryptic 3' splice site 126 nucleotides upstream. Consequently, aberrant splicing occurs, the sequence of the β-globin intron retains and translation into functional luciferase is hindered [261]. After treating HeLa pLuc/705 cells for 24 h, overall luminescence of each well was determined after adding luciferin (**Figure 23a**). PMO(705)–DBCO containing conjugate formulations were used in HeLa pLuc/705 cells in order to mask the additional 5' splice site leading to exon skipping and functional luciferase expression. The same XP library was screened in comparison to *#1195*. PMO(705)–XP 1:3 conjugate formulations containing *#1391*, *#1392*, *#1395*, and *#1396* increased luciferase activity level to at least 90-fold at a concentration of 625 µM. *#1395* containing PMO(705)–XP 1:3 conjugate formulations could even increase luciferase activity to nearly 100-fold at 0.3125 µM. With increasing concentration, all conjugate formulations showed clear decrease in luciferase activity. The negative correlation between high PMO–XP conjugate formulations and low luciferase activity can be explained with a metabolic activity assay (**Figure 23b**). All conjugate formulations led to lower metabolic activity of the cells presumably due to higher toxicity which led to the drop of

luciferase activity levels. For the selection of potential future best performers, luciferase activity levels as well as metabolic activity have to be considered in this reporter cell line.

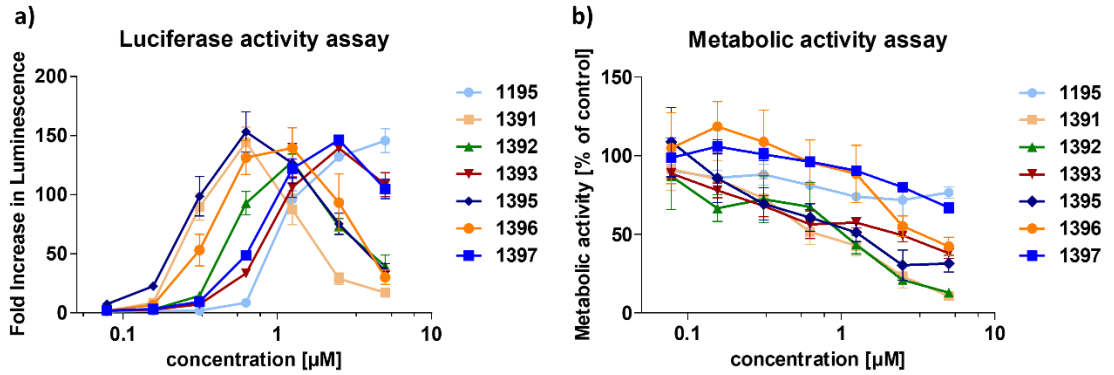

Figure 23 Structure-activity relationship of PMO(705)–XP 1:3 conjugate formulations. a) Splice switching activity in HeLa pLuc/705 cells after 24 h treatment with PMO(705)–XP 1:3 conjugate formulations (0.078-5 µM PMO). **b)** Metabolic activity of HeLa pLuc705 cells after 24 h treatment with PMO(705)–XP 1:3 conjugate formulations (0.078-5 µM PMO). Syntheses of *#1391,#1392, #1393, #1396, #1397* was performed by Dr. Yi Lin (Pharmaceutical Biotechnology, LMU München).

These findings in HeLa mCherry-DMDEx23 are in line with results in the well-established HeLa pLuc/705 cells which makes the new reporter system a suitable screening platform.

The best performing PMO conjugate formulations contained XP *#1392*, *#1395*, *#1396* and were additionally compared to previously established *#1195* conjugate formulation in experiments with short exposure times of 5 (**Figure 24a**), 15 (**Figure 24b**) and 30 min (**Figure 24c**).

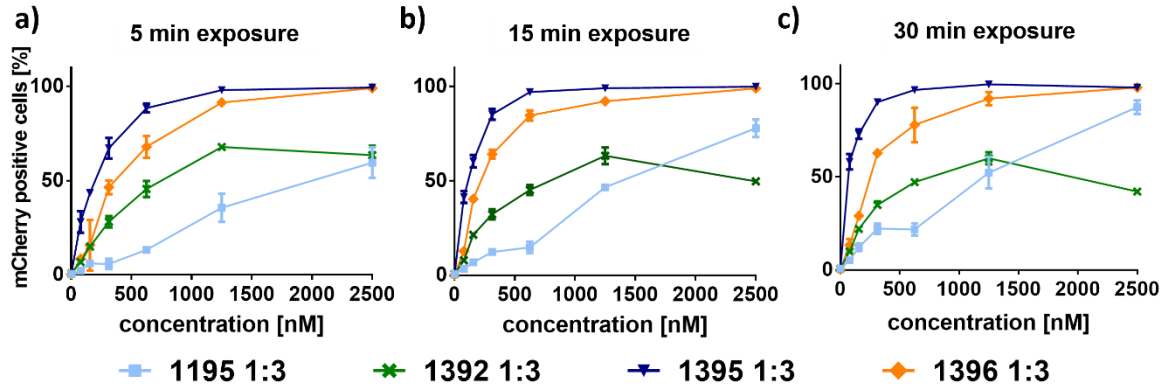

Figure 24 Structure-activity relationship of PMO(Ex23)–XP 1:3 conjugate formulations after short exposure times. Splice switching activity in HeLa mCherry-DMDEx23 cells after 5 min **(a)**, 15 min **(b)**, 30 min **(c)** exposure to PMO(Ex23)–XP 1:3 conjugate formulations (0.078-2.5 µM PMO) and subsequent incubation in fresh medium for 24 h. Syntheses of *#1392 and #1396* was performed by Dr. Yi Lin (Pharmaceutical Biotechnology, LMU München).

After the indicated exposure to PMO conjugate formulations, cells were incubated in fresh medium until 24 h since starting the experiment. Especially, XP *#1395* and *#1396* conjugate formulations turned out to be very potent and resulted in >45% mCherry positive cells even after exposure to a moderate PMO dose of 312.5 nM for 5 min only.

To assess favorable properties of PMO(Ex23)–1395 conjugate formulations in more detail, an additional comparison with PMO(Ex23)–1195 was carried out at low PMO concentrations between 2.4 and 312.5 nM (**Figure 25**). HeLa mCherry-DMDEx23 cells were treated for 24 h. The dose-response curves clearly illustrate much higher potency of *#1395*, which mediates splice switching already at PMO concentrations ≤5 nM.

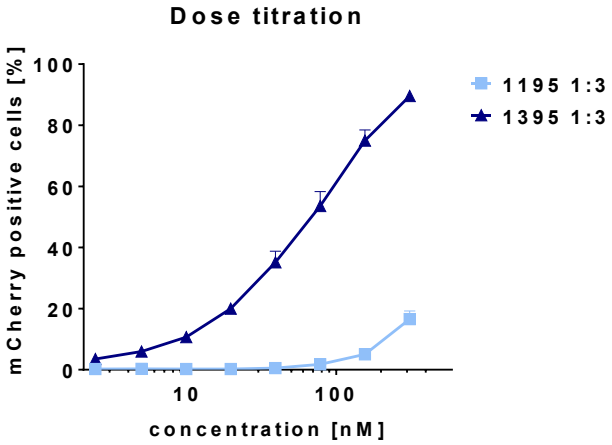

Figure 25 Dose titration of PMO(Ex23)–XP 1:3 conjugate formulations in nanomolar range. Dose-titration of PMO(Ex23)–1195 and –1395 conjugate formulations (2.4-312.5 nM PMO) with exposure of HeLa mCherry-DMDEx23 for 24 h. Percentage of mCherry expressing cells was determined 24 h after treatment. Data are presented as mean ± SD (n = 3).

To confirm the formation of PMO–XP nanomicelles with PMO(Ex23)–DBCO, transmission electron microscopy (TEM) was used for evaluation. Unformulated PMO(Ex23)–DBCO and conjugate formulations with already published *#1195* and new *#1395* was investigated at a concentration of 12.5 µM in HEPES buffer (**Figure 26a**). Unformulated PMO(Ex23)–DBCO did not self-assemble, whereas conjugate formulations with *#1195* and *#1395* at a molar ratio of 1:3 (PMO:XP) formed spherical nanomicelles with diameters of approximately 11.3 nm and approximately 14.7 nm, respectively (**Figure 26b**).

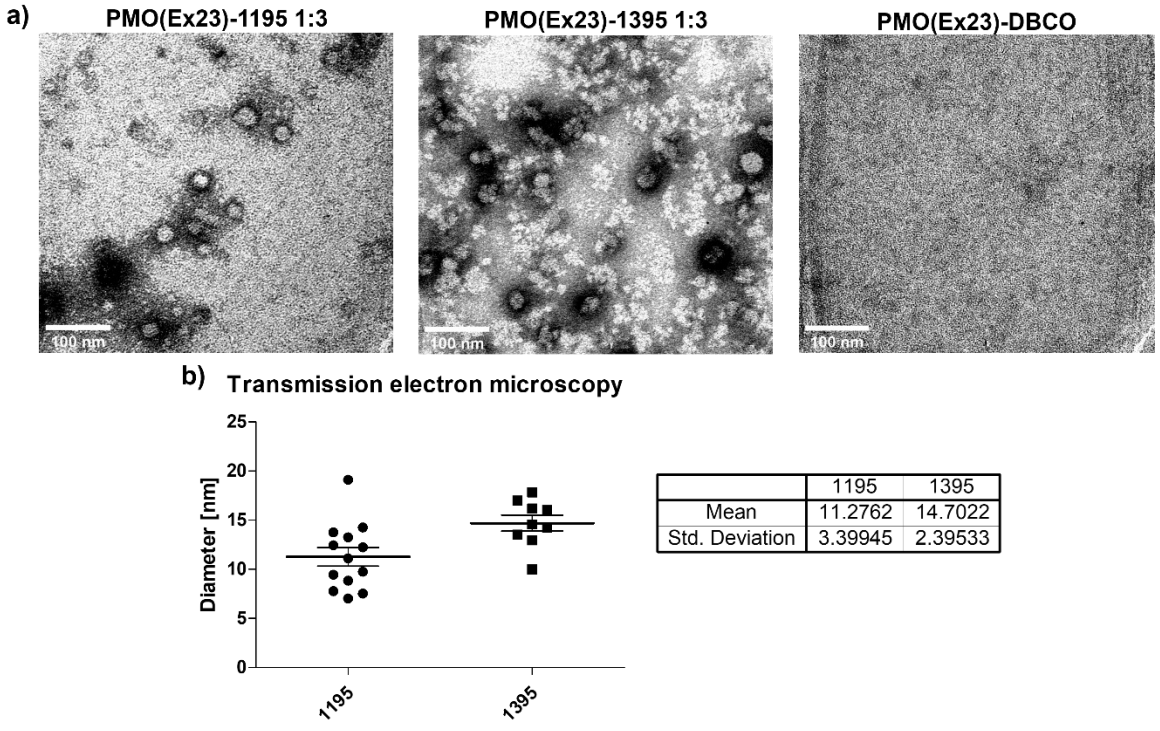

Figure 26 Nanomicelle formation of PMO(Ex23) conjugate formulations. a) Transmission electron microscopy (TEM) images of unformulated PMO(Ex23)–DBCO or conjugate formulations with *#1195* and *#1395* at a molar ratio of 1:3 (PMO:XP). **B)** Size distribution of nanomicelles detected in TEM. (*#1195* conjugate formulation : n=13; *#1395* conjugate formulation: n=9). TEM was performed by Susanne Kempter (Physics, soft condensed matter group, LMU München).

The high splice switching activity of the *#1395* conjugate formulation even after short exposure times suggests a favorable cellular uptake of the contained PMO cargo. To assess the difference of *#1195* and *#1395*, cellular uptake of conjugate formulations containing 5% Alexa Fluor 647 (AF647) labeled PMO into HeLa mCherry-DMDEx23 cells was determined by flow cytometry after 0.5 and 24 h incubation time (**Figure 27a,b**). Both conjugate formulations showed time- and concentration-dependent uptake characteristics, and at both time points, direct comparison confirmed a higher extent of PMO internalization mediated by the *#1395* conjugate formulation, which correlates with the increased splice switching activity. The observation, that effects of PMO(Ex23) treatment on splicing modulation could already be detected at much lower concentrations in HeLa mCherry-DMDEx23 cells, can be explained by two reasons: first, the detected AF647 signal in the case of uptake experiments results from 5% AF647-labeled PMO in the formulation, whereas each PMO(Ex23) molecule can be active in splice switching experiments. Second, PMO(Ex23) causes an amplifying effect on mCherry expression, since each molecule can modulate splicing of several mCherry-DMDEx23 pre-mRNAs and

each mature mRNA can be translated into protein repeatedly. In contrast, the intensity of AF647 is directly correlated with the PMO concentration. These considerations translate into the high sensitivity of the mCherry-DMDEx23 reporter system. Additionally, confocal laser scanning microscopy (CLSM) experiments confirmed beneficial cellular uptake of *#1395* PMO conjugate formulations (**Figure 27c**).

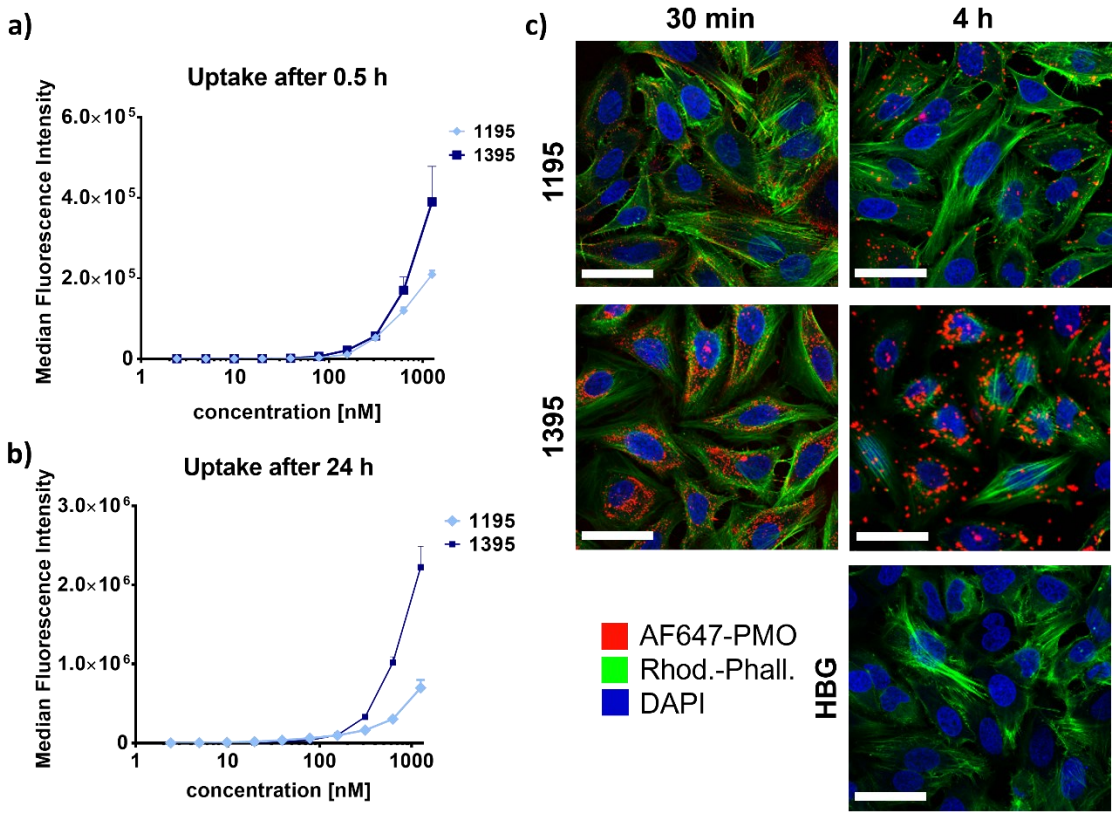

Figure 27 Cellular uptake of PMO–XP conjugate formulations. a,b) Cellular uptake of AF647-labeled PMO in HeLa mCherry-DMDEx23 cells 0.5 h (a) and 24 h (b) after treatment with PMO–1195 or PMO–1395 conjugate formulations containing 5% AF647–PMO(705) and 95% PMO(Ex23). Total PMO concentrations ranged from 2.4 nM to 1250 nM. **C)** CLSM images of HeLa wt cells after treatment with PMO–1195 and PMO–1395 conjugate formulations (5% AF647–PMO(705), 95% PMO(Ex23); 2.5 µM total PMO). Nuclei were stained with DAPI (blue), actin filaments with rhodamine phalloidin (green). AF647 fluorescence is indicated in red. Scale bar represents 50 µm. CLSM experiment was performed by Miriam Höhn (Pharmaceutical Biotechnology, LMU München).

After endocytotic uptake, nanoparticles are frequently entrapped in endosomes, which hampers the reach of other intracellular compartments. The internal volume of endosomes represents an acidic environment due to the activity of proton pumps, which is a frequently used trigger for inducing endosomolytic or fusogenic properties of delivery systems. To elucidate the impact of low endosomal pH on the delivery efficiency, treatments of HeLa mCherry-DMDEx23 cells with PMO(Ex23)–1195 and PMO(Ex23)–1395 conjugate formulations were performed in the presence and absence of bafilomycin

A1 (BafA1). BafA1 is an inhibitor of vacuolar-type H^+-ATPase (V-ATPase) and reduces endosomal acidification. Previous works could show that transfection with delivery systems based on ionizable structural motifs can be inhibited by BafA1.[184, 262-266] By using the mCherry-DMDEx23 reporter cells, the dependency of successful PMO delivery on the endosomal pH was evaluated on a functional level. The transfection efficiencies of *#1195* as well as *#1395* conjugate formulations were decreased in the presence of BafA1 compared to controls without BafA1 (**Figure 28a**). Especially, after 4 h PMO exposure time, BafA1 had significant influence on the *#1395* formulations. At the highest concentration, *#1395* containing formulations seem to overload the cells probably leading to endocytosis independent uptake to a certain extent. Regardless of the exposure time, BafA1 treatment seemed to decrease the MFI of mCherry expressing cells to a similar value (**Figure 28b**).

In order to confirm that the reporter gene expression was not influenced by BafA1 itself but by the PMO conjugate formulations, eGFP expression levels of each sample was evaluated simultaneously. As shown in **Figure 28c**, eGFP mean fluorescence intensities of cells did not differ in presence or absence of BafA1, whereas the ratio of mCherry expressing cells is influenced by the PMO which is contained in the conjugate formulation, the concentration and the presence and absence of BafA1. Especially after 4 h PMO exposure time, BafA1 had significant influence on the *#1395* conjugate formulations. These findings lead to the conclusion that the evaluated PMO–XP conjugate formulations depend on endosomal acidification during the intracellular delivery process.

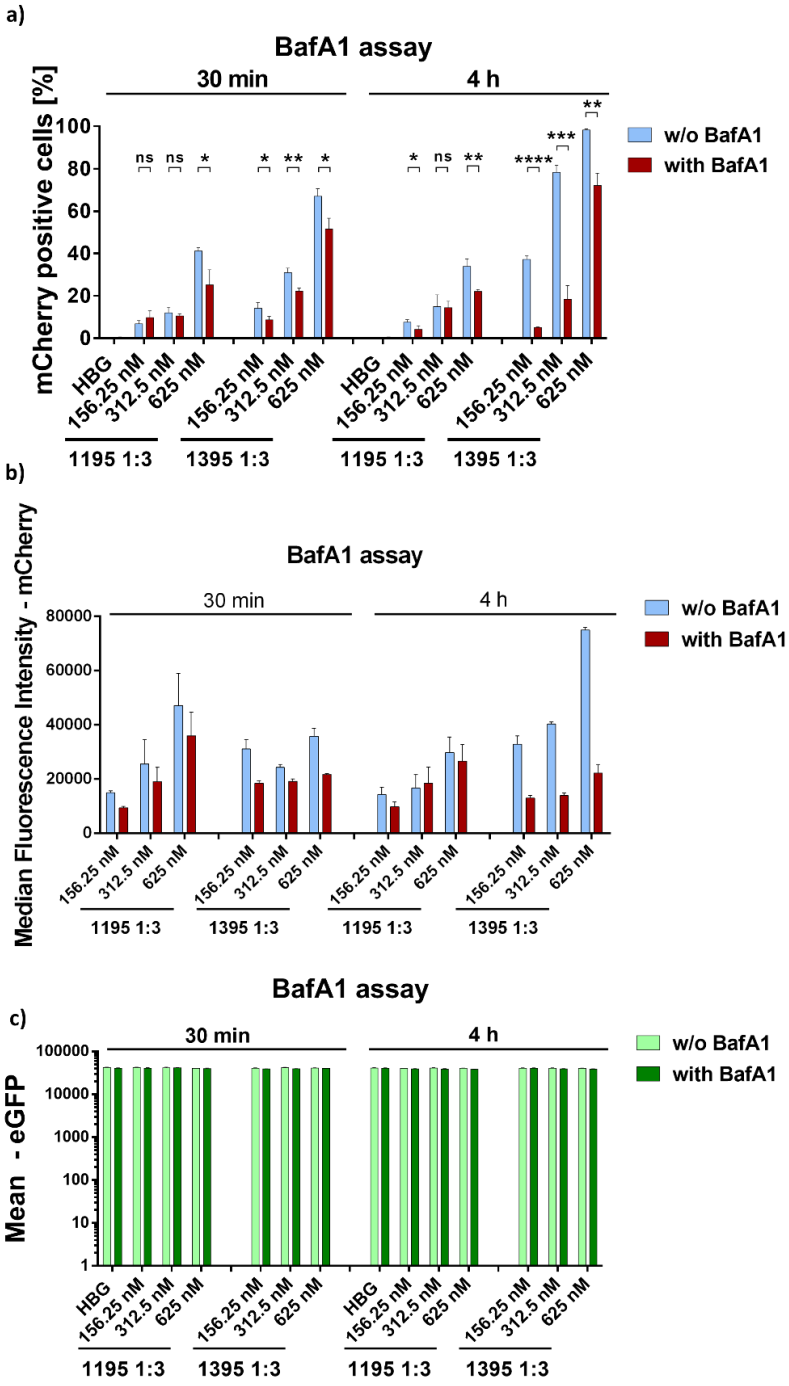

Figure 28 Influence of endosomal acidification on splice switching activity of PMO–XP conjugate formulations determined by V-ATPase inhibition with bafilomycin A1 (BafA1). HeLa mCherry-DMDEx23 were preincubated with BafA1 (200 nM) for 2 h and cells were treated with PMO(Ex23)–1195 or -1395 formulations. Medium was replaced by fresh medium 30 min or 4h after treatment and mCherry positive cells were quantified after a total incubation time of 24 h. Influence on mCherry expression regarding the ratio of mCherry expressing cells **(a)** and median fluorescence intensity of mCherry positive cell population **(b)** eGFP **(c)** expression. Statistical significance was estimated using the two-tailed student's t-test,(a) **** $p \leq 0.0001$, *** $p \leq 0.001$, ** $p \leq 0.01$, * $p \leq 0.05$. ns $p > 0.05$. Data are presented as mean ± SD (n = 3).

From the different flow cytometric evaluations determining transfection efficiencies at different exposure and incubation times and cellular uptake, it is visible that using *#1395* as carrier for PMO(Ex23) had a beneficial effect on PMO delivery over *#1195*. Beside the different used fatty acids, the number of protonatable amines in the backbones differs, which leads to a change in hydrophobicity of the XPs. In order to assess hydrophobicity of the PMO–1195 and PMO–1395 conjugate formulations, the $logD_{7.4}$ value was determined. PMO(Ex23)–1195 and –1395 conjugate formulations containing 5% AF647–PMO(705)–DBCO were prepared and $logD_{7.4}$ values were determined by quantifying AF647 fluorescence of the octanol and water phase after mixing and phase separation.[183, 247] The determined separation in octanol and water (**Figure 29a**) and the resulting $logD_{7.4}$ values (**Figure 29b**) indicate a higher hydrophobicity of the PMO–1395 conjugate formulation. As well known, higher hydrophobicity has a notable effect of nanoparticle interactions with cells and cellular uptake.[267, 268] The more hydrophobic PMO(Ex23)–1395 conjugate formulation in general improves nanomicelle-cell interaction which results in a higher and faster cellular uptake and therefore a higher transfection efficiency.

a)

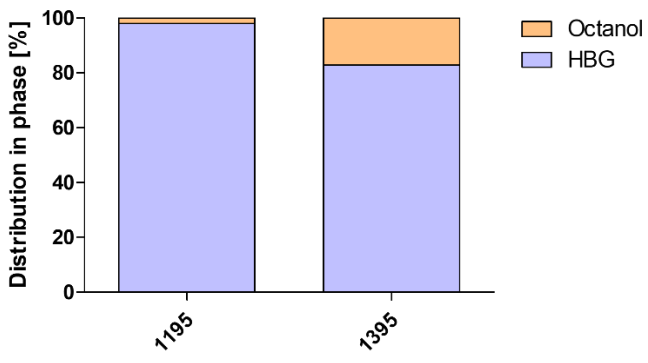

b)

Formulation	$LogD_{7.4}$(HBG)
1195	-1,69
1395	-0,68

Figure 29 Hydrophobicity of PMO(Ex23)–XP conjugate formulations. a) Distribution of PMO(Ex23)–XP conjugate formulations in HBG and octanol after phase separation experiment. **b)** Logarithmic octanol-HBG distribution coefficient at pH7.4 ($LogD_{7.4}$) resulting from phase separation experiment using XP *#1195* and *#1395* at a molar ratio of 1:3 (PMO : XP).

3.7 In Vivo Evaluation

The new mCherry-DMDEx23 reporter gene was designed to enable use of the same PMO sequence *in vitro*, which can also be used for DMD exon 23 skipping *in vivo*. The read-out system based on several subsequent PCRs starting transforming isolated mRNA into cDNA. Specific amplification via PCRs could finally yield DMD exon 20-24 sequence amplicons. Unaffected splicing resulted in full exon 20-24 sequence with a size of approximately 633 bp. Modulated splicing led to exon 23 skipping resulted in Δexon 23 sequence with a size of approximately 420 bp.

The *in vitro* screening identified the highest PMO delivery potency for the PMO–1395 conjugate formulation, which was therefore selected for *in vivo* evaluation. PMO(Ex23)–1395 as well as PMO(705)–1395 and unformulated PMO(Ex23) were intravenously injected into BALB/c mice (BALB/cByJRj, Janvier, Le Genest-Saint-Isle, France). After 48 h, DMD exon 23 skipping in brain, spleen, kidney, liver, lung, heart, and quadriceps femoris muscle was evaluated by RT-PCR *ex vivo*. **Figure 30** shows the gel electrophoresis of each organ and splicing modulation ratios shown on the right side of each data set which were determined by evaluating intensities of each band of each sample. The ratio of full sequence exon 20-24 including exon 23 was determined, leading to the full splice modulation ratio. The first group of mice served as negative control and were treated with the PMO–1395 1:3 conjugate formulation containing PMO(705)–DBCO (**Figure 30a**). PMO(705)–1395 1:3 did not show splice modulation. Since PMO(705) does not bind to the specific splice site in the DMD mRNA, no splice modulation was induced. The second group of mice was treated with free 3' primary amine modified PMO(Ex23) (**Figure 30b**). Since the sequence of PMO(Ex23) complementary binds to the splice site of the DMD intron 23, exon 23 skipping should be induced. Treatment with unmodified PMO(Ex23), leads to exon 23 skipping, especially in muscles. Conjugation and formulation with XP *#1395* led to an inhomogeneous distribution of splice modulation in all organs except from the muscle (**Figure 30c**).

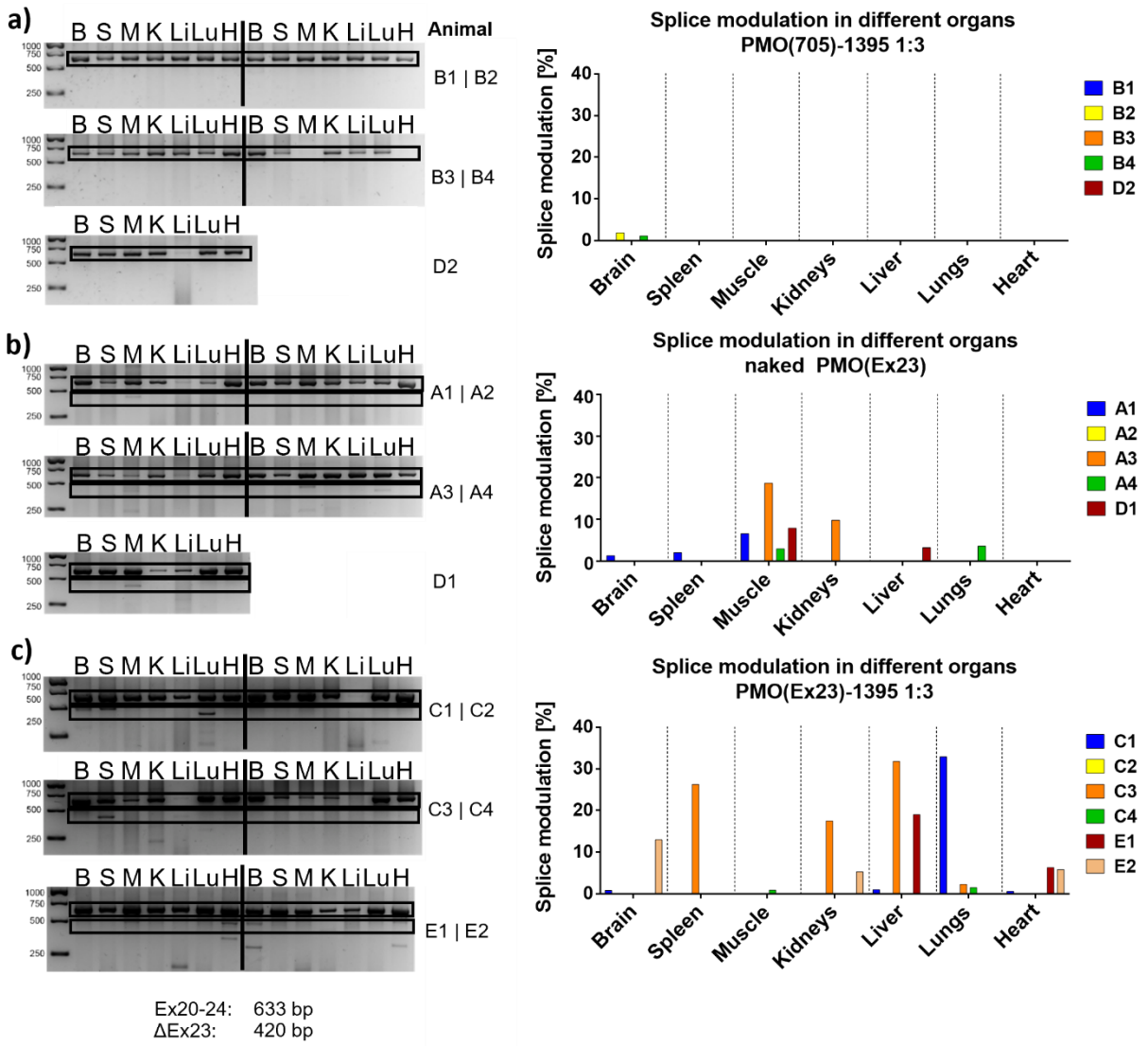

Figure 30 ***In vivo*** **splicing modulation of DMD mRNA in BALB/c mice determined by RT-PCR.** Total RNA was extracted from homogenized organs 48 h after intravenous injection of PMO conjugate formulations (375 µg PMO) and nested RT-PCR was conducted to amplify DMD Ex20-24. **a)** PMO(705)–1395 1:3 (n=5), **b)** free 3' primary amine modified PMO(Ex23) (n=5), and **c)** PMO(Ex23)–1395 1:3 (n=6). Single organs are indicated as: "B" = brain, "S" = spleen, "M" = quadriceps femoris muscle, "K" = kidneys, "Li" = liver, "Lu" = lung, "H" = heart. Ratios of splicing modulation were determined using ImageJ Software and shown on the right side of each data set. Animal experiments were performed by veterinarians Jana Pöhmerer and Dr. Ulrich Wilk.

Mean values of each splice modulation ratio enabled a better understanding and comparability of the different groups (**Figure 31a**). While unformulated PMO(Ex23) showed pre-dominant splice switching activity in the skeletal muscle, *#1395* led to a redistribution to different organs: with the PMO(Ex23)–1395 conjugate formulation exon skipping in the skeletal muscle was reduced; instead activity was observed in spleen, kidneys, liver, lung, and some splicing modulation was even observed in brain and heart. As this experiment is based on splice switching activity, a clear biodistribution is not

shown. Already published studies on biodistribution of unformulated PMOs showed less plasma protein binding due to the uncharged PMO backbone and renal excretion.[269] Slight exon skipping activity in the kidneys after treatment with unformulated PMO(Ex23) can therefore be explained with renal excretion.

The backbone modifications of *#1395* lead to slightly increased hydrophobicity of the conjugate formulations compared to PMO–1195 formulations which could be beneficial for crossing the blood-brain-barrier (BBB). In this experiment, mRNA was isolated from whole brain samples regardless of cell types. Exon skipping could take place in several neuronal cell types as well as in cerebral endothelial cells. In order to confirm BBB crossing, verification of splice switching activity in neurons has to be executed in the future. The decreased splice switching activity in skeletal muscles could be caused by entrapment of the PMO–1395 conjugate formulations in the interstitial space where exon skipping could not be induced.

Sanger sequencing confirmed successful exon 23 skipping (gel electrophoresis: **Figure 31b**, 633 bp band: **Figure 31c**, 420 bp band: **Figure 31d**). However, it has to be noted that the PMO(Ex23)–1395 group exhibited high variability and individual animals showed high splicing modulation, in contrast to others. It is speculated, that the high standard deviation could be caused by a suboptimal reconstitution of freeze-dried PMO conjugate formulations at high concentrations for *in vivo* application. In this case, further optimization of the conjugate formulation of concentrated *in vivo* samples, for instance by using cryo- and lyoprotectants during the freeze-drying process, could address issues with nanoformulation homogenicity in the future.

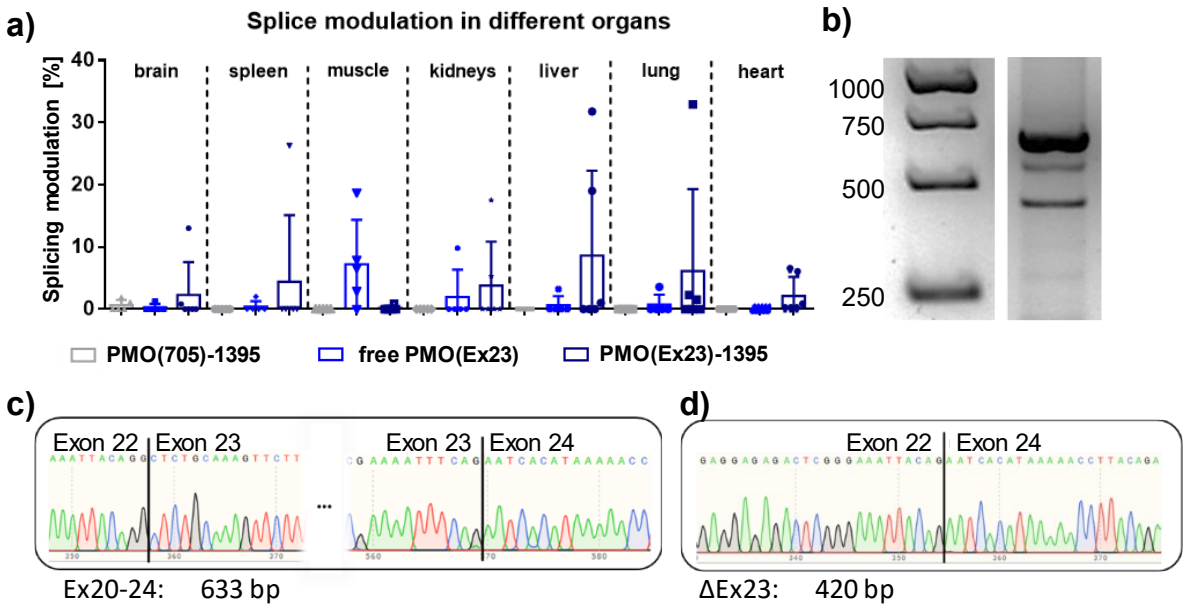

Figure 31 ***In vivo*** **mRNA splicing modulation in BALB/c mice. a)** Comparison of DMD mRNA splicing modulation in different organs of BALB/C mice determined *ex vivo* by RT-PCR 48 h after intravenous injection of PMO(Ex23)–1395, PMO(705)–1395 conjugate formulations or unformulated PMO(Ex23). Total RNA was extracted from homogenized organs and nested RT-PCR was conducted to amplify DMD Ex20-24. (PMO(705)–1395, n=5; free PMO(Ex23)–DBCO, n=5; PMO(Ex23)–1395, n=6). All formulations contained 375 µg PMO. **b)** Exemplary gel electrophoresis result showing splicing modulation in the lung of animal C1 treated with PMO(Ex23)–1395. **c, d)** Sanger sequencing of gel extracted bands corresponding to approx. 633 bp (c) and 420 bp (d) fragments. Expected sequences of complete DMD Ex20-24 (~633 bp, c) and after DMD exon 23 skipping (~420 bp, d) were found. Animal experiments were performed by veterinarians Jana Pöhmerer and Dr. Ulrich Wilk.

4. Summary

Nucleic acid therapeutics as an innovative class of biopharmaceuticals represent a versatile approach to address diseases at its roots. The variability of therapeutic nucleic acid sequences and chemical structures expands the flexibility, and the range of applications, since they are designed to target specific endogenous nucleic acid sequences or molecular structures. Despite the theoretical potential of therapeutic nucleic acids, safe and efficient delivery of sufficient therapeutic amount is limited due to its fast excretion and low cellular uptake. Therefore, development of potent, multifunctional, and flexible carrier systems is obligatory to obtain sufficient passage of several biological and physicochemical barriers including cargo packaging, intracellular delivery, endosomal escape, and cargo release at the target site. In order to overcome delivery hurdles of charged and uncharged nucleic acids, proteins, and other therapeutics, sequence-defined XPs consisting of α-amino acids, artificial amino acids, and different hydrophobic modifications were synthesized using solid-phase peptide synthesis. For the preinvestigation of delivery systems, specific and suitable *in vitro* reporter systems serve as tools for identification of potent carriers. The resulting knowledge is adapted to *in vivo* evaluation subsequently in order to determine potential therapeutic biopharmaceutical formulations.

A potential class of biopharmaceuticals includes phosphorodiamidate morpholino oligomers (PMOs), which are artificial and uncharged antisense oligonucleotides (ASOs). The uncharged backbone of PMOs results in favorable stability, nuclease-resistance, and immunogenicity and cytotoxicity profile. The ability of PMOs to modulate pre-mRNA splicing lead to modulation of cellular processes and restoration of functional gene expression. Due to this particular mechanism of action, specific *in vitro* models are essential to evaluate transfection efficiencies through splicing modulation. Transfer from *in vitro* to *in vivo* usually is accompanied with PMO modification, e.g., conjugation to fluorescent dye, which changes the molecule properties. A new positive read-out system based on mCherry and the murine *mdx* model to facilitate splice switching oligonucleotide (SSOs) formulation screenings was developed. This new platform provided the possibility to use the same PMO conjugate formulation compositions *in vitro* as *in vivo* without

additional modifications. The mCherry-DMDEx23 reporter consist of the split mCherry sequence which is interrupted by the *mdx* DMD exon 23 flanked by intronic sequences. The reporter cell line HeLa mCherry-DMDEx23 could be generated in which successful PMO delivery resulted in mCherry expression caused by *mdx* exon 23 skipping.

The application of the mCherry-DMDEx23 reporter was demonstrated by the screening of a series of XPs for PMO delivery. Potent XP–PMO conjugate formulations could be identified containing a more hydrophobic, ionizable backbone. Following a consequent *in vitro-in vivo* workflow, the best-performing conjugate formulation PMO(Ex23)–1395, identified *in vitro*, was subsequently tested *in vivo*. By using RT-PCR of *ex vivo* isolated mRNA, skipping of DMD exon 23 was confirmed in the spleen, kidneys, liver, and lung as well as to a minor extent in brain and heart of healthy BALB/c mice. In sum, this work presents a convenient workflow for development of SSO formulations based on a combination of the new DMD exon 23 skipping reporter and physiological DMD exon 23 skipping in mice. Furthermore, highly potent PMO conjugate formulations were identified, which cause a redistribution of PMO *in vivo* and could enable splicing modulation in tissues beyond skeletal muscle.

5. Appendix

5.1 Abbreviations

Abbreviation	
7mGpppN	7- Methylguanosine-triphosphate
ACN	Acetonitrile
AF647	Alexa Fluor 647
ASO	Antisense oligonucleotide
ATP	Adenosine triphosphate
BafA1	Bafilomycin A1
Boc	Tert-butoxycarbonyl protecting group
Boc2O	Di-tert-butyl dicarbonate
bp	Base pairs
cAMP	Cyclic adenosine monophosphate
cDNA	Complementary DNA
CFTR	Cystic fibrosis transmembrane conductance regulator
CLSM	Confocal laser scanning microscope
CPP	Cell penetrating peptide
cSNP	Coding single-nucleotide polymorphisms
DAPI	4′,6-diamidino-2-phenylindole
DBCO-NHS	Dibenzocyclooctyne-N-hydroxysuccinimidyl
DCM	Dichlormethane
Dde	1-(4,4-dimethyl-2,6-dioxocyclohexylidene)ethyl protecting group
DIPEA	N,N-Diisopropylethylamine
DMD	Duchenne Muscular Dystrophy
DMDEx23	Duchenne Muscular Dystrophy exon 23
DMEM	Dulbecco's Modified Eagle's Medium
DMF	N,N-Dimethylformamide
DMSO	Dimethyl sulfoxide
DNA	Deoxyribonucleic acid
EDTA	Ethylenediaminetetraacetic acid
eGFP	Enhanced Green fluorescent protein

EtOH	Ethanol
Ex23	Exon 23
FACS	Fluorescence-activated cell sorting
FBS	Fetal Bovine Serum
FC	Flow Cytometry
Fmoc	Fluorenylmethoxycarbonyl protecting group
fwd	Forward
GFPd2	Destabilized green fluorescent protein
HBG	Hepes-buffered glucose
HBTU	2-(1H-benzotriazole-1-yl)-1,1,3,3-tetramethyluronium hexafluorophosphate
HCl	Hydrochloric acid solution
HEPES	N-(2-hydroxethyl) piperazine-N‘-(2-ethansulfonic acid)
HGPS	Hutchinson-Gilford progeria syndrome
HOBt	1-Hydroxybenzotriazole
KCN	Potassium cyanide
kDa	Kilodalton
LB	Lysogeny broth
LenA	Linolenic acid
LinA	Linoleic acid
LMNA	Lamin A/C
MALDI-ToF	Matrix-assisted laser desorption and ionization time-of-flight
MAPT	Microtubule associated protein tau
MeOH	Methanol
mRNA	Messenger RNA
MTBE	Methyl tert-butyl ether
MTT	3-(4,5-dimethylthiazol-2-yl)-2,5-diphenyltetrazolium bromide
NHS	N-Hydroxysuccinimide
NMP	N-Methylpyrrolidone
OleA	Oleic acid
P/S	Penicillin/streptomycin
PAGE	Polyacrylamid gel electrophoresis

PB	Piggy Bac
PBS	Phosphate-buffered saline
PCR	Polymerase chain reaction
pDNA	Plasmid deoxyribonucleic acid
PFA	Paraformaldehyde
PMO	Phosphorodiamidate morpholino oligomer
PP	Polypropylene
pppN	5’ Triphosphate terminus
pre-mRNA	Precursor-mRNA
PTFE	Polytetrafluoroethylene
PVDF	Polyvinylidene difluoride
PyBOP	Benzotriazol-1-yl-oxy tripyrrolidinophosphonium hexafluorophosphate
rev	Reverse
RNA	Ribonucleic acid
RNP	Ribonucleoprotein
RP-HPLC	Reversed phase high-performance liquid chromatography
rpm	Revolutions per minute
RSD_n	Relative standard deviation of negative control cells
RSD_t	Relative standard deviation of transfected cells
RT	Room temperature
SD	Standard deviation
SDS-PAGE	Sodium dodecyl sulfate – polyacrylamide gel electrophoresis
SEC	Size exclusion chromatography
snRNP	Small nuclear ribonucleoproteins
SPAAC	Strain-promoted alkyne-azide cycloaddition
SPPS	Solid-phase peptide synthesis
SRE	Splicing regulatory elements
SSO	Splice switching oligonucleotide
Stp	Succinyl-tetraethylene pentamine
TE	Trypsin/EDTA
TEM	Transmission electron microscopy

TFA	Trifluoroacetic acid
TIS	Triisopropylsilane
wt	Wild type
XP	Xenopeptide

5.2 Analytics

5.2.1 Mass spectrometry

ID	Sequence (N → C)	Calculated mass [g/mol]	Measured mass [m/z]	Synthesized by
1195	K(N_3)-Y_3-Stp_2-K(G-K(LenA)$_2$)-Stp_2-Y_3	3069.9	3067.5	Anna-Lina Lessl
1391	K(N_3)-Y_3-Stp-K(K(OleA)$_2$)-Stp-Y_3	2479.2	2473.7	Yi Lin
1392	K(N_3)-Y_3-Stp-K(K(LinA)$_2$)-Stp-Y_3	2475.2	2471.5	Yi Lin
1393	K(N_3)-Y_3-Stp-K(K(LenA)$_2$)-Stp-Y_3	2471.12	2467.5	Yi Lin
1395	K(N_3)-Y_3-H-Stp-H-K(K(OleA)$_2$)-H-Stp-H-Y_3	3027.74	3025.4	Anna-Lina Lessl
1396	K(N_3)-Y_3-H-Stp-H-K(K(LinA)$_2$)-H-Stp-H-Y_3	3023.71	3018.3	Yi Lin
1397	K(N_3)-Y_3-H-Stp-H-K(K(LenA)$_2$)-H-Stp-H-Y_3	3019.67	3016.2	Yi Lin

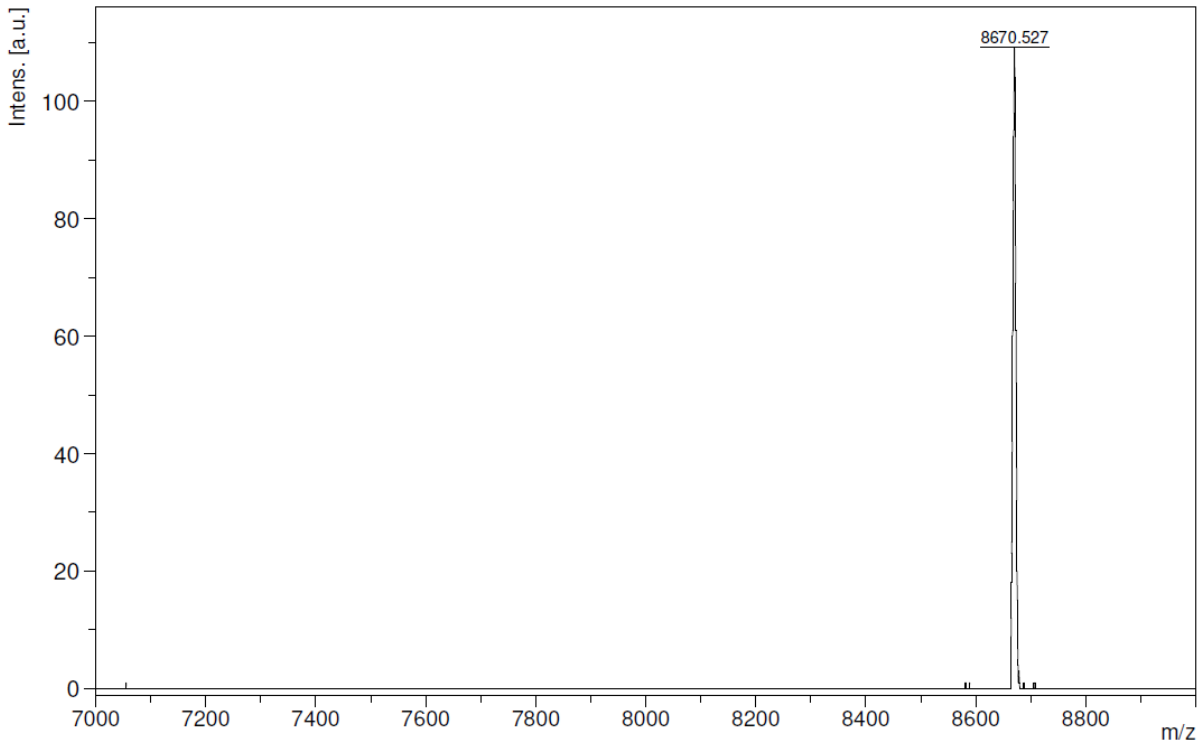

Figure 32 MALDI-ToF MS of PMO(705)–DBCO.

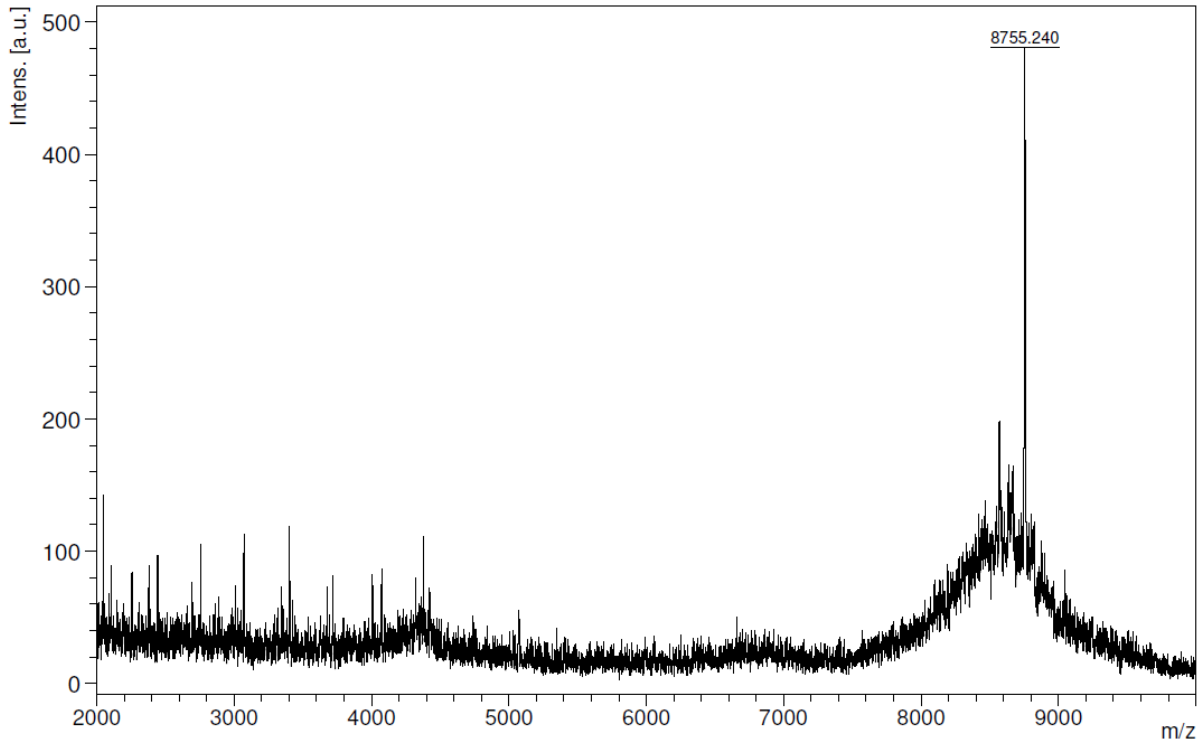

Figure 33 MALDI-ToF MS of PMO(Ex23)–DBCO.

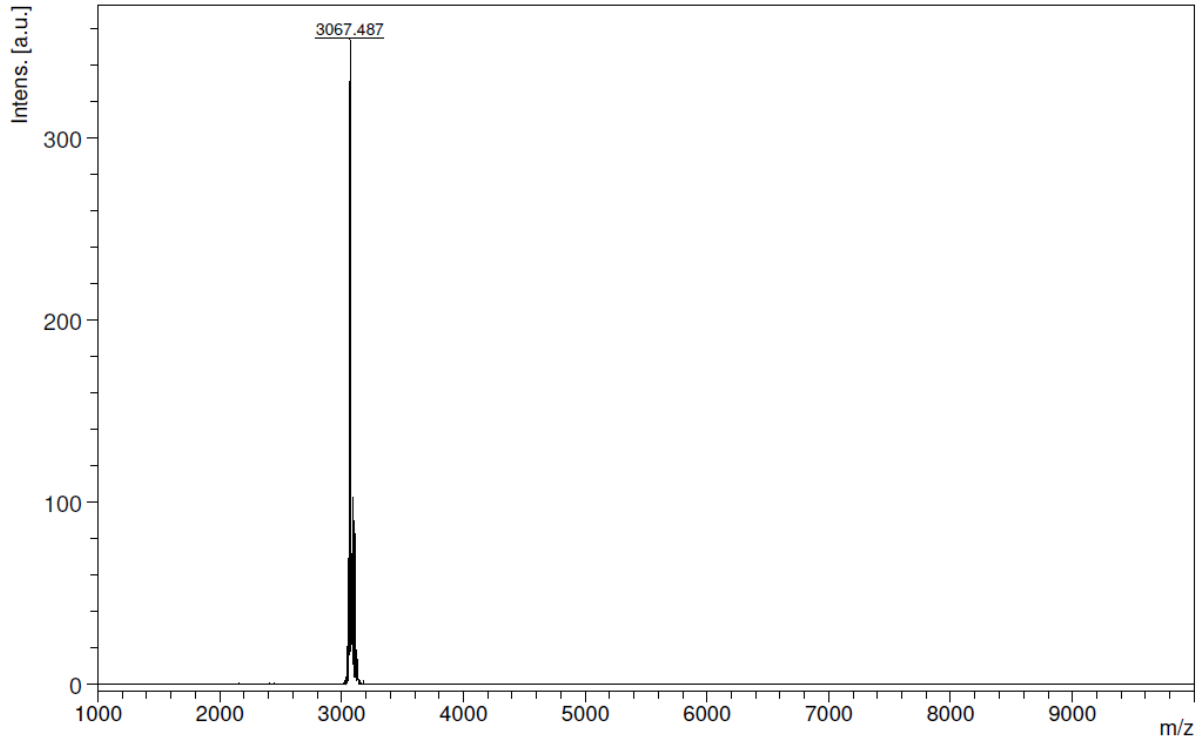

Figure 34 MALDI-ToF MS of *#1195*.

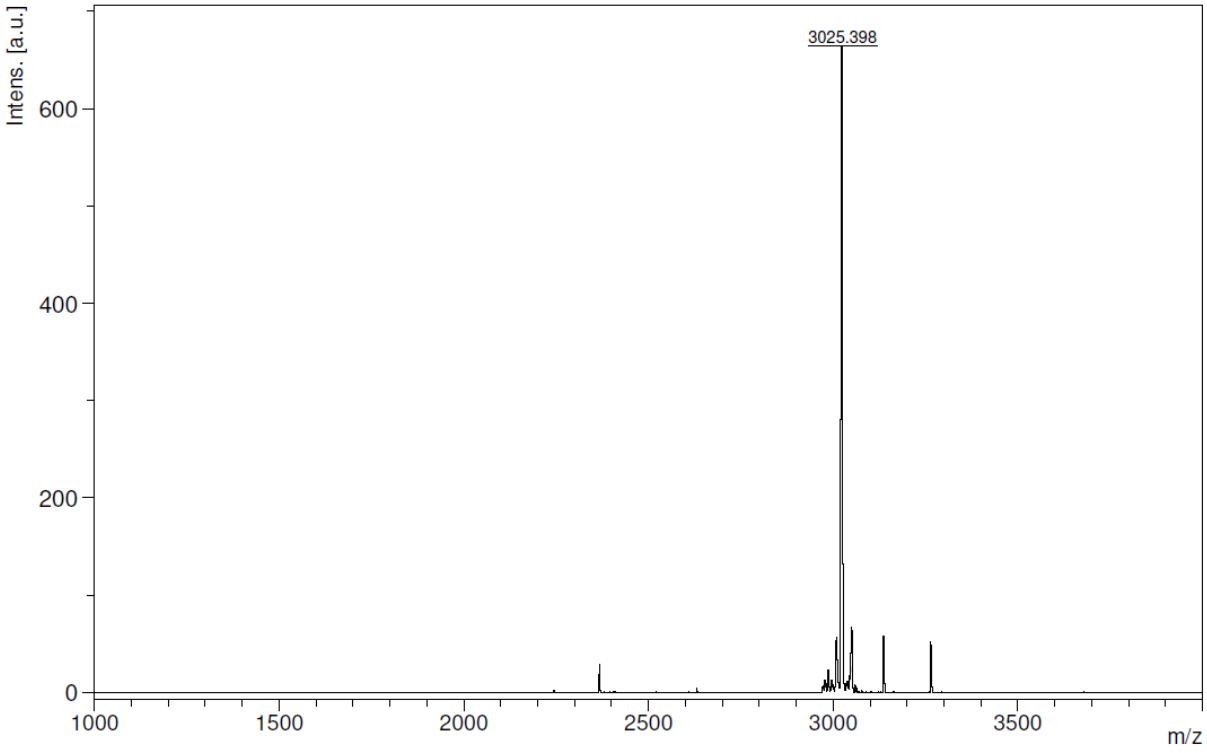

Figure 35 MALDI-ToF MS of *#1395*.

5.3 Plasmid maps and reporter gene sequence

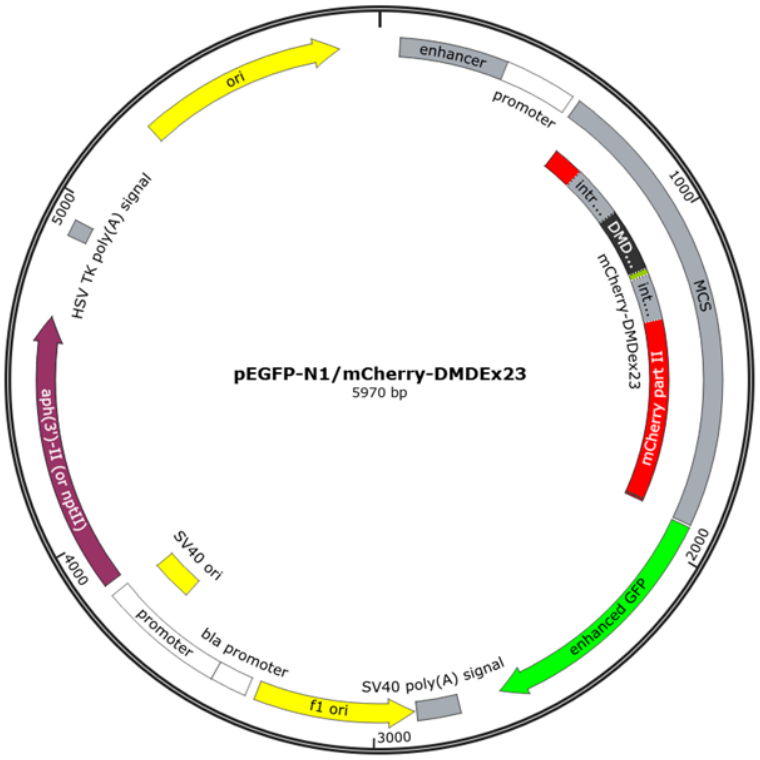

Figure 36 Plasmid map of pEFGP-N1/mCherry-DMDEx23. Deposited at Addgene (#211367).

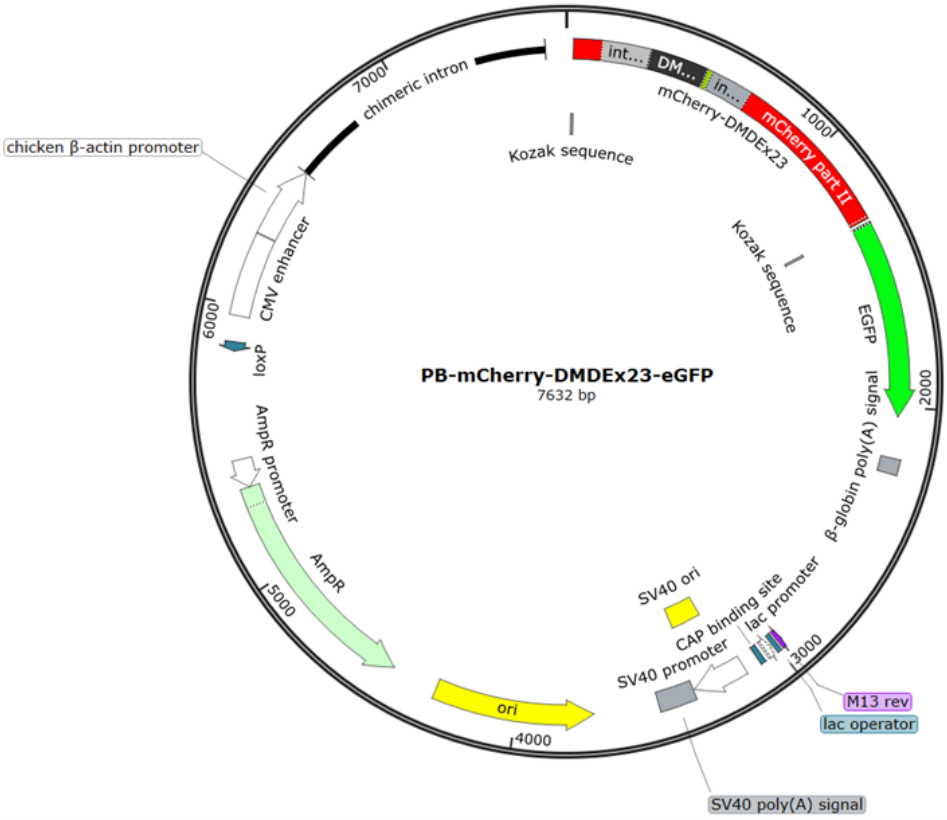

Figure 37 Plasmid map of PB-mCherry-DMDEx23-eGFP. Deposited at Addgene (#211366).

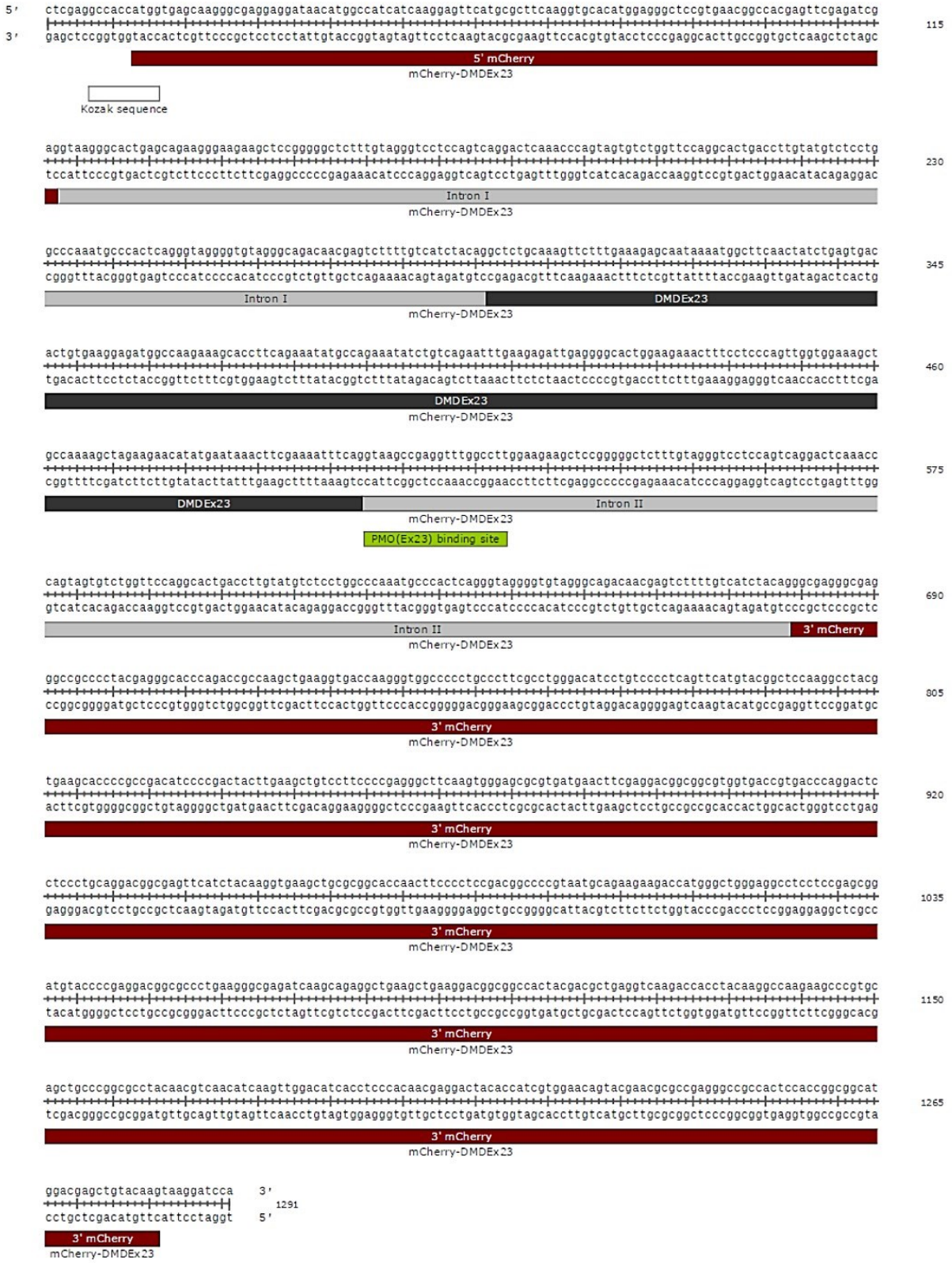

Figure 38 Sequence of the reporter gene mCherry-DMDEx23 with separate section labels and PMO(Ex23) binding site.

6. References

(1) Zschocke, J.; Byers, P. H.; Wilkie, A. O. M. Gregor Mendel and the concepts of dominance and recessiveness. *Nature Reviews Genetics* **2022**, *23* (7), 387-388.
(2) Lander, E. S.; Linton, L. M.; Birren, B.; Nusbaum, C.; Zody, M. C.; Baldwin, J.; Devon, K.; Dewar, K.; Doyle, M.; FitzHugh, W.; et al. Initial sequencing and analysis of the human genome. *Nature* **2001**, *409* (6822), 860-921.
(3) Lester, G.; Bonner David, M. THE OCCURRENCE OF β-GALACTOSIDASE IN ESCHERICHIA COLI. *Journal of Bacteriology* **1952**, *63* (6), 759-769.
(4) Jacob, F.; Monod, J. Genetic regulatory mechanisms in the synthesis of proteins. *Journal of Molecular Biology* **1961**, *3*, 318-356.
(5) Mendel, G. Versuche über Pflanzenhybriden. In *Versuche über Pflanzenhybriden*, Mendel, G. Ed.; Vieweg+Teubner Verlag, 1970; pp 21-64.
(6) Buccitelli, C.; Selbach, M. mRNAs, proteins and the emerging principles of gene expression control. *Nature Reviews Genetics* **2020**, *21* (10), 630-644.
(7) Gilbert, W. Why genes in pieces? *Nature* **1978**, *271* (5645), 501-501.
(8) Tahmasebi, S.; Sonenberg, N.; Hershey, J. W. B.; Mathews, M. B. Protein Synthesis and Translational Control: A Historical Perspective. *Cold Spring Harbor Perspectives in Biology* **2019**, *11* (9).
(9) Hocine, S.; Singer, R. H.; Grünwald, D. RNA processing and export. *Cold Spring Harbor Perspectives in Biology* **2010**, *2* (12), a000752.
(10) Shuman, S. Structure, mechanism, and evolution of the mRNA capping apparatus. *Progress in Nucleic Acid Research and Molecular Biology* **2001**, *66*, 1-40.
(11) Hsu, C. L.; Stevens, A. Yeast cells lacking 5'-->3' exoribonuclease 1 contain mRNA species that are poly(A) deficient and partially lack the 5' cap structure. *Molecular and Cellular Biology* **1993**, *13* (8), 4826-4835.
(12) Desterro, J.; Bak-Gordon, P.; Carmo-Fonseca, M. Targeting mRNA processing as an anticancer strategy. *Nature Reviews Drug Discovery* **2020**, *19* (2), 112-129.
(13) Licatalosi, D. D.; Darnell, R. B. RNA processing and its regulation: global insights into biological networks. *Nature Reviews Genetics* **2010**, *11* (1), 75-87.
(14) Drummond, D. R.; Armstrong, J.; Colman, A. The effect of capping and polyadenylation on the stability, movement and translation of synthetic messenger RNAs in Xenopus oocytes. *Nucleic Acids Research* **1985**, *13* (20), 7375-7394.
(15) Marasco, L. E.; Kornblihtt, A. R. The physiology of alternative splicing. *Nature Reviews Molecular Cell Biology* **2023**, *24* (4), 242-254.
(16) Gehring, N. H.; Roignant, J. Y. Anything but Ordinary - Emerging Splicing Mechanisms in Eukaryotic Gene Regulation. *Trend in Genetics* **2021**, *37* (4), 355-372.
(17) Black, A. J.; Gamarra, J. R.; Giudice, J. More than a messenger: Alternative splicing as a therapeutic target. *Biochimica et Biophysica Acta (BBA) - Gene Regulatory Mechanisms* **2019**, *1862* (11-12), 194395.
(18) Kornblihtt, A. R.; Schor, I. E.; Allo, M.; Dujardin, G.; Petrillo, E.; Munoz, M. J. Alternative splicing: a pivotal step between eukaryotic transcription and translation. *Nature Reviews Molecular Cell Biology* **2013**, *14* (3), 153-165.
(19) Baten, A. K.; Chang, B. C.; Halgamuge, S. K.; Li, J. Splice site identification using probabilistic parameters and SVM classification. *BMC Bioinformatics* **2006**, *7 Suppl 5* (Suppl 5), S15.
(20) Fu, X. D.; Ares, M., Jr. Context-dependent control of alternative splicing by RNA-binding proteins. *Nature Reviews Genetics* **2014**, *15* (10), 689-701.
(21) Wang, Y.; Liu, J.; Huang, B. O.; Xu, Y. M.; Li, J.; Huang, L. F.; Lin, J.; Zhang, J.; Min, Q. H.; Yang, W. M.; et al. Mechanism of alternative splicing and its regulation. *Biomedical Reports* **2015**, *3* (2), 152-158.
(22) Barash, Y.; Calarco, J. A.; Gao, W.; Pan, Q.; Wang, X.; Shai, O.; Blencowe, B. J.; Frey, B. J. Deciphering the splicing code. *Nature* **2010**, *465* (7294), 53-59.
(23) Griffith, M.; Griffith, O. L.; Mwenifumbo, J.; Goya, R.; Morrissy, A. S.; Morin, R. D.; Corbett, R.; Tang, M. J.; Hou, Y. C.; Pugh, T. J.; et al. Alternative expression analysis by RNA sequencing. *Nature Methods* **2010**, *7* (10), 843-847.
(24) Nilsen, T. W.; Graveley, B. R. Expansion of the eukaryotic proteome by alternative splicing. *Nature* **2010**, *463* (7280), 457-463.
(25) Black, D. L. Mechanisms of alternative pre-messenger RNA splicing. *Annual Review of Biochemistry* **2003**, *72*, 291-336.
(26) Cui, Y.; Cai, M.; Stanley, H. E. Comparative Analysis and Classification of Cassette Exons and Constitutive Exons. *BioMed Research International* **2017**, *2017*, 7323508.

(27) Wagner, N.; Celik, M. H.; Holzlwimmer, F. R.; Mertes, C.; Prokisch, H.; Yepez, V. A.; Gagneur, J. Aberrant splicing prediction across human tissues. *Nature Genetics* **2023**, *55* (5), 861-870.
(28) Vorechovský, I. Aberrant 3' splice sites in human disease genes: mutation pattern, nucleotide structure and comparison of computational tools that predict their utilization. *Nucleic Acids Research* **2006**, *34* (16), 4630-4641.
(29) Cartegni, L.; Chew, S. L.; Krainer, A. R. Listening to silence and understanding nonsense: exonic mutations that affect splicing. *Nature Reviews Genetics* **2002**, *3* (4), 285-298.
(30) Zakaria, N. A.; Bahar, R.; Abdullah, W. Z.; Mohamed Yusoff, A. A.; Shamsuddin, S.; Abdul Wahab, R.; Johan, M. F. Genetic Manipulation Strategies for beta-Thalassemia: A Review. *Frontiers in Pediatrics* **2022**, *10*, 901605.
(31) Fukumaki, Y.; Ghosh, P. K.; Benz, E. J., Jr.; Reddy, V. B.; Lebowitz, P.; Forget, B. G.; Weissman, S. M. Abnormally spliced messenger RNA in erythroid cells from patients with beta+ thalassemia and monkey cells expressing a cloned beta+-thalassemic gene. *Cell* **1982**, *28* (3), 585-593.
(32) Sierakowska, H.; Sambade, M. J.; Agrawal, S.; Kole, R. Repair of thalassemic human beta-globin mRNA in mammalian cells by antisense oligonucleotides. *Proceedings of the National Academy of Sciences USA* **1996**, *93* (23), 12840-12844.
(33) Thein, S. L. The molecular basis of beta-thalassemia. *Cold Spring Harbor Perspectives in Medicine* **2013**, *3* (5), a011700.
(34) Faustino, N. A.; Cooper, T. A. Pre-mRNA splicing and human disease. *Genes & Development* **2003**, *17* (4), 419-437.
(35) Deletang, K.; Taulan-Cadars, M. Splicing mutations in the CFTR gene as therapeutic targets. *Gene Therapy* **2022**, *29* (7-8), 399-406.
(36) Eriksson, M.; Brown, W. T.; Gordon, L. B.; Glynn, M. W.; Singer, J.; Scott, L.; Erdos, M. R.; Robbins, C. M.; Moses, T. Y.; Berglund, P.; et al. Recurrent de novo point mutations in lamin A cause Hutchinson–Gilford progeria syndrome. *Nature* **2003**, *423* (6937), 293-298.
(37) Lee, J. M.; Nobumori, C.; Tu, Y.; Choi, C.; Yang, S. H.; Jung, H. J.; Vickers, T. A.; Rigo, F.; Bennett, C. F.; Young, S. G.; et al. Modulation of LMNA splicing as a strategy to treat prelamin A diseases. *Journal of Clinical Investigation* **2016**, *126* (4), 1592-1602.
(38) Noda, A.; Mishima, S.; Hirai, Y.; Hamasaki, K.; Landes, R. D.; Mitani, H.; Haga, K.; Kiyono, T.; Nakamura, N.; Kodama, Y. Progerin, the protein responsible for the Hutchinson-Gilford progeria syndrome, increases the unrepaired DNA damages following exposure to ionizing radiation. *Genes and Environment* **2015**, *37*, 13.
(39) Goldman, R. D.; Shumaker, D. K.; Erdos, M. R.; Eriksson, M.; Goldman, A. E.; Gordon, L. B.; Gruenbaum, Y.; Khuon, S.; Mendez, M.; Varga, R.; et al. Accumulation of mutant lamin A causes progressive changes in nuclear architecture in Hutchinson-Gilford progeria syndrome. *Proceedings of the National Academy of Sciences USA* **2004**, *101* (24), 8963-8968.
(40) Cao, K.; Capell, B. C.; Erdos, M. R.; Djabali, K.; Collins, F. S. A lamin A protein isoform overexpressed in Hutchinson-Gilford progeria syndrome interferes with mitosis in progeria and normal cells. *Proceedings of the National Academy of Sciences USA* **2007**, *104* (12), 4949-4954.
(41) Singh, R. K.; Cooper, T. A. Pre-mRNA splicing in disease and therapeutics. *Trends in Molecular Medicine* **2012**, *18* (8), 472-482.
(42) Apicco, D. J.; Zhang, C.; Maziuk, B.; Jiang, L.; Ballance, H. I.; Boudeau, S.; Ung, C.; Li, H.; Wolozin, B. Dysregulation of RNA Splicing in Tauopathies. *Cell Reports* **2019**, *29* (13), 4377-4388 e4374.
(43) Chung, D. C.; Roemer, S.; Petrucelli, L.; Dickson, D. W. Cellular and pathological heterogeneity of primary tauopathies. *Molecular Neurodegeneration* **2021**, *16* (1), 57.
(44) Dawson, H. N.; Cantillana, V.; Chen, L.; Vitek, M. P. The tau N279K exon 10 splicing mutation recapitulates frontotemporal dementia and parkinsonism linked to chromosome 17 tauopathy in a mouse model. *Journal of Neuroscience* **2007**, *27* (34), 9155-9168.
(45) Schuyer, M.; van der Burg, M. E.; Henzen-Logmans, S. C.; Fieret, J. H.; Klijn, J. G.; Look, M. P.; Foekens, J. A.; Stoter, G.; Berns, E. M. Reduced expression of BAX is associated with poor prognosis in patients with epithelial ovarian cancer: a multifactorial analysis of TP53, p21, BAX and BCL-2. *British Journal of Cancer* **2001**, *85* (9), 1359-1367.
(46) Shkreta, L.; Bell, B.; Revil, T.; Venables, J. P.; Prinos, P.; Elela, S. A.; Chabot, B. Cancer-Associated Perturbations in Alternative Pre-messenger RNA Splicing. *Cancer Research and Treatment* **2013**, *158*, 41-94.
(47) Kwabi-Addo, B.; Ropiquet, F.; Giri, D.; Ittmann, M. Alternative splicing of fibroblast growth factor receptors in human prostate cancer. *Prostate* **2001**, *46* (2), 163-172.
(48) Aigner, A.; Juhl, H.; Malerczyk, C.; Tkybusch, A.; Benz, C. C.; Czubayko, F. Expression of a truncated 100 kDa HER2 splice variant acts as an endogenous inhibitor of tumour cell proliferation. *Oncogene* **2001**, *20* (17), 2101-2111.

(49) Mercatante, D. R.; Sazani, P.; Kole, R. Modification of alternative splicing by antisense oligonucleotides as a potential chemotherapy for cancer and other diseases. *Current Cancer Drug Targets* **2001**, *1* (3), 211-230.
(50) Hoffman, E. P.; Brown, R. H., Jr.; Kunkel, L. M. Dystrophin: The protein product of the duchenne muscular dystrophy locus. *Cell* **1987**, *51* (6), 919-928.
(51) Aoki, Y.; Yokota, T.; Nagata, T.; Nakamura, A.; Tanihata, J.; Saito, T.; Duguez, S. M.; Nagaraju, K.; Hoffman, E. P.; Partridge, T.; et al. Bodywide skipping of exons 45-55 in dystrophic mdx52 mice by systemic antisense delivery. *Proceedings of the National Academy of Sciences USA* **2012**, *109* (34), 13763-13768.
(52) Duchenne. The Pathology of Paralysis with Muscular Degeneration (Paralysie Myosclerotique), or Paralysis with Apparent Hypertrophy. *British Medical Journal* **1867**, *2* (363), 541-542.
(53) Duan, D.; Goemans, N.; Takeda, S.; Mercuri, E.; Aartsma-Rus, A. Duchenne muscular dystrophy. *Nature Reviews Disease Primers* **2021**, *7* (1), 13.
(54) Hara, Y.; Mizobe, Y.; Inoue, Y. U.; Hashimoto, Y.; Motohashi, N.; Masaki, Y.; Seio, K.; Takeda, S.; Nagata, T.; Wood, M. J. A.; et al. Novel EGFP reporter cell and mouse models for sensitive imaging and quantification of exon skipping. *Scientific Reports* **2020**, *10* (1), 10110.
(55) Wilton-Clark, H.; Yokota, T. Antisense and Gene Therapy Options for Duchenne Muscular Dystrophy Arising from Mutations in the N-Terminal Hotspot. *Genes (Basel)* **2022**, *13* (2).
(56) Yang, C.; Georgiou, M.; Atkinson, R.; Collin, J.; Al-Aama, J.; Nagaraja-Grellscheid, S.; Johnson, C.; Ali, R.; Armstrong, L.; Mozaffari-Jovin, S.; et al. Pre-mRNA Processing Factors and Retinitis Pigmentosa: RNA Splicing and Beyond. *Frontiers in Cell and Developmental Biology* **2021**, *9*, 700276.
(57) Martin, C. L.; Duvall, J. A.; Ilkin, Y.; Simon, J. S.; Arreaza, M. G.; Wilkes, K.; Alvarez-Retuerto, A.; Whichello, A.; Powell, C. M.; Rao, K.; et al. Cytogenetic and molecular characterization of A2BP1/FOX1 as a candidate gene for autism. *American Journal of Medical Genetics Part B: Neuropsychiatric Genetics* **2007**, *144B* (7), 869-876.
(58) Barnby, G.; Abbott, A.; Sykes, N.; Morris, A.; Weeks, D. E.; Mott, R.; Lamb, J.; Bailey, A. J.; Monaco, A. P. Candidate-gene screening and association analysis at the autism-susceptibility locus on chromosome 16p: evidence of association at GRIN2A and ABAT. *American Journal of Human Genetics* **2005**, *76* (6), 950-966.
(59) Voineagu, I.; Wang, X.; Johnston, P.; Lowe, J. K.; Tian, Y.; Horvath, S.; Mill, J.; Cantor, R. M.; Blencowe, B. J.; Geschwind, D. H. Transcriptomic analysis of autistic brain reveals convergent molecular pathology. *Nature* **2011**, *474* (7351), 380-384.
(60) Gehman, L. T.; Stoilov, P.; Maguire, J.; Damianov, A.; Lin, C. H.; Shiue, L.; Ares, M., Jr.; Mody, I.; Black, D. L. The splicing regulator Rbfox1 (A2BP1) controls neuronal excitation in the mammalian brain. *Nature Genetics* **2011**, *43* (7), 706-711.
(61) Perrone, B.; La Cognata, V.; Sprovieri, T.; Ungaro, C.; Conforti, F. L.; Andò, S.; Cavallaro, S. Alternative Splicing of ALS Genes: Misregulation and Potential Therapies. *Cellular and Molecular Neurobiology* **2020**, *40* (1), 1-14.
(62) Hughes, T.; Hansson, L.; Sonderby, I. E.; Athanasiu, L.; Zuber, V.; Tesli, M.; Song, J.; Hultman, C. M.; Bergen, S. E.; Landen, M.; et al. A Loss-of-Function Variant in a Minor Isoform of ANK3 Protects Against Bipolar Disorder and Schizophrenia. *Biological Psychiatry* **2016**, *80* (4), 323-330.
(63) Morikawa, T.; Manabe, T.; Ito, Y.; Yamada, S.; Yoshimi, A.; Nagai, T.; Ozaki, N.; Mayeda, A. The expression of HMGA1a is increased in lymphoblastoid cell lines from schizophrenia patients. *Neurochemistry International* **2010**, *56* (6-7), 736-739.
(64) Kim, H. K.; Pham, M. H. C.; Ko, K. S.; Rhee, B. D.; Han, J. Alternative splicing isoforms in health and disease. *Pflugers Archive* **2018**, *470* (7), 995-1016.
(65) Ohno, K.; Rahman, M. A.; Nazim, M.; Nasrin, F.; Lin, Y.; Takeda, J. I.; Masuda, A. Splicing regulation and dysregulation of cholinergic genes expressed at the neuromuscular junction. *Journal of Neurochemistry* **2017**, *142 Suppl 2*, 64-72.
(66) Poulos, M. G.; Batra, R.; Charizanis, K.; Swanson, M. S. Developments in RNA splicing and disease. *Cold Spring Harbor Perspectives in Biology* **2011**, *3* (1), a000778.
(67) Ren, P.; Lu, L.; Cai, S.; Chen, J.; Lin, W.; Han, F. Alternative Splicing: A New Cause and Potential Therapeutic Target in Autoimmune Disease. *Frontiers in Immunology* **2021**, *12*, 713540.
(68) Lopez-Pedrera, C.; Patino-Trives, A. M.; Cerdo, T.; Ortega-Castro, R.; Sanchez-Pareja, I.; Ibanez-Costa, A.; Munoz-Barrera, L.; Abalos-Aguilera, M. C.; Ruiz-Vilchez, D.; Segui Azpilcueta, P.; et al. Splicing machinery is profoundly altered in systemic lupus erythematosus and antiphospholipid syndrome and directly linked to key clinical features. *Journal of Autoimmunity* **2023**, *135*, 102990.
(69) Duncan, E.; Brown, M.; Shore, E. M. The revolution in human monogenic disease mapping. *Genes* **2014**, *5* (3), 792-803.
(70) Lächelt, U.; Wagner, E. Nucleic Acid Therapeutics Using Polyplexes: A Journey of 50 Years (and Beyond). *Chemical Reviews* **2015**, *115* (19), 11043-11078.

(71) Buning, H.; Fehse, B.; Ivics, Z.; Kochanek, S.; Koehl, U.; Kupatt, C.; Mussolino, C.; Nettelbeck, D. M.; Schambach, A.; Uckert, W.; et al. Gene Therapy "Made in Germany": A Historical Perspective, Analysis of the Status Quo, and Recommendations for Action by the German Society for Gene Therapy. *Human Gene Therapy* **2021**, *32* (19-20), 987-996.
(72) Ginn, S. L.; Amaya, A. K.; Alexander, I. E.; Edelstein, M.; Abedi, M. R. Gene therapy clinical trials worldwide to 2017: An update. *The Journal of Gene Medicine* **2018**, *20* (5), e3015.
(73) Hobernik, D.; Bros, M. DNA Vaccines-How Far From Clinical Use? *International Journal of Molecular Sciences* **2018**, *19* (11).
(74) Qin, F.; Xia, F.; Chen, H.; Cui, B.; Feng, Y.; Zhang, P.; Chen, J.; Luo, M. A Guide to Nucleic Acid Vaccines in the Prevention and Treatment of Infectious Diseases and Cancers: From Basic Principles to Current Applications. *Frontiers in Cell and Developmental Biology* **2021**, *9*, 633776.
(75) Liu, M. A. DNA and mRNA Vaccines for Chronic Viral Infections and Cancer: Rationale, Mechanisms, and Progress. *Cancers (Basel)* **2022**, *14* (23).
(76) Sun, W.; Shi, Q.; Zhang, H.; Yang, K.; Ke, Y.; Wang, Y.; Qiao, L. Advances in the techniques and methodologies of cancer gene therapy. *Discov Med* **2019**, *27* (146), 45-55.
(77) Grabbe, S.; Haas, H.; Diken, M.; Kranz, L. M.; Langguth, P.; Sahin, U. Translating nanoparticulate-personalized cancer vaccines into clinical applications: case study with RNA-lipoplexes for the treatment of melanoma. *Nanomedicine* **2016**, *11* (20), 2723-2734.
(78) Wittrup, A.; Lieberman, J. Knocking down disease: a progress report on siRNA therapeutics. *Nature Reviews Genetics* **2015**, *16* (9), 543-552.
(79) Freitag, F.; Wagner, E. Optimizing synthetic nucleic acid and protein nanocarriers: The chemical evolution approach. *Advanced Drug Delivery Reviews* **2021**, *168*, 30-54.
(80) Kulkarni, J. A.; Witzigmann, D.; Thomson, S. B.; Chen, S.; Leavitt, B. R.; Cullis, P. R.; van der Meel, R. The current landscape of nucleic acid therapeutics. *Nature Nanotechnology* **2021**, *16* (6), 630-643.
(81) Majeed, C. N.; Ma, C. D.; Xiao, T.; Rudnick, S.; Bonkovsky, H. L. Spotlight on Givosiran as a Treatment Option for Adults with Acute Hepatic Porphyria: Design, Development, and Place in Therapy. *Drug Design, Development and Therapy* **2022**, *16*, 1827-1845.
(82) Aartsma-Rus, A.; Corey, D. R. The 10th Oligonucleotide Therapy Approved: Golodirsen for Duchenne Muscular Dystrophy. *Nucleic Acid Therapeutics* **2020**, *30* (2), 67-70.
(83) Adams, D.; Gonzalez-Duarte, A.; O'Riordan, W. D.; Yang, C. C.; Ueda, M.; Kristen, A. V.; Tournev, I.; Schmidt, H. H.; Coelho, T.; Berk, J. L.; et al. Patisiran, an RNAi Therapeutic, for Hereditary Transthyretin Amyloidosis. *The New England Journal of Medicine* **2018**, *379* (1), 11-21.
(84) Stein, C. A.; Castanotto, D. FDA-Approved Oligonucleotide Therapies in 2017. *Molecular Therapy* **2017**, *25* (5), 1069-1075.
(85) Wagner, K. R.; Kuntz, N. L.; Koenig, E.; East, L.; Upadhyay, S.; Han, B.; Shieh, P. B. Safety, tolerability, and pharmacokinetics of casimersen in patients with Duchenne muscular dystrophy amenable to exon 45 skipping: A randomized, double-blind, placebo-controlled, dose-titration trial. *Muscle Nerve* **2021**, *64* (3), 285-292.
(86) Watanabe, N.; Nagata, T.; Satou, Y.; Masuda, S.; Saito, T.; Kitagawa, H.; Komaki, H.; Takagaki, K.; Takeda, S. NS-065/NCNP-01: An Antisense Oligonucleotide for Potential Treatment of Exon 53 Skipping in Duchenne Muscular Dystrophy. *Molecular Therapy - Nucleic Acids* **2018**, *13*, 442-449.
(87) Mendell, J. R.; Rodino-Klapac, L. R.; Sahenk, Z.; Roush, K.; Bird, L.; Lowes, L. P.; Alfano, L.; Gomez, A. M.; Lewis, S.; Kota, J.; et al. Eteplirsen for the treatment of Duchenne muscular dystrophy. *Annals of Neurology* **2013**, *74* (5), 637-647.
(88) Roshmi, R. R.; Yokota, T. Pharmacological Profile of Viltolarsen for the Treatment of Duchenne Muscular Dystrophy: A Japanese Experience. *Clinical pharmacology : advances and applications* **2021**, *13*, 235-242.
(89) Clemens, P. R.; Rao, V. K.; Connolly, A. M.; Harper, A. D.; Mah, J. K.; McDonald, C. M.; Smith, E. C.; Zaidman, C. M.; Nakagawa, T.; Investigators, C. D.; et al. Long-Term Functional Efficacy and Safety of Viltolarsen in Patients with Duchenne Muscular Dystrophy. *Journal of Neuromuscular Diseases* **2022**, *9* (4), 493-501.
(90) Frank, D. E.; Schnell, F. J.; Akana, C.; El-Husayni, S. H.; Desjardins, C. A.; Morgan, J.; Charleston, J. S.; Sardone, V.; Domingos, J.; Dickson, G.; et al. Increased dystrophin production with golodirsen in patients with Duchenne muscular dystrophy. *Neurology* **2020**, *94* (21), e2270-e2282.
(91) Servais, L.; Mercuri, E.; Straub, V.; Guglieri, M.; Seferian, A. M.; Scoto, M.; Leone, D.; Koenig, E.; Khan, N.; Dugar, A.; et al. Long-Term Safety and Efficacy Data of Golodirsen in Ambulatory Patients with Duchenne Muscular Dystrophy Amenable to Exon 53 Skipping: A First-in-human, Multicenter, Two-Part, Open-Label, Phase 1/2 Trial. *Nucleic Acid Therapeutics* **2022**, *32* (1), 29-39.
(92) Heydemann, A.; Siemionow, M. A Brief Review of Duchenne Muscular Dystrophy Treatment Options, with an Emphasis on Two Novel Strategies. *Biomedicines* **2023**, *11* (3).

(93) Roberts, T. C.; Langer, R.; Wood, M. J. A. Advances in oligonucleotide drug delivery. *Nature Reviews Drug Discovery* **2020**, *19* (10), 673-694.
(94) Heo, Y. A. Golodirsen: First Approval. *Drugs* **2020**, *80* (3), 329-333.
(95) Verbeke, R.; Lentacker, I.; De Smedt, S. C.; Dewitte, H. The dawn of mRNA vaccines: The COVID-19 case. *Journal of Controlled Release* **2021**, *333*, 511-520.
(96) Gillmore, J. D.; Gane, E.; Taubel, J.; Kao, J.; Fontana, M.; Maitland, M. L.; Seitzer, J.; O'Connell, D.; Walsh, K. R.; Wood, K.; et al. CRISPR-Cas9 In Vivo Gene Editing for Transthyretin Amyloidosis. *The New England Journal of Medicine* **2021**, *385* (6), 493-502.
(97) Wong, C. UK first to approve CRISPR treatment for diseases: what you need to know. *Nature* **2023**, *623* (7988), 676-677.
(98) Frangoul, H.; Altshuler, D.; Cappellini, M. D.; Chen, Y.-S.; Domm, J.; Eustace, B. K.; Foell, J.; de la Fuente, J.; Grupp, S.; Handgretinger, R.; et al. CRISPR-Cas9 Gene Editing for Sickle Cell Disease and β-Thalassemia. *New England Journal of Medicine* **2020**, *384* (3), 252-260.
(99) Di Fusco, D.; Dinallo, V.; Marafini, I.; Figliuzzi, M. M.; Romano, B.; Monteleone, G. Antisense Oligonucleotide: Basic Concepts and Therapeutic Application in Inflammatory Bowel Disease. *Frontiers in Pharmacology* **2019**, *10*, 305.
(100) Rinaldi, C.; Wood, M. J. A. Antisense oligonucleotides: the next frontier for treatment of neurological disorders. *Nature Reviews Neurology* **2018**, *14* (1), 9-21.
(101) Havens, M. A.; Hastings, M. L. Splice-switching antisense oligonucleotides as therapeutic drugs. *Nucleic Acids Research* **2016**, *44* (14), 6549-6563.
(102) Stephenson, M. L.; Zamecnik, P. C. Inhibition of Rous sarcoma viral RNA translation by a specific oligodeoxyribonucleotide. *Proceedings of the National Academy of Sciences USA* **1978**, *75* (1), 285-288.
(103) Bauman, J.; Jearawiriyapaisarn, N.; Kole, R. Therapeutic potential of splice-switching oligonucleotides. *Oligonucleotides* **2009**, *19* (1), 1-13.
(104) Kole, R.; Krainer, A. R.; Altman, S. RNA therapeutics: beyond RNA interference and antisense oligonucleotides. *Nature Reviews Drug Discovery* **2012**, *11* (2), 125-140.
(105) Re, R. The application of antisense technology to medicine. *Ochsner Journal* **2000**, *2* (4), 233-236.
(106) Summerton, J. Morpholino antisense oligomers: the case for an RNase H-independent structural type. *Biochimica et Biophysica Acta (BBA) - Gene Structure and Expression* **1999**, *1489* (1), 141-158.
(107) Wu, H.; Lima, W. F.; Zhang, H.; Fan, A.; Sun, H.; Crooke, S. T. Determination of the role of the human RNase H1 in the pharmacology of DNA-like antisense drugs. *Journal of Biological Chemistry* **2004**, *279* (17), 17181-17189.
(108) Summerton, J.; Weller, D. Morpholino antisense oligomers: design, preparation, and properties. *Antisense and Nucleic Acid Drug Development* **1997**, *7* (3), 187-195.
(109) Summerton, J. E. Invention and Early History of Morpholinos: From Pipe Dream to Practical Products. *Methods in Molecular Biology* **2017**, *1565*, 1-15.
(110) Manoharan, M. 2′-Carbohydrate modifications in antisense oligonucleotide therapy: importance of conformation, configuration and conjugation. *Biochimica et Biophysica Acta (BBA) - Gene Structure and Expression* **1999**, *1489* (1), 117-130.
(111) Gagliardi, M.; Ashizawa, A. T. The Challenges and Strategies of Antisense Oligonucleotide Drug Delivery. *Biomedicines* **2021**, *9* (4).
(112) Crooke, S. T.; Vickers, T. A.; Liang, X. H. Phosphorothioate modified oligonucleotide-protein interactions. *Nucleic Acids Research* **2020**, *48* (10), 5235-5253.
(113) Hinrich, A. J.; Jodelka, F. M.; Chang, J. L.; Brutman, D.; Bruno, A. M.; Briggs, C. A.; James, B. D.; Stutzmann, G. E.; Bennett, D. A.; Miller, S. A.; et al. Therapeutic correction of ApoER2 splicing in Alzheimer's disease mice using antisense oligonucleotides. *EMBO Molecular Medicine* **2016**, *8* (4), 328-345.
(114) Ottesen, E. W. ISS-N1 makes the First FDA-approved Drug for Spinal Muscular Atrophy. *Translational Neuroscience* **2017**, *8*, 1-6.
(115) McDonald, C. M.; Wong, B.; Flanigan, K. M.; Wilson, R.; de Kimpe, S.; Lourbakos, A.; Lin, Z.; Campion, G.; group, D. V. s. Placebo-controlled Phase 2 Trial of Drisapersen for Duchenne Muscular Dystrophy. *Annals of Clinical and Translational Neurology* **2018**, *5* (8), 913-926.
(116) Goemans, N.; Mercuri, E.; Belousova, E.; Komaki, H.; Dubrovsky, A.; McDonald, C. M.; Kraus, J. E.; Lourbakos, A.; Lin, Z.; Campion, G.; et al. A randomized placebo-controlled phase 3 trial of an antisense oligonucleotide, drisapersen, in Duchenne muscular dystrophy. *Neuromuscular Disorders* **2018**, *28* (1), 4-15.
(117) Evers, M. M.; Tran, H. D.; Zalachoras, I.; Meijer, O. C.; den Dunnen, J. T.; van Ommen, G. J.; Aartsma-Rus, A.; van Roon-Mom, W. M. Preventing formation of toxic N-terminal huntingtin fragments through antisense oligonucleotide-mediated protein modification. *Nucleic Acid Therapeutics* **2014**, *24* (1), 4-12.

(118) Disterer, P.; Al-Shawi, R.; Ellmerich, S.; Waddington, S. N.; Owen, J. S.; Simons, J. P.; Khoo, B. Exon skipping of hepatic APOB pre-mRNA with splice-switching oligonucleotides reduces LDL cholesterol in vivo. *Molecular Therapy* **2013**, *21* (3), 602-609.
(119) Bauman, J. A.; Li, S. D.; Yang, A.; Huang, L.; Kole, R. Anti-tumor activity of splice-switching oligonucleotides. *Nucleic Acids Research* **2010**, *38* (22), 8348-8356.
(120) Grünweiler, A.; Hartmann, R. K. Locked Nucleic Acid Oligonucleotides. *BioDrugs* **2007**, *21* (4), 235-243.
(121) Nielsen, P. E.; Egholm, M.; Berg, R. H.; Buchardt, O. Peptide nucleic acids (PNAs): potential antisense and anti-gene agents. *Anticancer Drug Des* **1993**, *8* (1), 53-63.
(122) Lee, H. T.; Kim, S. K.; Yoon, J. W. Antisense peptide nucleic acids as a potential anti-infective agent. *Journal of Microbiology* **2019**, *57* (6), 423-430.
(123) Shimizu-Motohashi, Y.; Komaki, H.; Motohashi, N.; Takeda, S.; Yokota, T.; Aoki, Y. Restoring Dystrophin Expression in Duchenne Muscular Dystrophy: Current Status of Therapeutic Approaches. *Journal of Personalized Medicine* **2019**, *9* (1).
(124) Wood, M. J. A.; Talbot, K.; Bowerman, M. Spinal muscular atrophy: antisense oligonucleotide therapy opens the door to an integrated therapeutic landscape. *Human Molecular Genetics* **2017**, *26* (R2), R151-R159.
(125) Crawford, T. O.; Pardo, C. A. The Neurobiology of Childhood Spinal Muscular Atrophy. *Neurobiology of Disease* **1996**, *3* (2), 97-110.
(126) Lefebvre, S.; Bürglen, L.; Reboullet, S.; Clermont, O.; Burlet, P.; Viollet, L.; Benichou, B.; Cruaud, C.; Millasseau, P.; Zeviani, M.; et al. Identification and characterization of a spinal muscular atrophy-determining gene. *Cell* **1995**, *80* (1), 155-165.
(127) Murray, L. M.; Comley, L. H.; Thomson, D.; Parkinson, N.; Talbot, K.; Gillingwater, T. H. Selective vulnerability of motor neurons and dissociation of pre- and post-synaptic pathology at the neuromuscular junction in mouse models of spinal muscular atrophy. *Human Molecular Genetics* **2008**, *17* (7), 949-962.
(128) Levin, A. A. Treating Disease at the RNA Level with Oligonucleotides. *The New England Journal of Medicine* **2019**, *380* (1), 57-70.
(129) Echigoya, Y.; Lim, K. R. Q.; Nakamura, A.; Yokota, T. Multiple Exon Skipping in the Duchenne Muscular Dystrophy Hot Spots: Prospects and Challenges. *Journal of Personalized Medicine* **2018**, *8* (4).
(130) Gieron-Korthals, M.; Fernandez, R. New Developments in Diagnosis, Treatment, and Management of Duchenne Muscular Dystrophy. *Advances in Pediatrics* **2020**, *67*, 183-196.
(131) Lim, K. R.; Maruyama, R.; Yokota, T. Eteplirsen in the treatment of Duchenne muscular dystrophy. *Drug Design, Development and Therapy* **2017**, *11*, 533-545.
(132) Mendell, J. R.; Goemans, N.; Lowes, L. P.; Alfano, L. N.; Berry, K.; Shao, J.; Kaye, E. M.; Mercuri, E.; Eteplirsen Study, G.; Telethon Foundation, D. M. D. I. N. Longitudinal effect of eteplirsen versus historical control on ambulation in Duchenne muscular dystrophy. *Annals of Neurology* **2016**, *79* (2), 257-271.
(133) Kim, J.; Hu, C.; Moufawad El Achkar, C.; Black, L. E.; Douville, J.; Larson, A.; Pendergast, M. K.; Goldkind, S. F.; Lee, E. A.; Kuniholm, A.; et al. Patient-Customized Oligonucleotide Therapy for a Rare Genetic Disease. *The New England Journal of Medicine* **2019**, *381* (17), 1644-1652.
(134) Mole, S. E.; Cotman, S. L. Genetics of the neuronal ceroid lipofuscinoses (Batten disease). *Biochimica et Biophysica Acta* **2015**, *1852* (10 Pt B), 2237-2241.
(135) Radke, J.; Stenzel, W.; Goebel, H. H. Human NCL Neuropathology. *Biochimica et Biophysica Acta* **2015**, *1852* (10 Pt B), 2262-2266.
(136) Aartsma-Rus, A.; Garanto, A.; van Roon-Mom, W.; McConnell, E. M.; Suslovitch, V.; Yan, W. X.; Watts, J. K.; Yu, T. W. Consensus Guidelines for the Design and In Vitro Preclinical Efficacy Testing N-of-1 Exon Skipping Antisense Oligonucleotides. *Nucleic Acid Therapeutics* **2023**, *33* (1), 17-25.
(137) Hagedorn, P. H.; Yakimov, V.; Ottosen, S.; Kammler, S.; Nielsen, N. F.; Hog, A. M.; Hedtjarn, M.; Meldgaard, M.; Moller, M. R.; Orum, H.; et al. Hepatotoxic potential of therapeutic oligonucleotides can be predicted from their sequence and modification pattern. *Nucleic Acid Therapeutics* **2013**, *23* (5), 302-310.
(138) Bege, M.; Borbas, A. The Medicinal Chemistry of Artificial Nucleic Acids and Therapeutic Oligonucleotides. *Pharmaceuticals* **2022**, *15* (8).
(139) Roehr, B. Fomivirsen approved for CMV retinitis. *Journal of International Association of Physicians in AIDS Care* **1998**, *4* (10), 14-16.
(140) Egli, M.; Manoharan, M. Chemistry, structure and function of approved oligonucleotide therapeutics. *Nucleic Acids Research* **2023**, *51* (6), 2529-2573.
(141) Grillone, L. R.; Lanz, R. Fomivirsen. *Drugs Today (Barc)* **2001**, *37* (4), 245-255.
(142) Sanghvi, Y. S. A status update of modified oligonucleotides for chemotherapeutics applications. *Current Protocols in Nucleic Acid Chemistry* **2011**, *Chapter 4*, Unit 4.1.1-22.

(143) Bubela, T.; McCabe, C. Value-engineered translation: developing biotherapeutics that align with health-system needs. *American Journal of Managed Care* **2014**, *20* (10 Spec No), E3.
(144) Merki, E.; Graham, M. J.; Mullick, A. E.; Miller, E. R.; Crooke, R. M.; Pitas, R. E.; Witztum, J. L.; Tsimikas, S. Antisense oligonucleotide directed to human apolipoprotein B-100 reduces lipoprotein(a) levels and oxidized phospholipids on human apolipoprotein B-100 particles in lipoprotein(a) transgenic mice. *Circulation* **2008**, *118* (7), 743-753.
(145) El Harchaoui, K.; Akdim, F.; Stroes, E. S.; Trip, M. D.; Kastelein, J. J. Current and future pharmacologic options for the management of patients unable to achieve low-density lipoprotein-cholesterol goals with statins. *American Journal of Cardiovascular Drugs* **2008**, *8* (4), 233-242.
(146) Duell, P. B.; Santos, R. D.; Kirwan, B. A.; Witztum, J. L.; Tsimikas, S.; Kastelein, J. J. P. Long-term mipomersen treatment is associated with a reduction in cardiovascular events in patients with familial hypercholesterolemia. *Journal of Clinical Lipidology* **2016**, *10* (4), 1011-1021.
(147) Finkel, R. S.; Mercuri, E.; Darras, B. T.; Connolly, A. M.; Kuntz, N. L.; Kirschner, J.; Chiriboga, C. A.; Saito, K.; Servais, L.; Tizzano, E.; et al. Nusinersen versus Sham Control in Infantile-Onset Spinal Muscular Atrophy. *The New England Journal of Medicine* **2017**, *377* (18), 1723-1732.
(148) Wurster, C. D.; Ludolph, A. C. Nusinersen for spinal muscular atrophy. *Therapeutic Advances in Neurological Disorders* **2018**, *11*, 1756285618754459.
(149) Gales, L. Tegsedi (Inotersen): An Antisense Oligonucleotide Approved for the Treatment of Adult Patients with Hereditary Transthyretin Amyloidosis. *Pharmaceuticals* **2019**, *12* (2).
(150) Mathew, V.; Wang, A. K. Inotersen: new promise for the treatment of hereditary transthyretin amyloidosis. *Drug Design, Development and Therapy* **2019**, *13*, 1515-1525.
(151) Paik, J.; Duggan, S. Volanesorsen: First Global Approval. *Drugs* **2019**, *79* (12), 1349-1354.
(152) Dhillon, S. Viltolarsen: First Approval. *Drugs* **2020**, *80* (10), 1027-1031.
(153) Shirley, M. Casimersen: First Approval. *Drugs* **2021**, *81* (7), 875-879.
(154) Goncalves, C.; Akhter, S.; Pichon, C.; Midoux, P. Intracellular Availability of pDNA and mRNA after Transfection: A Comparative Study among Polyplexes, Lipoplexes, and Lipopolyplexes. *Molecular Pharmaceutics* **2016**, *13* (9), 3153-3163.
(155) Scholz, C.; Wagner, E. Therapeutic plasmid DNA versus siRNA delivery: common and different tasks for synthetic carriers. *Journal of Controlled Release* **2012**, *161* (2), 554-565.
(156) Jackson, D. A.; Symons, R. H.; Berg, P. Biochemical method for inserting new genetic information into DNA of Simian Virus 40: circular SV40 DNA molecules containing lambda phage genes and the galactose operon of Escherichia coli. *Proceedings of the National Academy of Sciences USA* **1972**, *69* (10), 2904-2909.
(157) Travieso, T.; Li, J.; Mahesh, S.; Mello, J.; Blasi, M. The use of viral vectors in vaccine development. *NPJ Vaccines* **2022**, *7* (1), 75.
(158) Kotterman, M. A.; Chalberg, T. W.; Schaffer, D. V. Viral Vectors for Gene Therapy: Translational and Clinical Outlook. *Annual Review of Biomedical Engineering* **2015**, *17*, 63-89.
(159) Thomas, C. E.; Ehrhardt, A.; Kay, M. A. Progress and problems with the use of viral vectors for gene therapy. *Nature Reviews Genetics* **2003**, *4* (5), 346-358.
(160) Belting, M.; Wittrup, A. Developments in macromolecular drug delivery. *Methods in Molecular Biology* **2009**, *480*, 1-10.
(161) Blanco, E.; Shen, H.; Ferrari, M. Principles of nanoparticle design for overcoming biological barriers to drug delivery. *Nature Biotechnology* **2015**, *33* (9), 941-951.
(162) Kuhn, J.; Klein, P. M.; Al Danaf, N.; Nordin, J. Z.; Reinhard, S.; Loy, D. M.; Höhn, M.; El Andaloussi, S.; Lamb, D. C.; Wagner, E.; et al. Supramolecular Assembly of Aminoethylene-Lipopeptide PMO Conjugates into RNA Splice-Switching Nanomicelles. *Advanced Functional Materials* **2019**, *29* (48).
(163) Lynch, I.; Salvati, A.; Dawson, K. A. Protein-nanoparticle interactions: What does the cell see? *Nature Nanotechnology* **2009**, *4* (9), 546-547.
(164) Walkey, C. D.; Chan, W. C. Understanding and controlling the interaction of nanomaterials with proteins in a physiological environment. *Chemical Society Reviews* **2012**, *41* (7), 2780-2799.
(165) Conner, S. D.; Schmid, S. L. Regulated portals of entry into the cell. *Nature* **2003**, *422* (6927), 37-44.
(166) Behzadi, S.; Serpooshan, V.; Tao, W.; Hamaly, M. A.; Alkawareek, M. Y.; Dreaden, E. C.; Brown, D.; Alkilany, A. M.; Farokhzad, O. C.; Mahmoudi, M. Cellular uptake of nanoparticles: journey inside the cell. *Chemical Society Reviews* **2017**, *46* (14), 4218-4244.
(167) Frohlich, E. The role of surface charge in cellular uptake and cytotoxicity of medical nanoparticles. *International Journal of Nanomedicine* **2012**, *7*, 5577-5591.
(168) Lin, J.; Zhang, H.; Chen, Z.; Zheng, Y. Penetration of Lipid Membranes by Gold Nanoparticles: Insights into Cellular Uptake, Cytotoxicity, and Their Relationship. *ACS Nano* **2010**, *4* (9), 5421-5429.
(169) Nangia, S.; Sureshkumar, R. Effects of nanoparticle charge and shape anisotropy on translocation through cell membranes. *Langmuir* **2012**, *28* (51), 17666-17671.

(170) Zhu, M.; Nie, G.; Meng, H.; Xia, T.; Nel, A.; Zhao, Y. Physicochemical properties determine nanomaterial cellular uptake, transport, and fate. *Accounts of Chemical Research* **2013**, *46* (3), 622-631.
(171) Reinhard, S.; Wagner, E. Sequence-Defined Cationic Lipo-Oligomers Containing Unsaturated Fatty Acids for Transfection. *Methods in Molecular Biology* **2019**, *1943*, 1-25.
(172) Smith, S. A.; Selby, L. I.; Johnston, A. P. R.; Such, G. K. The Endosomal Escape of Nanoparticles: Toward More Efficient Cellular Delivery. *Bioconjugate Chemistry* **2019**, *30* (2), 263-272.
(173) Scott, C. C.; Vacca, F.; Gruenberg, J. Endosome maturation, transport and functions. *Seminars in Cell & Developmental Biology* **2014**, *31*, 2-10.
(174) Behr, J.-P. The Proton Sponge: a Trick to Enter Cells the Viruses Did Not Exploit. *CHIMIA* **1997**, *51* (1-2), 34.
(175) Bus, T.; Traeger, A.; Schubert, U. S. The great escape: how cationic polyplexes overcome the endosomal barrier. *Journal of Materials Chemistry B* **2018**, *6* (43), 6904-6918.
(176) Choudhury, C. K.; Kumar, A.; Roy, S. Characterization of Conformation and Interaction of Gene Delivery Vector Polyethylenimine with Phospholipid Bilayer at Different Protonation State. *Biomacromolecules* **2013**, *14* (10), 3759-3768.
(177) Vermeulen, L. M. P.; De Smedt, S. C.; Remaut, K.; Braeckmans, K. The proton sponge hypothesis: Fable or fact? *European Journal of Pharmaceutics and Biopharmaceutics* **2018**, *129*, 184-190.
(178) ur Rehman, Z.; Hoekstra, D.; Zuhorn, I. S. Mechanism of polyplex- and lipoplex-mediated delivery of nucleic acids: real-time visualization of transient membrane destabilization without endosomal lysis. *ACS Nano* **2013**, *7* (5), 3767-3777.
(179) Bieber, T.; Meissner, W.; Kostin, S.; Niemann, A.; Elsasser, H. P. Intracellular route and transcriptional competence of polyethylenimine-DNA complexes. *Journal of Controlled Release* **2002**, *82* (2-3), 441-454.
(180) Ray, M.; Tang, R.; Jiang, Z.; Rotello, V. M. Quantitative tracking of protein trafficking to the nucleus using cytosolic protein delivery by nanoparticle-stabilized nanocapsules. *Bioconjugate Chemistry* **2015**, *26* (6), 1004-1007.
(181) Boussif, O.; Lezoualc'h, F.; Zanta, M. A.; Mergny, M. D.; Scherman, D.; Demeneix, B.; Behr, J. P. A versatile vector for gene and oligonucleotide transfer into cells in culture and in vivo: polyethylenimine. *Proceedings of the National Academy of Sciences USA* **1995**, *92* (16), 7297-7301.
(182) Liu, X.; Zhang, P.; He, D.; Rodl, W.; Preiss, T.; Radler, J. O.; Wagner, E.; Lachelt, U. pH-Reversible Cationic RNase A Conjugates for Enhanced Cellular Delivery and Tumor Cell Killing. *Biomacromolecules* **2016**, *17* (1), 173-182.
(183) Lin, Y.; Luo, X.; Burghardt, T.; Dorrer, S.; Hohn, M.; Wagner, E.; Lachelt, U. Chemical Evolution of Amphiphilic Xenopeptides for Potentiated Cas9 Ribonucleoprotein Delivery. *Journal of the American Chemical Society* **2023**, *145* (28), 15171-15179.
(184) Thalmayr, S.; Grau, M.; Peng, L.; Pohmerer, J.; Wilk, U.; Folda, P.; Yazdi, M.; Weidinger, E.; Burghardt, T.; Hohn, M.; et al. Molecular Chameleon Carriers for Nucleic Acid Delivery: The Sweet Spot between Lipoplexes and Polyplexes. *Advanced Materials* **2023**, *35* (25), e2211105.
(185) Wyman, T. B.; Nicol, F.; Zelphati, O.; Scaria, P. V.; Plank, C.; Szoka, F. C. Design, Synthesis, and Characterization of a Cationic Peptide That Binds to Nucleic Acids and Permeabilizes Bilayers. *Biochemistry* **1997**, *36* (10), 3008-3017.
(186) Betts, C.; Saleh, A. F.; Arzumanov, A. A.; Hammond, S. M.; Godfrey, C.; Coursindel, T.; Gait, M. J.; Wood, M. J. Pip6-PMO, A New Generation of Peptide-oligonucleotide Conjugates With Improved Cardiac Exon Skipping Activity for DMD Treatment. *Molecular Therapy - Nucleic Acids* **2012**, *1* (8), e38.
(187) Pardridge, W. M.; Boado, R. J. Enhanced cellular uptake of biotinylated antisense oligonucleotide or peptide mediated by avidin, a cationic protein. *FEBS Letters* **1991**, *288* (1-2), 30-32.
(188) Felgner, P. L.; Gadek, T. R.; Holm, M.; Roman, R.; Chan, H. W.; Wenz, M.; Northrop, J. P.; Ringold, G. M.; Danielsen, M. Lipofection: a highly efficient, lipid-mediated DNA-transfection procedure. *Proceedings of the National Academy of Sciences USA* **1987**, *84* (21), 7413-7417.
(189) Zhang, P.; He, D.; Klein, P. M.; Liu, X.; Röder, R.; Döblinger, M.; Wagner, E. Enhanced Intracellular Protein Transduction by Sequence Defined Tetra-Oleoyl Oligoaminoamides Targeted for Cancer Therapy. *Advanced Functional Materials* **2015**, *25* (42), 6627-6636.
(190) Bangham, A. D.; Standish, M. M.; Watkins, J. C. Diffusion of univalent ions across the lamellae of swollen phospholipids. *Journal of Molecular Biology* **1965**, *13* (1), 238-IN227.
(191) Woodle, M. C.; Lasic, D. D. Sterically stabilized liposomes. *Biochimica et Biophysica Acta (BBA) - Reviews on Biomembranes* **1992**, *1113* (2), 171-199.
(192) Bulbake, U.; Doppalapudi, S.; Kommineni, N.; Khan, W. Liposomal Formulations in Clinical Use: An Updated Review. *Pharmaceutics* **2017**, *9* (2).

(193) Sebastiani, F.; Yanez Arteta, M.; Lindfors, L.; Cárdenas, M. Screening of the binding affinity of serum proteins to lipid nanoparticles in a cell free environment. *Journal of Colloid and Interface Science* **2022**, *610*, 766-774.
(194) Palchetti, S.; Pozzi, D.; Capriotti, A. L.; Barbera, G.; Chiozzi, R. Z.; Digiacomo, L.; Peruzzi, G.; Caracciolo, G.; Laganà, A. Influence of dynamic flow environment on nanoparticle-protein corona: From protein patterns to uptake in cancer cells. *Colloids and Surfaces B: Biointerfaces* **2017**, *153*, 263-271.
(195) Kulkarni, J. A.; Witzigmann, D.; Chen, S.; Cullis, P. R.; van der Meel, R. Lipid Nanoparticle Technology for Clinical Translation of siRNA Therapeutics. *ACS Applied Materials & Interfaces* **2019**, *52* (9), 2435-2444.
(196) Akinc, A.; Maier, M. A.; Manoharan, M.; Fitzgerald, K.; Jayaraman, M.; Barros, S.; Ansell, S.; Du, X.; Hope, M. J.; Madden, T. D.; et al. The Onpattro story and the clinical translation of nanomedicines containing nucleic acid-based drugs. *Nature Nanotechnology* **2019**, *14* (12), 1084-1087.
(197) Mukai, H.; Ogawa, K.; Kato, N.; Kawakami, S. Recent advances in lipid nanoparticles for delivery of nucleic acid, mRNA, and gene editing-based therapeutics. *Drug Metabolism and Pharmacokinetics* **2022**, *44*, 100450.
(198) Fawell, S.; Seery, J.; Daikh, Y.; Moore, C.; Chen, L. L.; Pepinsky, B.; Barsoum, J. Tat-mediated delivery of heterologous proteins into cells. *Proceedings of the National Academy of Sciences USA* **1994**, *91* (2), 664-668.
(199) Shen, X.; Corey, D. R. Chemistry, mechanism and clinical status of antisense oligonucleotides and duplex RNAs. *Nucleic Acids Research* **2018**, *46* (4), 1584-1600.
(200) Dhuri, K.; Bechtold, C.; Quijano, E.; Pham, H.; Gupta, A.; Vikram, A.; Bahal, R. Antisense Oligonucleotides: An Emerging Area in Drug Discovery and Development. *Journal of Clinical Medicine* **2020**, *9* (6).
(201) Cirak, S.; Arechavala-Gomeza, V.; Guglieri, M.; Feng, L.; Torelli, S.; Anthony, K.; Abbs, S.; Garralda, M. E.; Bourke, J.; Wells, D. J.; et al. Exon skipping and dystrophin restoration in patients with Duchenne muscular dystrophy after systemic phosphorodiamidate morpholino oligomer treatment: an open-label, phase 2, dose-escalation study. *Lancet* **2011**, *378* (9791), 595-605.
(202) McMahon, B. M.; Mays, D.; Lipsky, J.; Stewart, J. A.; Fauq, A.; Richelson, E. Pharmacokinetics and Tissue Distribution of a Peptide Nucleic Acid After Intravenous Administration. *Antisense and Nucleic Acid Drug Development* **2002**, *12* (2), 65-70.
(203) Amantana, A.; Moulton, H. M.; Cate, M. L.; Reddy, M. T.; Whitehead, T.; Hassinger, J. N.; Youngblood, D. S.; Iversen, P. L. Pharmacokinetics, Biodistribution, Stability and Toxicity of a Cell-Penetrating Peptide–Morpholino Oligomer Conjugate. *Bioconjugate Chemistry* **2007**, *18* (4), 1325-1331.
(204) Abes, S.; Moulton, H. M.; Clair, P.; Prevot, P.; Youngblood, D. S.; Wu, R. P.; Iversen, P. L.; Lebleu, B. Vectorization of morpholino oligomers by the (R-Ahx-R)4 peptide allows efficient splicing correction in the absence of endosomolytic agents. *Journal of Controlled Release* **2006**, *116* (3), 304-313.
(205) Lebleu, B.; Moulton, H. M.; Abes, R.; Ivanova, G. D.; Abes, S.; Stein, D. A.; Iversen, P. L.; Arzumanov, A. A.; Gait, M. J. Cell penetrating peptide conjugates of steric block oligonucleotides. *Advanced Drug Delivery Reviews* **2008**, *60* (4-5), 517-529.
(206) Moulton, H. M.; Nelson, M. H.; Hatlevig, S. A.; Reddy, M. T.; Iversen, P. L. Cellular Uptake of Antisense Morpholino Oligomers Conjugated to Arginine-Rich Peptides. *Bioconjugate Chemistry* **2004**, *15* (2), 290-299.
(207) Shiraishi, T.; Nielsen, P. E. Peptide nucleic acid (PNA) cell penetrating peptide (CPP) conjugates as carriers for cellular delivery of antisense oligomers. *Artificial DNA: PNA & XNA* **2011**, *2* (3), 90-99.
(208) Gan, L.; Wu, L. C. L.; Wood, J. A.; Yao, M.; Treleaven, C. M.; Estrella, N. L.; Wentworth, B. M.; Hanson, G. J.; Passini, M. A. A cell-penetrating peptide enhances delivery and efficacy of phosphorodiamidate morpholino oligomers in mdx mice. *Molecular Therapy - Nucleic Acids* **2022**, *30*, 17-27.
(209) Morcos, P. A.; Li, Y.; Jiang, S. Vivo-Morpholinos: a non-peptide transporter delivers Morpholinos into a wide array of mouse tissues. *Biotechniques* **2008**, *45* (6), 613-614, 616, 618 passim.
(210) Warren, T. K.; Shurtleff, A. C.; Bavari, S. Advanced morpholino oligomers: a novel approach to antiviral therapy. *Antiviral Research* **2012**, *94* (1), 80-88.
(211) Shen, G.; Fang, H.; Song, Y.; Bielska, A. A.; Wang, Z.; Taylor, J.-S. A. Phospholipid Conjugate for Intracellular Delivery of Peptide Nucleic Acids. *Bioconjugate Chemistry* **2009**, *20* (9), 1729-1736.
(212) Betts, C. A.; McClorey, G.; Healicon, R.; Hammond, S. M.; Manzano, R.; Muses, S.; Ball, V.; Godfrey, C.; Merritt, T. M.; van Westering, T.; et al. Cmah-dystrophin deficient mdx mice display an accelerated cardiac phenotype that is improved following peptide-PMO exon skipping treatment. *Human Molecular Genetics* **2019**, *28* (3), 396-406.
(213) Betts, C. A.; Saleh, A. F.; Carr, C. A.; Hammond, S. M.; Coenen-Stass, A. M.; Godfrey, C.; McClorey, G.; Varela, M. A.; Roberts, T. C.; Clarke, K.; et al. Prevention of exercised induced cardiomyopathy following Pip-PMO treatment in dystrophic mdx mice. *Scientific Reports* **2015**, *5*, 8986.

(214) Hammond, S. M.; Hazell, G.; Shabanpoor, F.; Saleh, A. F.; Bowerman, M.; Sleigh, J. N.; Meijboom, K. E.; Zhou, H.; Muntoni, F.; Talbot, K.; et al. Systemic peptide-mediated oligonucleotide therapy improves long-term survival in spinal muscular atrophy. *Proceedings of the National Academy of Sciences USA* **2016**, *113* (39), 10962-10967.
(215) Vives, E.; Brodin, P.; Lebleu, B. A truncated HIV-1 Tat protein basic domain rapidly translocates through the plasma membrane and accumulates in the cell nucleus. *Journal of Biological Chemistry* **1997**, *272* (25), 16010-16017.
(216) Mishra, A.; Lai, G. H.; Schmidt, N. W.; Sun, V. Z.; Rodriguez, A. R.; Tong, R.; Tang, L.; Cheng, J.; Deming, T. J.; Kamei, D. T.; et al. Translocation of HIV TAT peptide and analogues induced by multiplexed membrane and cytoskeletal interactions. *Proceedings of the National Academy of Sciences USA* **2011**, *108* (41), 16883-16888.
(217) Lattig-Tunnemann, G.; Prinz, M.; Hoffmann, D.; Behlke, J.; Palm-Apergi, C.; Morano, I.; Herce, H. D.; Cardoso, M. C. Backbone rigidity and static presentation of guanidinium groups increases cellular uptake of arginine-rich cell-penetrating peptides. *Nature Communications* **2011**, *2*, 453.
(218) Ezzat, K.; Aoki, Y.; Koo, T.; McClorey, G.; Benner, L.; Coenen-Stass, A.; O'Donovan, L.; Lehto, T.; Garcia-Guerra, A.; Nordin, J.; et al. Self-Assembly into Nanoparticles Is Essential for Receptor Mediated Uptake of Therapeutic Antisense Oligonucleotides. *Nano Letters* **2015**, *15* (7), 4364-4373.
(219) Brooks, H.; Lebleu, B.; Vives, E. Tat peptide-mediated cellular delivery: back to basics. *Advanced Drug Delivery Reviews* **2005**, *57* (4), 559-577.
(220) Herce, H. D.; Garcia, A. E.; Cardoso, M. C. Fundamental molecular mechanism for the cellular uptake of guanidinium-rich molecules. *Journal of the American Chemical Society* **2014**, *136* (50), 17459-17467.
(221) Boisguerin, P.; Deshayes, S.; Gait, M. J.; O'Donovan, L.; Godfrey, C.; Betts, C. A.; Wood, M. J.; Lebleu, B. Delivery of therapeutic oligonucleotides with cell penetrating peptides. *Advanced Drug Delivery Reviews* **2015**, *87*, 52-67.
(222) El-Sayed, A.; Harashima, H. Endocytosis of gene delivery vectors: from clathrin-dependent to lipid raft-mediated endocytosis. *Molecular Therapy* **2013**, *21* (6), 1118-1130.
(223) Kim, J.; Woo, S.; de Gusmao, C. M.; Zhao, B.; Chin, D. H.; DiDonato, R. L.; Nguyen, M. A.; Nakayama, T.; Hu, C. A.; Soucy, A.; et al. A framework for individualized splice-switching oligonucleotide therapy. *Nature* **2023**, *619* (7971), 828-836.
(224) Schaffert, D.; Troiber, C.; Salcher, E. E.; Frohlich, T.; Martin, I.; Badgujar, N.; Dohmen, C.; Edinger, D.; Klager, R.; Maiwald, G.; et al. Solid-phase synthesis of sequence-defined T-, i-, and U-shape polymers for pDNA and siRNA delivery. *Angewandte Chemie International Edition* **2011**, *50* (38), 8986-8989.
(225) He, D.; Muller, K.; Krhac Levacic, A.; Kos, P.; Lachelt, U.; Wagner, E. Combinatorial Optimization of Sequence-Defined Oligo(ethanamino)amides for Folate Receptor-Targeted pDNA and siRNA Delivery. *Bioconjugate Chemistry* **2016**, *27* (3), 647-659.
(226) Lin, Y.; Wilk, U.; Pöhmerer, J.; Hörterer, E.; Höhn, M.; Luo, X.; Mai, H.; Wagner, E.; Lächelt, U. Folate Receptor-Mediated Delivery of Cas9 RNP for Enhanced Immune Checkpoint Disruption in Cancer Cells. *Small* **2023**, *19* (2), e2205318.
(227) Benli-Hoppe, T.; Göl Öztürk, Ş.; Öztürk, Ö.; Berger, S.; Wagner, E.; Yazdi, M. Transferrin Receptor Targeted Polyplexes Completely Comprised of Sequence-Defined Components. *Macromolecular Rapid Communications* **2022**, *43* (12), e2100602.
(228) Krhač Levačić, A.; Berger, S.; Müller, J.; Wegner, A.; Lächelt, U.; Dohmen, C.; Rudolph, C.; Wagner, E. Dynamic mRNA polyplexes benefit from bioreducible cleavage sites for in vitro and in vivo transfer. *Journal of Controlled Release* **2021**, *339*, 27-40.
(229) Truebenbach, I.; Kern, S.; Loy, D. M.; Hohn, M.; Gorges, J.; Kazmaier, U.; Wagner, E. Combination Chemotherapy of L1210 Tumors in Mice with Pretubulysin and Methotrexate Lipo-Oligomer Nanoparticles. *Molecular Pharmaceutics* **2019**, *16* (6), 2405-2417.
(230) Steinborn, B.; Truebenbach, I.; Morys, S.; Lachelt, U.; Wagner, E.; Zhang, W. Epidermal growth factor receptor targeted methotrexate and small interfering RNA co-delivery. *The Journal of Gene Medicine* **2018**, *20* (7-8), e3041. .
(231) Dohmen, C.; Edinger, D.; Fröhlich, T.; Schreiner, L.; Lächelt, U.; Troiber, C.; Rädler, J.; Hadwiger, P.; Vornlocher, H.-P.; Wagner, E. Nanosized Multifunctional Polyplexes for Receptor-Mediated SiRNA Delivery. *ACS Nano* **2012**, *6* (6), 5198-5208.
(232) Salcher, E. E.; Kos, P.; Frohlich, T.; Badgujar, N.; Scheible, M.; Wagner, E. Sequence-defined four-arm oligo(ethanamino)amides for pDNA and siRNA delivery: Impact of building blocks on efficacy. *Journal of Controlled Release* **2012**, *164* (3), 380-386.
(233) Beckert, L.; Kostka, L.; Kessel, E.; Krhac Levacic, A.; Kostkova, H.; Etrych, T.; Lachelt, U.; Wagner, E. Acid-labile pHPMA modification of four-arm oligoaminoamide pDNA polyplexes balances shielding and gene

transfer activity in vitro and in vivo. *European Journal of Pharmaceutics and Biopharmaceutics* **2016**, *105*, 85-96.
(234) Scholz, C.; Kos, P.; Wagner, E. Comb-like oligoaminoethane carriers: change in topology improves pDNA delivery. *Bioconjugate Chemistry* **2014**, *25* (2), 251-261.
(235) Schaffert, D.; Badgujar, N.; Wagner, E. Novel Fmoc-Polyamino Acids for Solid-Phase Synthesis of Defined Polyamidoamines. *Organic Letters* **2011**, *13* (7), 1586-1589.
(236) Frohlich, T.; Edinger, D.; Klager, R.; Troiber, C.; Salcher, E.; Badgujar, N.; Martin, I.; Schaffert, D.; Cengizeroglu, A.; Hadwiger, P.; et al. Structure-activity relationships of siRNA carriers based on sequence-defined oligo (ethane amino) amides. *Journal of Controlled Release* **2012**, *160* (3), 532-541.
(237) Kos, P.; Lachelt, U.; Herrmann, A.; Mickler, F. M.; Doblinger, M.; He, D.; Krhac Levacic, A.; Morys, S.; Brauchle, C.; Wagner, E. Histidine-rich stabilized polyplexes for cMet-directed tumor-targeted gene transfer. *Nanoscale* **2015**, *7* (12), 5350-5362.
(238) Troiber, C.; Edinger, D.; Kos, P.; Schreiner, L.; Kläger, R.; Herrmann, A.; Wagner, E. Stabilizing effect of tyrosine trimers on pDNA and siRNA polyplexes. *Biomaterials* **2013**, *34* (5), 1624-1633.
(239) Shin, M. L.; Hänsch, G.; Mayer, M. M. Effect of agents that produce membrane disorder on lysis of erythrocytes by complement. *Proceedings of the National Academy of Sciences USA* **1981**, *78* (4), 2522-2525.
(240) Reinhard, S.; Zhang, W.; Wagner, E. Optimized Solid-Phase-Assisted Synthesis of Oleic Acid Containing siRNA Nanocarriers. *Medicinal Chemistry Journal* **2017**, *12* (17), 1464-1470.
(241) Klein, P. M.; Kern, S.; Lee, D.-J.; Schmaus, J.; Höhn, M.; Gorges, J.; Kazmaier, U.; Wagner, E. Folate receptor-directed orthogonal click-functionalization of siRNA lipopolyplexes for tumor cell killing in vivo. *Biomaterials* **2018**, *178*, 630-642.
(242) Luo, J.; Höhn, M.; Reinhard, S.; Loy, D. M.; Klein, P. M.; Wagner, E. IL4-Receptor-Targeted Dual Antitumoral Apoptotic Peptide—siRNA Conjugate Lipoplexes. *Advanced Functional Materials* **2019**, *29* (25).
(243) Rui, Y.; Wilson, D. R.; Sanders, K.; Green, J. J. Reducible Branched Ester-Amine Quadpolymers (rBEAQs) Codelivering Plasmid DNA and RNA Oligonucleotides Enable CRISPR/Cas9 Genome Editing. *ACS Applied Materials & Interfaces* **2019**, *11* (11), 10472-10480.
(244) Hammond, S. M.; McClorey, G.; Nordin, J. Z.; Godfrey, C.; Stenler, S.; Lennox, K. A.; Smith, C. I.; Jacobi, A. M.; Varela, M. A.; Lee, Y.; et al. Correlating In Vitro Splice Switching Activity With Systemic In Vivo Delivery Using Novel ZEN-modified Oligonucleotides. *Molecular Therapy - Nucleic Acids* **2014**, *3* (11), e212.
(245) Gee, P.; Lung, M. S. Y.; Okuzaki, Y.; Sasakawa, N.; Iguchi, T.; Makita, Y.; Hozumi, H.; Miura, Y.; Yang, L. F.; Iwasaki, M.; et al. Extracellular nanovesicles for packaging of CRISPR-Cas9 protein and sgRNA to induce therapeutic exon skipping. *Nature Communications* **2020**, *11* (1), 1334.
(246) Yin, H.; Moulton, H. M.; Seow, Y.; Boyd, C.; Boutilier, J.; Iverson, P.; Wood, M. J. Cell-penetrating peptide-conjugated antisense oligonucleotides restore systemic muscle and cardiac dystrophin expression and function. *Human Molecular Genetics* **2008**, *17* (24), 3909-3918.
(247) Kim, H. J.; Ogura, S.; Otabe, T.; Kamegawa, R.; Sato, M.; Kataoka, K.; Miyata, K. Fine-Tuning of Hydrophobicity in Amphiphilic Polyaspartamide Derivatives for Rapid and Transient Expression of Messenger RNA Directed Toward Genome Engineering in Brain. *ACS Central Science* **2019**, *5* (11), 1866-1875.
(248) Scherer, W. F.; Syverton, J. T.; Gey, G. O. Studies on the propagation in vitro of poliomyelitis viruses. IV. Viral multiplication in a stable strain of human malignant epithelial cells (strain HeLa) derived from an epidermoid carcinoma of the cervix. *Journal of Experimental Medicine* **1953**, *97* (5), 695-710.
(249) Wilton-Clark, H.; Yokota, T. Antisense and Gene Therapy Options for Duchenne Muscular Dystrophy Arising from Mutations in the N-Terminal Hotspot. *Genes* **2022**, *13* (2), 257.
(250) Kaushal, J.; Singh, S.; Nautiyal, D.; Rao, G. K.; Singh, A. K.; Kumar, A. Themed collection Bioorthogonal and click chemistry: Celebrating the 2022 Nobel Prize in Chemistry. *New Journal of Chemistry* **2022**, *46*, 14757-14781.
(251) Agard, N. J.; Prescher, J. A.; Bertozzi, C. R. A Strain-Promoted [3 + 2] Azide–Alkyne Cycloaddition for Covalent Modification of Biomolecules in Living Systems. *Journal of the American Chemical Society* **2004**, *126* (46), 15046-15047.
(252) Zhang, H.; Lyu, Z.; Fan, Y.; Evans, C. R.; Barber, K. W.; Banerjee, K.; Igoshin, O. A.; Rinehart, J.; Ling, J. Metabolic stress promotes stop-codon readthrough and phenotypic heterogeneity. *Proceedings of the National Academy of Sciences USA* **2020**, *117* (36), 22167-22172.
(253) Kwan, T.; Thompson, S. R. Noncanonical Translation Initiation in Eukaryotes. *Cold Spring Harbor Perspectives in Biology* **2019**, *11* (4).
(254) Dai, C.; Cao, Z.; Wu, Y.; Yi, H.; Jiang, D.; Li, W. Improved fusion protein expression of EGFP via the mutation of both Kozak and the initial ATG codon. *Cellular and Molecular Biology Letters* **2007**, *12* (3), 362-369.

(255) Chen, Q.; Luo, W.; Veach, R. A.; Hickman, A. B.; Wilson, M. H.; Dyda, F. Structural basis of seamless excision and specific targeting by piggyBac transposase. *Nature Communications* **2020**, *11* (1), 3446.
(256) Laptev, I. A.; Raevskaya, N. M.; Filimonova, N. A.; Sineoky, S. P. The piggyBac Transposon as a Tool in Genetic Engineering. *Applied Biochemistry and Microbiology* **2018**, *53* (9), 874-881.
(257) Li, X.; Burnight, E. R.; Cooney, A. L.; Malani, N.; Brady, T.; Sander, J. D.; Staber, J.; Wheelan, S. J.; Joung, J. K.; McCray, P. B., Jr.; et al. piggyBac transposase tools for genome engineering. *Proceedings of the National Academy of Sciences USA* **2013**, *110* (25), E2279-2287.
(258) Wu, S. C.; Meir, Y. J.; Coates, C. J.; Handler, A. M.; Pelczar, P.; Moisyadi, S.; Kaminski, J. M. piggyBac is a flexible and highly active transposon as compared to sleeping beauty, Tol2, and Mos1 in mammalian cells. *Proceedings of the National Academy of Sciences USA* **2006**, *103* (41), 15008-15013.
(259) Day, C. D.; Lee, E.; Kobayashi, J.; Holappa, L. D.; Albert, H.; Ow, D. W. Transgene integration into the same chromosome location can produce alleles that express at a predictable level, or alleles that are differentially silenced. *Genes & Development* **2000**, *14* (22), 2869-2880.
(260) Rock, K. L.; Kono, H. The inflammatory response to cell death. *Annual Review of Pathology* **2008**, *3*, 99-126.
(261) Kang, S. H.; Cho, M. J.; Kole, R. Up-regulation of luciferase gene expression with antisense oligonucleotides: implications and applications in functional assay development. *Biochemistry* **1998**, *37* (18), 6235-6239.
(262) Bowman, E. J.; Siebers, A.; Altendorf, K. Bafilomycins: a class of inhibitors of membrane ATPases from microorganisms, animal cells, and plant cells. *Proceedings of the National Academy of Sciences USA* **1988**, *85* (21), 7972-7976.
(263) Crider, B. P.; Xie, X. S.; Stone, D. K. Bafilomycin inhibits proton flow through the H+ channel of vacuolar proton pumps. *Journal of Biological Chemistry* **1994**, *269* (26), 17379-17381.
(264) Clague, M. J.; Urbé, S.; Aniento, F.; Gruenberg, J. Vacuolar ATPase activity is required for endosomal carrier vesicle formation. *Journal of Biological Chemistry* **1994**, *269* (1), 21-24.
(265) Kichler, A.; Leborgne, C.; Coeytaux, E.; Danos, O. Polyethylenimine-mediated gene delivery: a mechanistic study. *The Journal of Gene Medicine* **2001**, *3* (2), 135-144.
(266) Akinc, A.; Thomas, M.; Klibanov, A. M.; Langer, R. Exploring polyethylenimine-mediated DNA transfection and the proton sponge hypothesis. *The Journal of Gene Medicine* **2005**, *7* (5), 657-663.
(267) Sabourian, P.; Yazdani, G.; Ashraf, S. S.; Frounchi, M.; Mashayekhan, S.; Kiani, S.; Kakkar, A. Effect of Physico-Chemical Properties of Nanoparticles on Their Intracellular Uptake. *International Journal of Molecular Sciences* **2020**, *21* (21).
(268) Anderson, C. R.; Gnopo, Y. D. M.; Gambinossi, F.; Mylon, S. E.; Ferri, J. K. Modulation of cell responses to Ag-(MeO2MA-co-OEGMA): Effects of nanoparticle surface hydrophobicity and serum proteins on cellular uptake and toxicity. *Journal of Biomedical Materials Research Part A* **2018**, *106* (4), 1061-1071.
(269) Heemskerk, H. A.; de Winter, C. L.; de Kimpe, S. J.; van Kuik-Romeijn, P.; Heuvelmans, N.; Platenburg, G. J.; van Ommen, G. J.; van Deutekom, J. C.; Aartsma-Rus, A. In vivo comparison of 2'-O-methyl phosphorothioate and morpholino antisense oligonucleotides for Duchenne muscular dystrophy exon skipping. *The Journal of Gene Medicine* **2009**, *11* (3), 257-266.

7. Publications

Original articles

Öztürk Ö, Lessl AL, Höhn M, Wuttke S, Nielsen PE, Wagner E, Lächelt U. *Peptide nucleic acid-zirconium coordination nanoparticles*. Sci Rep. 2023 Aug 30;13(1):14222.

DOI: 10.1038/s41598-023-40916-w

Lessl AL, Pöhmerer J, Lin Y, Wilk U, Höhn M, Hörterer E, Wagner E, Lächelt U. *mCherry on Top: A Positive Read-Out Cellular Platform for Screening DMD Exon Skipping Xenopeptide-PMO Conjugates*. Bioconjugate Chemistry 2023 Nov 22.

DOI: 10.1021/acs.bioconjchem.3c00408

Patent application

Wagner E, Lächelt U, Lin Y, **Lessl A-L**, Yazdi M, *Novel artificial amino acid containing lipo-oligomers for ribonucleoprotein and oligonucleotide delivery*, PCT application number: PCT/EP2023/080853

Poster presentation

Lessl A.-L., Kuhn J, Klein P. M., El Danaf N., Lamb D.C., Wagner E. and Lächelt U., *Splice-switching in tumor cells by artificial cationic lipopeptide–PMO conjugates*. 24th Annual meeting of the German local chapter of the Controlled Release Society, Planegg/Munich, Germany (February 2020).

8. Acknowledgements

I would like to express my gratitude to several people who supported and guided me throughout my PhD, leading me on this academic journey.

First of all, I would like to thank Prof. Dr. Ernst Wagner for giving me the opportunity to work on my PhD thesis within his research group. I want to thank you for every productive scientific discussion and input where I have learned a lot during the whole time. Your passion and fascination for science was a motivation and encouragement.

In addition, I would like to express my deep gratitude to Prof. Dr. Ulrich Lächelt for his supervision and support. It was an honor to be part of the “Lächelt subgroup”. Your guidance, support, and the weekly meetings made a significant difference. Thank you for every nice word of appreciation, commendation, and encouragement, especially during moments of desperation. I learned a lot from you, not only in terms of science and research but also in leading a group. Your scientific creativity was an inspiration teaching me to develop my own ideas and to never lose my curiosity.

I want to thank our small “Lächelt Lab” subgroup for having supportive and interesting discussions every week. Thank you Dr. Yi Lin, Dr. Faqian Shen, and Dr. Özgür Öztürk.

I would like to thank all of the people how directly contributed to this work: Dr. Elisa Hörterer, with whom I successfully established the PCR-based *in vivo* evaluation method; Jana Pöhmerer and Dr. Ulrich Wilk (aka Pöhmerich), who performed the required animal experiments; Dr. Yi Lin, for establishing of the new xenopeptide library; Miriam Höhn, for her support not only regarding CLSM but also as mental support during my PCR trouble shooting; and Melina Grau and Tobias Burghardt, for the MALDI-ToF measurements. Special thanks to Susanne Kempter, for performing TEM, and Lisa Richter, for conducting cell sorting.

I want to thank all of the people who contributed with their immense experience in different topics. Special thanks to Prof. Dr. Elvir Becirovic, whose support during the splicing reporter design and inspiring quote, 'Welcome to the weird world of splicing,' greatly enriched this project phase. I also extend my appreciation to Wolfgang Rödl, Ursula Biebl, Melinda Kiss, and Dr. Andreas Roidl for your support in different areas

I want to express my gratitude to you, Janin, for brightening up every single day in the lab and beyond. Thank you for navigating the delicate balance between sanity and insanity with me multiple times over the past years. Thank you for being as weirdly passionate about natural phenomena (such as the white color of snow and the consequences) as I am, as well as our shared experiences, from attempting to tame a crow to skydiving. Thank you for becoming my close friend in the past 4 years. I look forward to many more exciting things we will go through in the future.

. -.. . .-.. --. .- ... . / ..-. ..-- .-. / .. -- -- . .-. -.-.-- / -.. .- -. -.- . / -.. .- ... ... / . ... / -.. .. -.-. .... / --. .. -... –

Actually, this journey began in 2015 when I started working as a student research assistant in my second bachelor semester. It was during this time that I got to know many funny, helpful, friendly, and unique individuals. There are so many people who accompanied me along the way. I want to express my gratitude to Dr. Ines Truebenbach and Dr. Jasmin Hotz for being the best supervisors during my Bachelor's and Master's theses, as well as Dr. Dominik Loy, Dr. Sören Reinhardt, Dr. Philipp Klein, and Dr. Stephan Morys.

I want to thank many more members of the group who enriched my time: Ricarda, Johanna, Eric, Mina, Sophie, Franzi, Simone, Vicky, Paul, Fengrong, and Xianjin. From Mate tea taste tests to half-marathons, we experienced a lot.

In paying tribute to Markus Kovac, whose infectious joy, laugh, and light-heartedness brightened up all our days. His enduring positivity and the countless shared cups of coffee made it possible to have a break from challenging and stressful moments. Even though Markus is no longer with us, his lively spirit continues to influence this group, reminding us of the lasting imprint left by their friendship.

I would like to express my gratitude to my parents, who has shaped me into this independent, courageous, curious, self-determined, and persistent woman that I am today. I want to thank my grandparents who always encouraged me to stay curious and get to the bottom of things. My siblings always played an important role in my childhood and earlier adulthood, especially in terms of resilience, patience, and assertiveness. I love you!

Finally, I would like to express my deepest gratitude to Konstantin, whose unwavering support and steadfast encouragement have been essential throughout this doctoral journey. Your presence has been my constant source of strength, providing a safe haven in times of academic storms and a steady anchor when the seas of research seemed tumultuous. Your belief in my capabilities fueled my determination, and your patience during the demanding phases of this journey sustained me. Thank you for being my sanctuary and my confidant. I am grateful beyond words for your unwavering presence and the countless moments of support. Thank you for your love!

In the immortal words of Albus Dumbledore, "Happiness can be found even in the darkest of times if one only remembers to turn on the light." Thank you all for being the Lumos in my academic journey.

With immense gratitude and a pocket full of Bertie Bott's Every Flavor Beans,
Anna - Defender of the Thesis and Conqueror of Academic Dragons.

Mischief managed